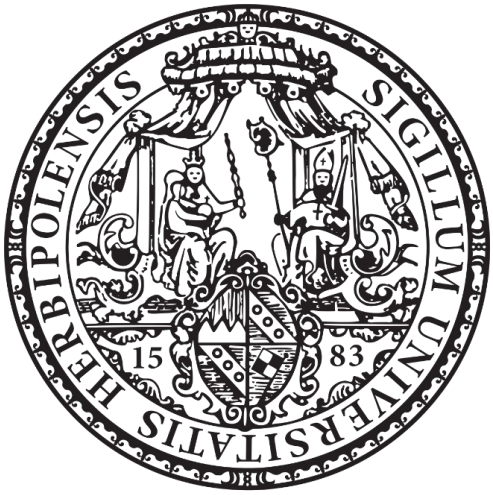

The HSV-1 ICP22 protein selectively impairs histone repositioning upon Pol II transcription downstream of genes

Das HSV-1 ICP22 Protein stört selektiv die Repositionierung von Histonen bei der Transkription durch Pol-II unterhalb von Genen

Doctoral thesis for a doctoral degree

at the Graduate School of Life Sciences

Julius-Maximilians-Universität Würzburg

Section: Infection and immunity

submitted by

Lara Djaković

from Rijeka, Croatia

Würzburg 2021

Submitted on:

……

Office stamp

Members of the *Promotionskomitee*:

Chairperson:	Prof. Dr. sc. Christian Janzen
Primary Supervisor:	Prof. Dr. med. Lars Dölken
Supervisor (Second):	Prof. Dr. sc. Utz Fischer
Supervisor (Third):	Prof. Dr. sc. Florian Erhard

Date of Public Defense: ……..

Date of Receipt of Certificates: ……

Affidavit

I hereby declare that my thesis entitled "**The HSV-1 ICP22 protein selectively impairs histone repositioning upon Pol II transcription downstream of genes**" is the result of my own work. I did not receive any help or support from commercial consultants. All sources and/or materials applied are listed and specified in the thesis.
Furthermore, I verify that this thesis has not yet been submitted as part of another examination process neither in identical nor similar form.

Würzburg, June 2021

_____

Lara Djaković

Eidesstattliche Erklärung

Hiermit erkläre ich an Eides statt, die Dissertation „**Das HSV-1 ICP22 Protein stört selektiv die Repositionierung von Histonen bei der Transkription durch Pol-II unterhalb von Genen**" eigenständig, d.h. insbesondere selbständig und ohne Hilfe eines kommerziellen Promotionsberaters, angefertigt und keine anderen als die von mir angegebenen Quellen und Hilfsmittel verwendet zu haben.
Ich erkläre außerdem, dass die Dissertation weder in gleicher noch in ähnlicher Form bereits in einem anderen Prüfungsverfahren vorgelegen hat.

Würzburg, Juni 2021

_____

Lara Djaković

ACKNOWLEDGMENTS

As I am now at the end of the PhD journey, I would like to take this opportunity to thank many who have been part of my life over the years.

First, I want to express my sincere gratitude and appreciation to my primary supervisor, Prof. Dr. Lars Dölken. His insightful comments, guidance, experience as well as excellent tools in the lab helped me grow as a scientist and complete my work. I am beyond grateful I had a supervisor who I could approach not only with work-related topics and who was always willing to help or show his support in some way.

I would also like to give my warm thanks the other two members of my committee, Prof. Dr. Utz Fischer and Prof. Dr. Florian Erhard. Thank you both for participating in valuable scientific discussions during our meetings, sharing your insights but also providing constructive criticisms to strengthen my work. Many thanks also goes to Prof. Dr. Caroline Friedel for analyzing the sequencing data.

I wish to express my thanks to the current and former lab members of the Dölken group; Dr. Thomas Hennig (Tomaš) for supervising me during my time here, sharing his knowledge and raising my spirit in difficult times, my ride or die conference partner Dr. Adam Whisnant for all the scientific but also less scientific discussions, Manivel Lodha for all the useful comments and enjoyable lunch breaks, Arnhild Grothey for assisting me with my work when needed, Dr. Bhupesh Prusty for providing helpful suggestions for my work and finally, Julian Hock for sharing all the struggles of the first PhD year with me. My thanks also goes to Dr. Bhaskar Jha, Dr. Marissa Baptista, Marina, Oliver, Sina, Kourosh, Mara, Kathy, Chris, and Eli for making a friendly and enjoyable atmosphere in the lab. Additionally, I want to thank the former lab members of the SSS group, Sherry and Maria for all the nice times we have spent together, inside and outside of the lab.

Special thanks goes to the Internet for showing the job position to Andrea Milić who decided to join our lab and made my last few years here much more enjoyable. Gospođo, thank you for all the times you've helped me with my experiments without expecting anything in return. Thank

you for carrying heavy boxes and picking up stuff that were too high for me to pick up. I am grateful I had someone like you to share my happy, but also less happy moments with. While we might no longer be colleagues at work, you will never stop being my friend.

Again, I want to thank my 'Tigers' (Luka, Andrea, Manivel and Adam) for making my life in Würzburg much more fulfilled during these unpredictable COVID-19 times. We were each other's family and I will always have you in my heart wherever I go. Thank you for all the memorable weekends we've spent gaming, cooking and just hanging out together.

I want to thank my parents and grandma for their love, support and constant encouragement. Thank you, mum and dad, for driving 800 km just to spend a few days with me. Also, thank you for understanding when my days were low and I wasn't the best conversation partner. I still don't know where the road will take me next, but if dad managed to survive my 12h flight to Las Vegas, he will survive anything!

My biggest thanks goes to Luka Zurak. Thank you for all the patience and being there for me throughout this journey even when I was a pain in the neck. Thank you for doing all the house chores, delicious meals and even blow drying my hair when I was too tired to do it myself. Just having someone like you to come home to everyday is something I wouldn't change for anything.

TABLE OF CONTENTS

APPENDIX

Metric prefixes

Abbreviation	Long-term
c	centi
in	inch
k	kilo
m	mili
n	nano
µ	micro

Units

Abbreviation	Long-term
°C	degree Celsius
Da	Dalton
g	gram
G force	gravitational force
h	hour
L	liter
m	meter
M	mol
min	minute
sec	second
U	unit
w/v	weight per volume
v/v	volume per volume

Other abbreviations

Abbreviation	Long-term
%	percent
4E-BP1	4E-binding protein 1
4-sU	4-thiouridine
aa	amino acid
amiRNA	artificial microRNA
AMP	ampicillin
ATAC-seq	assay for transposase-accessible chromatin using sequencing
ATP	adenosine triphosphate
BAC	bacterial artificial chromosome
BHK	baby hamster kidney cell line
bp	base pair
C	cytosine
cdc2	cell division control protein 2
CDS	coding sequence
CH_3	methyl group
ChIP	chromatin immunoprecipitation followed by sequencing
CMC	carboxymethylcellulose
CO_2	carbon dioxide
CPE	cytopathic effect
CPSF	cleavage and polyadenylation specificity factor
Cq	quantification cycle
CstF	cleavage stimulating factor
CTD	carboxyl-terminal domain

CVSC	capsid vertex-specific component
DAPI	4', 6-diamidino-2-phenylindole
ddH20	double distilled water
DDR	DNA damage response
DMEM	Dulbecco's modified eagle medium
DNA	deoxyribonucleic acid
DNase	deoxyribonuclease
dOCR	downstream open chromatin region
DoG	downstream-of-gene containing transcript
DoTT	disruption of transcription termination
Dox	doxycycline
DRG	dorsal root ganglia
DSB	double strand break
dsDNA	double-stranded DNA
DSIF	DRB sensitivity inducing factor
DST	desalting
dUTPase	deoxyuridine triphosphatase
E gene	early gene
EBV	Epstein-Barr virus
EC	elongation complex
EDTA	ethylenediaminetetraacetic acid
eGFP	green fluorescent protein
eIF	eukaryotic initiation factor
EM	electron microscopy
ER	endoplasmic reticulum
ET	electron tomography
FACT	facilitates chromatin transaction
FCS	fetal calf serum

FPKM	fragments per kilobase of transcript per million mapped reads
G	guanine
GAG	glycosaminoglycan
gD	glycoprotein D (e.g.)
HCF-1	host cell factor-1
HCl	hydrochloric acid
HCMV	human cytomegalovirus
HDAC1	histone deacetylase 1
HDM	histone demethylases
HEK 293T	human embryonic kidney 293 cells with T antigen
HF	high fidelity
HFFF	human fetal foreskin fibroblasts
HHV-6A	human herpesvirus 6A
HHV-6B	human herpesvirus 6B
HHV-7	human herpesvirus 7
HMT	histone methyltransferase
hpi	hours post infection
HPLC	high performance liquid chromatography
Hsc70	heat shock cognate protein 70
HSE	herpes simplex encephalitis
HSK	herpetic stromal keratitis
HSV-1	herpes simplex virus 1
HSV-2	herpes simplex virus 2
hTERT	human telomerase reverse transcriptase Immortalized cell line
IAV	influenza virus infection
ICP0	infected cell protein 0 (e.g.)

IE gene	immediate-early gene
IF	immunofluorescence
IFN	interferon
IgG	immunoglobulin
Int	integrator
IR_L	internal repeat of the long region
IR_S	internal repeat of the short region
ISG	interferon stimulated gene
JNK	c-Jun N-terminal kinase
KD	knock-down
KSHV	Kaposi's sarcoma–associated herpesvirus
L gene	late gene
LB	lysogeny broth
LiCl	lithium chloride
MCS	multiple cloning site
Med	mediator
MEF	mouse embryo fibroblasts
MEM NEAA	minimum essential medium non-essential amino acids
$MgCl_2$	magnesium chloride
MOI	multiplicity of infection
mRNA	messenger RNA
NaCl	sodium chloride
Na-DOC	sodium deoxycholate
ND10	nuclear domain 10
NEC	nuclear egress complex
NH_3	amino group
NLS	nuclear localization signal
NP	nuclear protein

NP-40	nonyl phenoxypolyethoxylethanol
NS1	non-structural protein 1
OCR	open chromatin region
Oct1	octamer binding protein 1
ORF	open reading frame
ori	origin of replication
PAA	phosphonoacetic acid
PAS	polyadenylation signal
PBS	phosphate-buffered saline
PCR	polymerase chain reaction
PenStrep	penicillin-streptomycin
PFA	paraformaldehyde
PFU	plaque forming unit
Phe	phenylalanine
PKR	protein kinase R
PML	promyelocytic leukemia
PMSF	phenylmethylsulfonyl fluoride
Pol II	RNA polymerase II
PP1	protein phosphatase 1
PPP	promoter proximal pausing
PTM	post translational modification
qPCR	quantitative polymerase chain reaction
qRT	reverse transcriptase
REST	re1-silencing transcription factor
RNA	ribonucleic acid
RNase	ribonuclease
RNF	ring finger protein
rpm	revolutions per minute
rRNA	ribosomal RNA

RSB	resuspension buffer
RT	room temperature
SAM	S-adenosyl methionine
SAP145	spliceosome associated protein 145
SAPK	stress activated protein kinase
SDS	sodium dodecyl sulfate
SDS-PAGE	SDS-polyacrylamide gel electrophoresis
Ser	serine
SETD2	SET domain containing 2
snRNA	small nuclear RNA
SOC	super optimal broth medium
Spt16	suppressor of Ty 16
ssDNA	single-stranded DNA
SSRP1	structure specific recognition protein 1
TAF-I	template activating factor
TBP	TATA-binding protein
TES	transcription end site
TF	transcription factor
TG	trigeminal ganglia
TGN	trans-Golgi network
Thr	threonine
TK	thymidine kinase
TRIS	tris(hydroxymethyl)aminomethane
TR_L	terminal repeat of the long region
TR_S	terminal repeat of the short region
TSS	transcriptional start site
Tyr	tyrosine
U	unit
U-2 OS	human bone osteosarcoma epithelial cells

Ubc13	ubiquitin-conjugating enzyme 13
UbcH5a	ubiquitin-conjugating enzyme H5a
UD	unique dual
UDG	uracil-DNA glycosylase
U_L	unique-long
UPS	upstream sequence
U_S	unique-short
UTR	untranslated region
Vero	African green monkey kidney cells
vhs	virion host shut-off
VICE	virus-induced chaperon-enriched
VP5	virion protein 5 (e.g.)
VRC	viral replication compartment
VZV	varicella-zoster virus
WB	western blot
WT	wild type
XRN2	5'-3' Exoribonuclease 2
γ1	leaky-late gene
γ2	true-late gene

SUMMARY

Herpes Simplex Virus type 1 (HSV-1) is an ubiquitous neurotropic human pathogen that infects a large majority of the world's population. It is the causative agent of the common cold sore but also responsible for life-threatening infections (e.g., encephalitis), particularly in immunocompromised individuals and neonates. Like other herpesviruses, HSV-1 takes over the cellular RNA machinery to facilitate productive infection while efficiently shutting down host gene expression by targeting multiple steps of RNA metabolism. The two viral proteins, vhs and ICP27, play a crucial role in this process. Delivered by the tegument of the incoming virus, the virion host shut-off (vhs) endonuclease rapidly starts cleaving both cellular and viral mRNAs. With the onset of viral gene expression, the HSV-1 immediate-early protein ICP27 promotes the expression of viral early and late genes through various mechanisms, including mRNA processing, export, and translation.

Prior research by the Dölken lab demonstrated that lytic HSV-1 infection results in the disruption of transcription termination (DoTT) of most cellular genes by the viral ICP27 protein. This significantly contributes to HSV-1 induced host shut-off. DoTT results in transcription for tens of thousands of nucleotides beyond poly(A) sites and into downstream genes. Interestingly, this was found to be accompanied by a dramatic increase in chromatin accessibility downstream of the affected poly(A) sites. This is consistent with the formation of extensive downstream open chromatin regions (dOCR) and indicative of impaired histone repositioning in the wake of RNA polymerase II (Pol II) downstream of the affected poly(A) sites.

In my PhD thesis, I demonstrate that dOCR formation is dependent on the viral ICP22 protein when poly(A) read-through transcription is triggered by the ectopic expression of ICP27 or salt stress. I show that dOCR formation occurs when a high level of transcriptional activity arises downstream of genes due to the HSV-1-induced DoTT. To investigate whether histone composition is affected downstream of genes, I established the ChIPmentation approach to study associated changes and the influence of DoTT and dOCR formation on major histone modification marks. In HSV-1 WT infection, dOCR formation was reflected in alterations of canonical H1 histone downstream of affected genes, which was absent in ΔICP22 infection. To elucidate the

underlying molecular mechanism, two major histone chaperones SPT6 and FACT (SPT16 and SSRP1), which govern histone repositioning and may thus play a role in H1 homeostasis, were extensively studied. Both histone chaperones have been recently shown to be recruited to the viral genome by interactions with ICP22 protein. To investigate whether the depletion of SSRP1 or SPT6 would complement the loss of ICP22 to induce dOCR, T-HF cells with doxycycline-inducible knock-down of either of the two factors were generated. ATAC-seq analysis revealed that the interaction between the two histone chaperones and ICP22 is not involved in HSV-1-induced dOCR formation, suggesting the involvement of other proteins. In summary, this work sheds new light on a fundamental molecular mechanism of the cellular transcriptional machinery that is manipulated by the concerted actions of the two HSV-1 immediate-early proteins ICP22 and ICP27.

ZUSAMMENFASSUNG

HSV-1 ist ein weit verbreitetes, neurotropisches Virus, mit welchem ein Großteil der Weltbevölkerung infiziert ist. Es verursacht milde Infektionen wie Herpes labialis, aber kann auch lebensbedrohliche Infektionen des Nervensystems (z. B. Enzephalitis) in immunsupprimierten Menschen und Neugeborenen auslösen. Um sich lytisch zu vermehren, programmiert HSV-1 die Transkriptions- und Translationsmaschinerie der Zelle effizient um und hemmt gleichzeitig an mehreren Punkten zelluläre Genexpression. Zwei virale Proteine, vhs und ICP27, spielen dabei eine entscheidende Rolle. Vhs wird im Tegument des Virions mit dem Inokulum in die Zelle geliefert und baut so zelluläre Transkripte ab noch bevor virale Genexpression startet. ICP27 wird also sogenanntes „immediate-early" Gen als eines der ersten viralen Proteine exprimiert und kann unterstützt auf mehreren Ebenen (RNA Prozessierung, Export und Translation) die Expression der viralen „early" und „late" Gene.

Unsere Gruppe hat diesbezüglich gezeigt, dass die Terminierung der Transkription (sogenanntes „DoTT") durch das virale Protein ICP27 in der lytischen Infektion gestört wird. Dies trägt maßgeblich zur Abschaltung der zellulären Genexpression bei. Die Störung der Terminierung führt dazu, dass RNA Polymerase II bis zu >100 Kilobasen nach dem Polyadenylierungssignal weiter transkribiert. Durch die Aktivität der RNA Polymerase II wird in den 3' Regionen der betroffenen Gene das Chromatin gelockert (sogenanntes „dOCR"). Dies steht im Einklang mit einer Öffnung des Chromatins durch gehemmte Histon-Neupositionierung, verursacht durch die Transkription der betroffenen Genomregionen.

Im Rahmen meiner Doktorarbeit konnte ich mittels Hochdurchsatzsequenzieranalyse von Transposon-zugänglichem Chromatin (ATAC-seq) zeigen, dass offenes Chromatin durch das virale Protein ICP22 verursacht wird. Dieser Effekt konnte unterdessen nur beobachtet werden, wenn die Terminierung der Transkription, entweder durch die gleichzeitige Expression von ICP27 oder stressinduziert z.B. durch hypertonen Lösungen, gestört wurde. Das Ausmaß an offenem Chromatin korrelierte dabei mit der Transkriptionsaktivität der entsprechenden Genomregionen.

Durch bioinformatische Analysen von Hochdurchsatzsequenzierungen von Wildtyp Virus und ICP22-defizitären Mutanten infizierten Zellen konnte ich einen Cluster von stark exprimierten Genen mit ausgeprägter DoTT identifizieren, der besonders stark von der Chromatinöffnung betroffen war. Um zu testen, ob die Histone in den betroffenen Regionen durch die Induktion von dOCR verändert wurden, habe ich ein neues Chromatin-Immunpräzipitations Verfahren namens ChIPmentation etabliert und hiermit die mit der Induktion von dOCR assoziierten Histonvarianten untersucht. Dabei fiel auf, dass das H1 Histon gezielt in von dOCR betroffenen Regionen verloren ging. Um den zu Grunde liegenden Mechanismus zu untersuchen, habe ich die Rolle der beiden Histonchaperonen SPT6 und FACT (SPT16 und SSRP1) ausgiebig charakterisiert. Diese regulieren normalerweise die Repositionierung von Histonen im Zuge der Pol II Transkription. Beide Faktoren werden zudem durch ICP22 in die viralen DNA Replikationzentren im Nukleus rekrutiert, was den Positionierungsdefekt von H1 hervorrufen könnte. Um diese Hypothese zu testen, wurden beide Proteine durch induzierbare shRNA Knockdowns depletiert und mittels ATAC-seq untersucht, ob dies in der Infektion mit ICP22-defizitären Mutanten zur Öffnung des Chromatin führt. Hierbei zeigte sich allerdings, dass die Depletion dieser beider Histonchaperone kein offenes Chromatin bei Infektion mit der ICP22 Knockout Mutante erzeugt. Zudem fiel auf, dass SSRP1 selektiv dazu beitrug, Chromatin in transkribierten Regionen geschlossen zu halten. Offensichtlich spielen daher die beiden Histonchaperonen keine Rolle bei der ICP22-induzierten Öffnung des zellulären Chromatins unterhalb von Genen.

1. INTRODUCTION

Herpesviridae

The *Herpesviridae* is a large family of double-stranded DNA (dsDNA) viruses that infect a wide range of vertebrates including mammals, reptiles and birds [1]. Thus far, nine herpesviruses are known to infect humans: Herpes Simplex Virus 1 (HSV-1), Herpes Simplex Virus 2 (HSV-2), Human Cytomegalovirus (HCMV), Varicella-Zoster Virus (VZV), Epstein-Barr Virus (EBV), Human herpesviruses 6A (HHV-6A), Human herpesviruses 6B (HHV-6B), Human herpesviruses 7 (HHV-7) and Kaposi's sarcoma–associated herpesvirus (KSHV) [2,3].

Based on their biological and physical properties including genome organization and cell tropism, these viruses are classified into three subfamilies - Alphaherpesvirinae, Betaherpesvirinae and Gammaherpesvirinae. Members of the Alphaherpesvirinae subfamily – HSV-1, HSV-2 and VZV – are defined by: a variable host range, relatively short reproductive cycles, rapid spread in the cell culture, efficient destruction of infected cells and the ability to establish latency primarily, although not solely, in trigeminal ganglia (TG) or dorsal root ganglia (DRG) [3–5].

1.1. Herpes Simplex Virus 1 (HSV-1)

1.1.1. Pathology

HSV-1 is an ubiquitous human pathogen and a causative agent of the common orolabial lesions ('cold-sore') affecting nearly two-thirds of the world's population. Typically, HSV-1 is acquired during childhood through direct contact with mucocutaneous lesions or via contact with oral secretions during asymptomatic shedding [6]. The seroprevalence of HSV-1 infection is higher than HSV-2, although they share about 83 % of the base sequence homology [7]. In contrast to HSV-1, HSV-2 is primarily sexually transmitted and thus infections usually arise later in life [8]. Although the two viruses generally infect different parts of the body, with HSV-2 more frequently infecting genital epithelial cells, HSV-1 has become responsible for more than 50 % of the first-episode genital herpes in recent years. Of note, genital HSV-1 infections are usually less severe clinically

and cause fewer recurrences than observed for HSV-2 [9].

HSV-1 undergoes productive infection in epithelial cells at the site of inoculation and establishes latent infection in neurons. Here, the virus remains quiescent lifelong with occasional reactivation as a result of different psychological and physical factors [10]. In an immunocompetent host, primary HSV-1 infection is often asymptomatic, while immunocompromised individuals commonly develop severe, or even life-threatening infections. This includes HSV-1 pneumonia, herpetic stromal keratitis (HSK), the leading cause of infectious corneal blindness, and herpes simplex encephalitis (HSE). After primary infection, recurrence rates are highly variable with disease severity directly related to the degree of immunodeficiency [5]. In neonates, HSV-1 is associated with increased mortality and morbidity that results from transmission from mother to child *in utero* or via intrapartum contact [3]. Despite the availability of effective antiviral agents, such as acyclovir, the incidence of neonatal HSV-1 infection is ~1 in 3,000 to 1 in 5,000 deliveries per year [12]. Localized infections of the orofacial area are rarely fatal, however, infants with disseminated infections or those involving the central nervous system are at high risk of permanent neurological impairment or mortality. Accordingly, efficient prevention as well as timely diagnosis and therapy are crucial for preventing severe clinical outcomes.

1.1.2. Virion structure

Early studies revealed the structure of HSV-1 particle through electron microscopy (EM) and electron tomography (ET), defining it as a spherical particle with diameter ranging from 186 nm to 225 nm, each containing an icosahedral nucleocapsid with an external diameter of 125 nm [13,14]. The HSV-1 particle, as illustrated in Figure 1, consists of four elements: (I) an electron-dense core containing the viral dsDNA, (II) an icosahedral capsid encompassing the core, (III) a partially ordered layer called *tegument* that surrounds nucleocapsid and (IV) the envelope, an outer lipid bilayer with viral glycoproteins embedded in it [3].

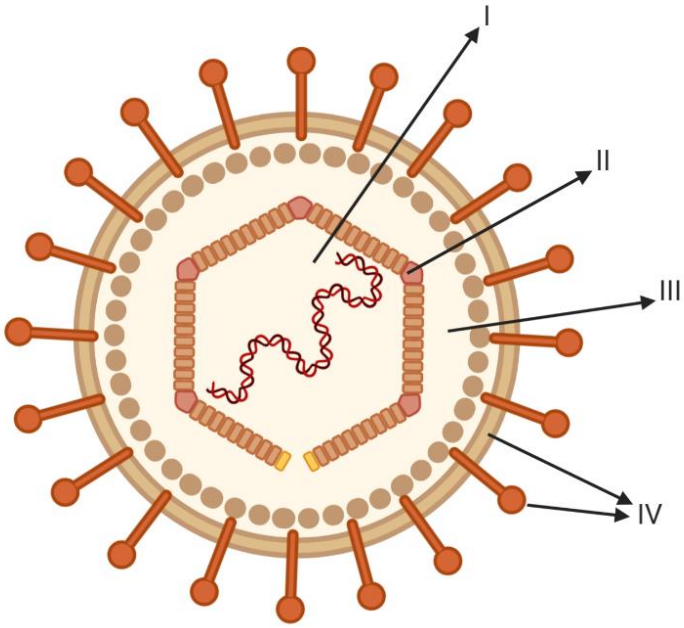

Figure 1. Structure of the HSV-1 virion.

The HSV-1 virion is comprised of four features: **(I)** dsDNA, packaged as a tightly wrapped spool inside the core; **(II)** an icosahedral capsid; **(III)** a tegument layer containing viral proteins; and **(IV)** a viral lipid envelope studded with gly oproteins.

Adapted from "HSV-1", by BioRender.com (2020). Retrieved from https://app.biorender.com/biorender-illustrations.

The HSV-1 core contains dsDNA genome whose negative charge is neutralized by tightly bound polyamines spermidine and spermine [15] The viral capsid surrounding the core is composed of 162 capsomers, including 150 hexons and 11 pentons arranged in a T=16 icosahedral symmetry [16]. Virion protein 5 (VP5, *U_L19*), a major capsid protein and three less abundant proteins (VP26, VP23, and VP19c) are comprising the outer shell of the capsid surrounded by the tightly adhering tegument [17]. The most structurally complex layer of the HSV-1 is the tegument that comprises over 20 proteins, with VP16 (*U_L48*), virion-host shutoff (vhs, *U_L41*), VP22 (*U_L49*) and VP1-2 (*U_L36*) as the most studied among them [18] The envelope, consisted of a lipid membrane, carries 13 distinct viral glycoproteins essential for virus entry into the host cell and viral morphogenesis [19].

1.1.3. Genome structure

HSV-1 genome is a linear dsDNA that encodes more than 80 proteins and is approximately 152 000 bp long, varying slightly between laboratory strains and clinical isolates [20,21]. However, a recent revised annotation of the HSV-1 genome revealed the complexity of HSV-1 gene expression by identifying novel 201 viral transcripts and 284 Open-Reading Frames (ORFs) [22].

A high G+C composition is one of the most unusual characteristics of herpesviruses, particularly α-herpesviruses. Both HSV-1 and HSV-2 have a high G+C contents of 68 % and 70 %, respectively, while the average G+C composition of other herpesviruses is 54.4 ± 11.5 % [23].

Structurally, as depicted in Figure 2, the HSV-1 genome is divided into distinct components, comprising two covalently linked regions, designated as unique long (U_L, 82 % of the genome) and unique short (U_S, 18 % of the genome), each flanked by inverted copies of large repeats known as the terminal and internal repeats of the long region (TR_L and IR_L) and the short region (TR_S and IR_S) [3].

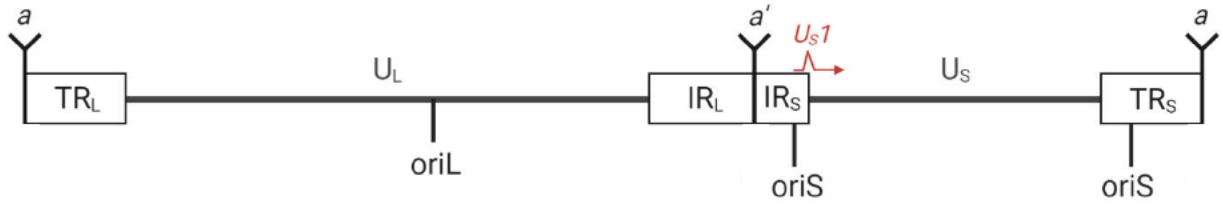

Figure 2. Genomic structure of HSV-1.

The full schematic representation of HSV-1 genome depicting unique long (U_L) and a unique short region (U_S), flanked by terminal and internal repeat sequences of the long (TR_L and IR_L) and short (TR_S and IR_S) region. A repeat sequence (*a*) at the genome termini is present at the IRL-IRs junction (*a'*). *U_S1* indicates the location of the ICP22 protein. Positions of three origins of replication are indicated with two within the U_S region (oriS) and one in the U_L region (oriL).

The short segment, known as the "*a*" sequence is repeated in one or more copies at the junction between IR_L-IR_s and at the both ends of the genome, with only one copy present at the termini of TR_S [24]. The inverted orientation of the "*a*" sequence at the IR_L-IR_s junction enables inversion of

the orientation of the unique regions, relative to one another, thus yielding four genomic isomers in equimolar concentrations and with equal functionality [25].

HSV-1 genome contains three origins of replication; one copy of oriL located within the U_L region and two copies of oriS located within short repeat regions, IR_S and TR_S. Mutations of oriL or both copies of oriS do not prevent viral replication *in vitro*, suggesting that oriL and oriS can substitute functionally for one another during lytic infection [26].

1.1.4. Productive infection

The HSV-1 life cycle *in vitro* involves several major steps; attachment and entry into the host cell, capsid migration through cytoplasm and viral genome delivery into the nucleus, expression of viral genes in a regulated temporal cascade, genome replication, virion assembly and egress of new viral particles. A schematic representation of these steps is shown in Figure 3.

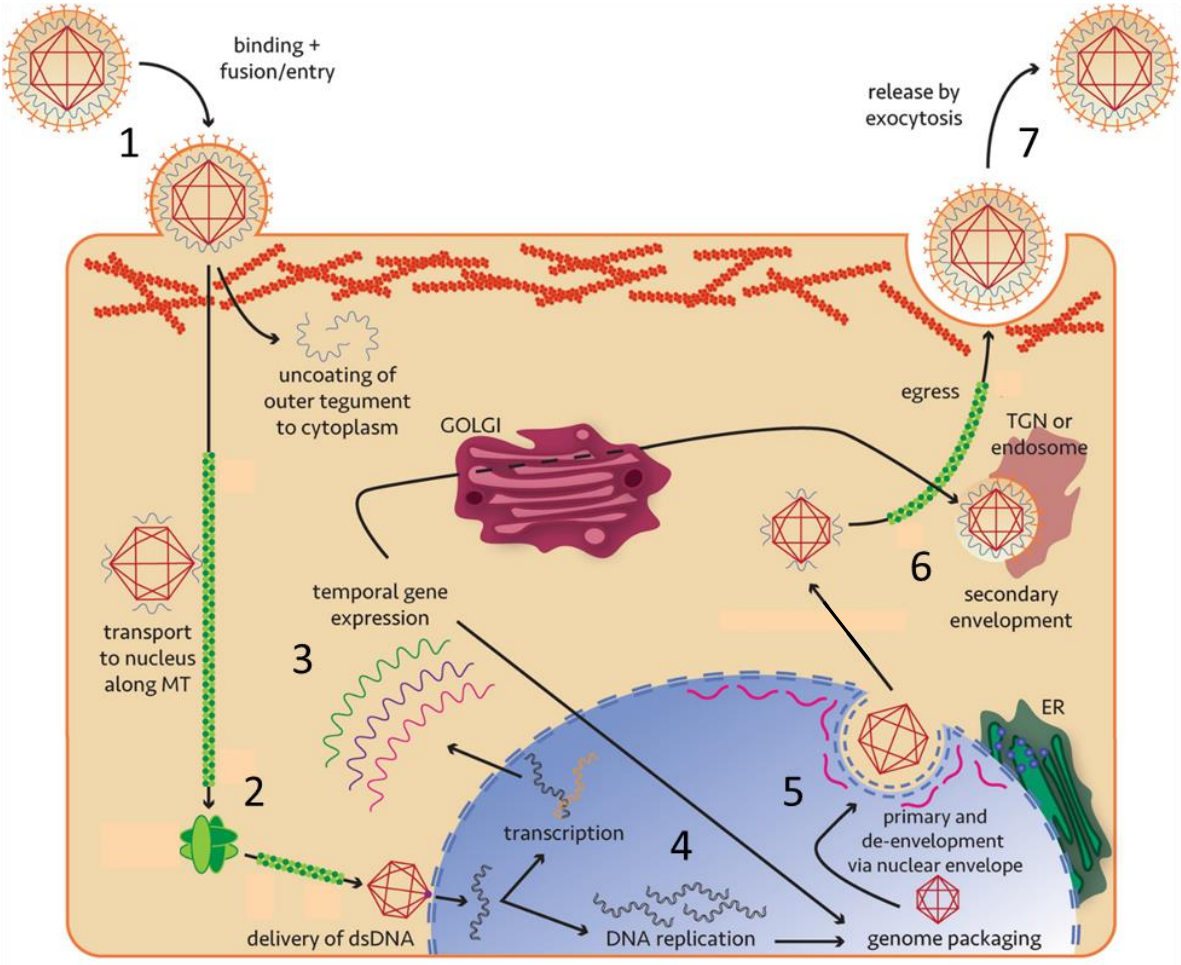

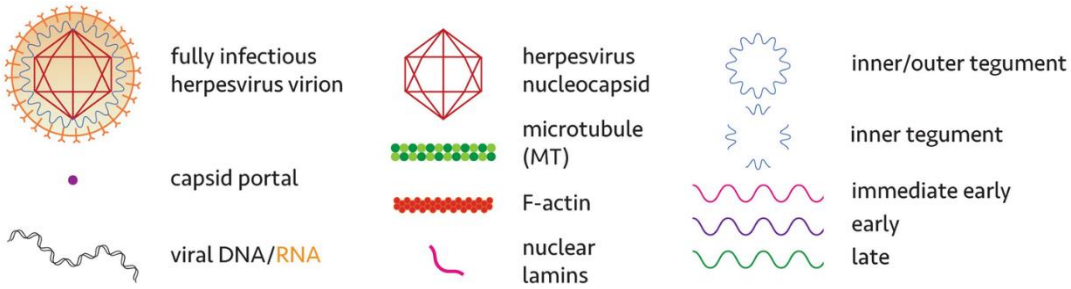

Figure 3. Schematic model of HSV-1 productive infection.

HSV-1 life cycle consists of: **1)** virion attachment facilitated by viral glycoproteins and entry into the host cell via fusion; **2)** transport across cytoplasm via microtubule-based motor proteins, kinesin and dynein, and delivery of the viral DNA to the nucleus through a capsid portal; **3)** transcription and translation of viral genes in a temporal manner with immediate-early (IE, α), early (E, β) and late (L, γ) proteins involved in key maturation stages; **4)** viral DNA replication; **5)** capsid assembly and genome packaging in the nucleus followed by nuclear egress (primary envelopment and de-envelopment step); **6)** nucleocapsid maturation through attaining tegument layer and envelope proteins processed via the endoplasmic reticulum (ER)/Golgi and transport along microtubules via the trans-Golgi network (TGN) (secondary envelopment) **7)** egress of newly assembled viral particles by exocytosis.

Taken and adapted from Denes, Christopher E et al. "Cytoskeletons in the Closet-Subversion in Alphaherpesvirus Infections." Viruses vol. 10,2 79. 13 Feb. 2018 [27]

1.1.4.1. Attachment and viral entry

To enter a host cell and initiate infection, HSV-1 undergoes a complex multistage process that requires interaction between surface-expressed cellular receptors and viral glycoproteins. Whether HSV-1 enters the cell by fusion of the envelope with the plasma membrane or endocytosis depends on the respective cell type. However, the viral glycoproteins required for the interaction are the same irrespective of the pathway of entry [28,29]. In the process of productive infection, HSV-1 loosely attaches to the cellular membrane through interaction of viral glycoproteins gC and gB with glycosaminoglycans (GAGs) such as heparan sulfate. In the following step, high-affinity binding of gD to one of the three cellular receptors: Nectin-1, herpesvirus entry mediator (HVEM) or 3-O-sulfated heparan sulfate (3-OS HS) induces a conformational change in gD that promotes recruitment of gH-gL and gB as components of fusion complex. Finally, this

complex of viral glycoproteins and cellular receptors mediates fusion of the envelope with the cellular membrane and penetration of the viral particle into the host cell [3,30].

Upon entry into the cytoplasm, the majority of the tegument proteins are released into the cytoplasm with small number still bound to the viral capsid, such as VP1-2, U_L37 and U_S3. Tegument proteins released from the nucleocapsid subsequently perform their functions in regulation of gene expression, viral envelopment and immune modulation as it will be discussed in the following chapters [31,32]. HSV-1 capsids rely on the cellular machinery to be transported to the nuclear pore. This utilizes the microtubular network and is mediated by the molecular motor cytoplasmic dynein/dynactin complex [33]. Once the capsid reaches the nucleus, the viral tegument protein VP1-2 together with the host nuclear factor importin-β and nuclear pore complex proteins (NPCs) govern capsid docking onto nuclear pores, as well as the release of the linear HSV-1 genome from the capsid and its delivery into the nucleus [31]. Upon entry into the nucleus, the linear dsDNA genome undergoes rapid circularization in the absence of protein synthesis. This step is essential in the productive life cycle of HSV-1 because it generates circular molecules that function as a template for viral replication [34].

1.1.4.2. Intrinsic immunity

Mammalian cells have evolved complex defense mechanisms to respond to disturbances caused by viral infections. As HSV-1 enters a host cell, several intrinsic pathways provide a primary defense mechanism in combating infection. Intrinsic immunity represents an interferon (IFN)-independent antiviral response mediated by constitutively expressed host restriction factors that directly act to control the viral gene expression [35]. Numerous studies identified different intrinsic restriction factors that rapidly associate with the incoming viral genomes and induce genome silencing under low multiplicity of infection (MOI) and absence of viral countermeasures. Some of the most common include: (I) nuclear domain 10 (ND10), also known as promyelocytic leukemia (PMLs) bodies, (II) DNA damage response (DDR) proteins and (III) epigenetic regulators. Infected cell protein 0 (ICP0), an immediate-early protein of HSV-1, successfully counteracts all pathways of intrinsic immunity indicating its essential role in promoting viral fitness [35].

ND10 are spherical subnuclear structures consisted of multiple cellular proteins that are either constitutively present at ND10 or only under certain conditions, depending on the function of

ND10 and type of stress. Major components localized permanently at the ND10 are PML, SP100, ATRX and hDaxx that together with several other proteins act as a cellular restriction machinery representing the first line of intracellular defense against invading pathogen [36].

ND10 structures have been identified as target sites for many DNA and RNA viruses during the course of infection [37]. Upon nuclear entry, ND10 bodies localize adjacent to the newly entered viral DNA in attempt to repress HSV-1 gene expression [38,39]. However, the virus has evolved to circumvent this through the E3-ubiquitin ligase activity of the viral ICP0 protein. ICP0 in conjunction with ubiquitin-conjugating enzyme 5a (UbcH5a) mediates proteasome-dependent degradation of PML and SP100, while the residual parts of ND10 get infiltrated by viral proteins and become a part of viral replication compartments (VRCs) [40–43].

To monitor damage of the genomic DNA, ensure fidelity of replication and recognize invading linear viral DNA, cells have developed a sophisticated DNA repair machinery [44,45]. Ring finger protein-8 and -168 (RNF8 and RNF168) are histone E3-ubiquitin ligases essential in cellular response to double strand breaks (DSBs), one of the most deleterious types of DNA damage [46]. They play a critical role in responding to incoming linear and non-chromatinized HSV-1 genomes by recruiting repair factors to the sites of apparent or seeming DNA damage.

The HSV-1 ICP0 protein degrades RNF8, thereby preventing the recruitment of downstream DNA repair proteins to the incoming viral genomes or sites of cellular DNA damage [47]. RNF8, together with E2-conjugating enzyme Ubc13, ubiquitinates histone variants H2A and H2AX that consequentially lead to the accumulation of downstream repair proteins such as RNF168, BRCA1 and 53BP1. However, the presence of ICP0 blocks this pathway by inducing proteasome-mediated degradation of both RNF8 and RNF168, thereby leading to reduced levels of ubiquitinated H2A and H2AX [47,48].

HSV-1 DNA inside the virion is not associated with histones; instead, the negative charge of the DNA is balanced by polyamine spermine with better DNA compaction than histones, due to its higher positive charge density for the same mass. This provides an advantage over histones for compacting the large HSV-1 DNA genome into the small volume of the capsid [49,50]. However, during lytic infection, HSV-1 rapidly undergoes canonical nucleosome assembly. As the host cell

starts to silence the invading viral genomes, the initial chromatin state of the viral genome exhibits heterochromatin marks such as H3K9me3 and H3K27me3 [51]. Balance and accessibility of chromatin regulatory components is crucial for the regulation of lytic HSV-1 infection. If heterochromatin marks bind to lytic gene promoters, gene silencing takes over and latent infection ensues. In contrast, if the suppressive chromatin state transitions into a permissive state at the viral IE gene promoters, the first wave of viral IE gene expression will commence and subsequently activate the lytic viral gene expression program [52].

Throughout the course of infection, viral genomes show a gradual removal of chromatin and euchromatin modification marks on the remaining histones. Mutant viruses lacking VP16 (*U_L48*) and ICP0 show increased heterochromatin association with viral lytic promoters, indicating that tegument and IE proteins promote lytic gene expression by recruiting marks of euchromatin to promote lytic infection [53].

The VP16/HCF1/Oct1 complex recruits several histone modification enzymes including histone H3K9 demethylases, LSD1 and histone H3K4 methyltransferases, Set1, thus limiting the accumulation of repressive marks (H3K9-me) and promoting the installation of positive transcriptional activating marks (H3K4-me). Upon inhibition of LSD1, repressive chromatin on viral IE gene promoters starts accumulating and silencing of the viral genome takes place [54,55].

Among its many roles in promoting viral fitness, ICP0 shows an important transactivator function in modifying chromatin features of viral genome through interaction with cellular repressor complexes. CoREST is a corepressor of the RE1-silencing transcription factor (REST) that together form a complex to recruit chromatin-modifying enzymes, such as HDAC1/2 to induce condensed chromatin state and silence gene expression [56]. ICP0 helps to avoid this by mediating the displacement of histone deacetylase-1 HDAC1 from the (CoREST/REST)-HDAC1/2 complex, enabling expression of β and γ genes and blocking the silencing of the HSV-1 DNA [57]. Furthermore, the HSV-1 viral kinases U_S3 and U_L13 phosphorylate HDAC1 and CoREST/REST, respectively, which are then exported to the cytoplasm in an HSV-1-dependent manner [57–59].

1.1.4.3. Transcription

Transcription of the HSV-1 DNA takes place in the host nucleus and essentially relies on cellular RNA Polymerase II (Pol II) to express all viral genes [60]. HSV-1 genes are expressed in a coordinated

temporal cascade that can be divided into three kinetic classes: immediate-early (IE or α), early (E or β) and late (L or γ). However, late genes can be further divided into leaky-late (γ1) and true-late (γ2) genes, depending on the extent to which they depend on the viral DNA replication for expression. γ1 genes are expressed at low levels prior to DNA replication and are substantially upregulated at late times because of the increase in the number of newly synthesized genomes, while γ2 are expressed strictly after and are dependent upon viral DNA synthesis [61].

The immediate-early genes are the first viral genes to be transcribed upon infection, with a peak transcription between 2 and 4 hours post infection (hpi) [62]. They perform several functions important for regulating both cellular and viral gene expression [3]. HSV-1 encodes for five IE proteins ICP4 (*RS1*), ICP22 (U_S1), ICP27 (U_L54), ICP0 (*RL2*) and ICP47 (U_S12), out of which ICP4 and ICP27 are essential for productive infection [63]. Immediate-early gene expression occurs in the absence of *de novo* viral protein synthesis and is highly stimulated by the α-transcriptional transactivator VP16 [64,65]. Once released from the tegument, VP16 binds to the cellular host cell factor 1 (HCF-1) protein and subsequently gets transported into the nucleus. Once inside the nucleus, VP16-HCF-1 complex binds to the octamer binding protein 1 (Oct1) and forms stable activator complex on 'TAATGARAT' regulatory elements present in each α-gene promoter [66]. To activate the transcription of α-genes, VP16 recruits numerous cellular transcription factors, including transcription factor IIB (TFIIB), TFIIH, TATA-binding protein (TBP) and TBP-associated factors (TAFs) and promotes the formation of Pol II preinitiation complex [67]. VP16 has also been reported to recruit histone modification factors (histone acetyltransferases p300/CBP, histone methyltransferase SUVH39H1, histone demethylase JMJD2A) and promote chromatin remodeling through ATP-dependent SWI/SNF ATPase complex [68]. At 4 hours post infection, α-gene expression begins to decrease primarily due to vhs and ICP4, with the latter negatively regulating expression of its own mRNA by directly binding to the promoter region [69,70].

Activation of early gene transcription requires ICP4 and is increased by ICP0 [71]. Early genes are highly transcribed between 4 and 6 hpi and their products are mainly required for (I) viral genome replication; (II) transcription of the late viral genes together with ICP27; and (III) accumulation of some of the early and late viral mRNAs in the cytoplasm [72]. Some of the most intensively studied

β genes include, ICP8 (*U_L29*), thymidine kinase (*U_L23*) and viral DNA polymerase (*U_L30*), all involved in the viral DNA synthesis.

Late genes are expressed once the viral DNA replication has initiated. Viral α proteins ICP4, ICP22, and ICP27, and β-gene products, such as ICP8, are necessary for the expression of late genes [73]. Many of the γ genes encode viral structural proteins, and their expression enables the production of progeny virion particles [74].

1.1.4.4. Translation

HSV-1 relies on the cellular translation machinery to facilitate synthesis of viral proteins, while successfully blocking the expression of cellular proteins [75]. It does so by employing several strategies, including (I) enhancement of translation initiation; (II) prevention of translation shut down by host stress kinases; (III) degradation of cellular mRNAs competing for translation machinery [75].

Translation of mRNAs by the ribosome can be divided into three stages - initiation, elongation, and termination — each of which requires specific cellular proteins [76]. In eukaryotic cells, initiation of protein synthesis starts with the binding of the multi-subunit translation initiation complex eIF4F (eukaryotic Initiation Factor 4F), important for mediating recruitment of ribosomes to mRNA. Many viruses target eIF4F to destabilize and gain control of the host translation machinery [77]. HSV-1 stimulates eIF4F to translate viral mRNAs through action of three proteins. U_S3, viral serine/threonine kinase, activates protein synthesis complex mTORC1 to inhibit the translational repressor 4E-binding protein 1 (4E-BP1) and release eIF4E from the complex [77,78]. The viral β protein ICP6 (*U_L39*) was shown to promote the assembly of the eIF4F complex by associating with eIF4G, a large scaffolding protein [79]. Finally, through the action of ICP27, the cap binding activity of the eIF4E can be increased by p38-dependent phosphorylation [80].

Cellular stress kinases, such as protein kinase R (PKR) and endoplasmic reticulum (ER) stress kinase PERK, block translation initiation of both cellular and viral mRNA by phosphorylating eukaryotic translation initiation factor 2 (eIF2α). HSV-1 encodes two viral proteins that counteract the global shut down of protein synthesis, namely U_S11 and ICP34.5. U_S11 prevents

the activation of PKR and can also bind and inactivate PACT, a protein activator of PKR, while ICP34.5 antagonizes the PKR signaling pathway through mediating dephosphorylation of the eIF2α [81,82].

The virion host shutoff protein (vhs) is a tegument protein with endoribonuclease activity that dramatically alters the cellular translation profile. It degrades both cellular and viral mRNAs leading to shut-off of host protein synthesis. We could show that both tegument-associated and *de novo* expressed vhs cooperate to continuously degrade about 20 to 30 % of all cellular mRNAs per hour until at least 8 hpi [83]. Through vhs-mediated degradation of cellular mRNAs, viral mRNAs have improved access to the cellular translation machinery [84].

Vhs also plays a major role in productive infection by helping HSV-1 to evade the host innate immunity. It efficiently degrades the mRNAs of interferon stimulating genes (ISGs) and thereby interferes with the antiviral function of many ISGs. Higher levels of IFNβ and ISG production were observed in vhs-null mutant, when compared to the wild type (WT) virus, suggesting that vhs also has a role in dampening IFN production [85]. Furthermore, vhs can reduce dsRNA in infected cells by either dampening the accumulation of partially complementary viral mRNAs, reducing the potential for generating dsRNA, or by cleaving dsRNA after its formation [86]. In the later stages of infection, the nuclease activity of newly synthesized vhs is dampened by the viral proteins VP16 and VP22, ensuring sufficient accumulation of viral γ-gene products and efficient virus production [87].

1.1.4.5. Replication

Viral DNA replication takes place in the nucleus of the infected cell in large domains termed viral replication compartments (VRCs). VRCs are membrane-less structures that facilitate the spatial organization of viral processes and recruit viral and cellular factors required for gene expression, DNA replication, and encapsidation [88].

HSV-1 DNA replication can be divided into two stages, origin-dependent and origin-independent replication. Origin-dependent replication initiates at the one of the three origins of replication (oriS or oriL) within the HSV-1 genome and initially proceeds via a theta replication mechanism. With ongoing DNA synthesis, origin-independent replication takes over through rolling-circle

replication mechanism to produce most of the progeny DNA in an infected cell [89].

Seven viral proteins are essential for HSV-1 origin-dependent DNA replication: U_L9, ICP8 (*U_L29*), U_L5, U_L8, U_L52, U_L30, and U_L42 [90]. The origin-binding protein U_L9 binds specifically to the CGTTCGCACTT sequence in either oriS or oriL, induces a bend in the viral DNA and forms a single-stranded stem-loop structure. To unwind dsDNA, ssDNA-binding protein ICP8 forms specific complex by binding to U_L9 C-terminal domain and stimulates its DNA helicase activity [91,92]. Together, they recruit the viral helicase-primase complex composed of U_L5, U_L8, and U_L52 that binds to the ssDNA and synthesizes short oligoribonucleotide primers, the first step in the initiation of DNA replication [93]. Finally, the viral DNA polymerase U_L30, with 3'-5' exonuclease activity, continues to synthetize the DNA from the oligoribonucleotide primer in a complex with the processivity factor U_L42 [94].

HSV-1 encodes several other proteins that are dispensable for the viral replication *in vitro* but are likely to be essential for nucleotide metabolism, viral DNA synthesis and repair in neurons. Viral proteins that contribute to the viral DNA synthesis but are not essential *in vitro* include thymidine kinase (*U_L23*), ribonucleotide reductase (*U_L39* and *U_L40*), deoxyuridine triphosphatase (dUTPase, *U_L50*), alkaline nuclease (*U_L12*) and uracil-DNA glycosylase (UDG, *U_L2*) [95].

1.1.4.6. Assembly and egress

HSV-1 capsid assembly occurs in the nucleus of the infected cell where procapsids assemble around a protein scaffold and subsequently mature [17]. Internal scaffold proteins are not present in the mature virion but are necessary for the formation of the procapsid prior to encapsidation of the viral DNA [96]. Three γ proteins form the scaffold, VP21, pre-VP22a and VP24. The major structural components of the HSV-1 capsid shell are VP5, VP19c, VP23, and VP26 [17]. VP5, the major capsid protein, in association with scaffold proteins makes up the hexons and pentons. The VP19c-VP23 complex stabilizes the capsid shell structure. If either one is absent, capsid shells are not formed. VP26 is located on the outer tips of VP5 hexons [97].

Three types of viral capsids – A, B and C – can be identified in the nucleus of infected cells due to their different sedimentation behavior [98]. A and B capsids are abortive capsid forms: A capsids lack both viral DNA and scaffold proteins, while B capsids still contain internal scaffold proteins

but no viral DNA. C capsids contain viral DNA and mature into infectious virions by budding through the nuclear membrane [16].

Encapsidation and retention of the viral DNA requires at least seven viral genes: *U_L6*, *U_L15*, *U_L17*, *U_L25*, *U_L28*, *U_L32*, and *U_L33* [16,99]. The portal complex that is constituted by 12 U_L6 proteins is an integral capsid component present in both procapsids and mature capsids and serves as a portal for viral DNA entry into the capsid [100]. The terminase complex, which consists of UL28, UL15, and UL33, is responsible for the cleavage of the concatemer DNA at specific packaging sequences, termed *pac1* and *pac2*, to release unit length viral genomes into the capsid [101]. U_L17 and U_L25, the two minor capsid proteins, form a heterodimeric structure termed capsid vertex-specific component (CVSC) that stabilizes DNA-containing capsids [102]. Although a precise role of U_L32 still remains elusive, it is believed it modulates disulfide bond formation during procapsid assembly and maturation [103].

Once formed in the nucleus, mature nucleocapsid must traverse the nuclear membrane, cytoplasm, and plasma membrane to exit the cell ("envelopment-de-envelopment-re-envelopment" process of viral egress) [4]. Primary envelopment, promoted by the viral nuclear egress complex (NEC), involves budding of the mature nucleocapsid through the inner nuclear membrane. Viral UL31 and UL34 proteins that form NEC are essential in circumventing barriers essential for the viral egress [104]. Both proteins promote disruption of the nuclear lamina and dispersal of the cellular chromatin. Before leaving the nucleus, mature nucleocapsids acquire the inner tegument proteins – VP1/2, UL37, vhs, VP22 and VP16, associated with the inner tails of the glycoproteins. The next step, de-envelopment includes the fusion of the envelope of the virion in the perinuclear space with the outer nuclear membrane releasing the capsids and tegument into the cytoplasm. During secondary envelopment, tegument-coated capsids are budding into cytoplasmic membranes, including the Golgi apparatus, the trans-Golgi network (TGN) or endosomes, thereby constituting infectious virions within the respective vesicles. Lastly, transport of these vesicles that contain HSV-1 infectious virions to the cell surface goes through exocytosis pathways [3].

1.1.5. Immediate-early protein ICP22

The ICP22 polypeptide is encoded by *U_S1* gene which initiates within the IRs sequence of the HSV-1 genome and is comprised of 420 amino acids (aa) (Figure 1). This 68-kDa nuclear-localized phosphoprotein extensively interacts with host cell components, thereby regulating several processes in the infected cell as illustrated in Figure 4 [3,105,106].

ICP22 is not essential for DNA replication in 'permissive' cell types, such as Vero (African green monkey kidney) and HEp-2 cells (Human Epithelial type 2). However, *in vivo* and in primary human fibroblasts and rodent cell lines, referred to as 'restrictive' cells, ICP22 is required for efficient HSV-1 growth [107,108]. In restrictive cells, infected with ICP22 mutant virus, late gene expression is markedly reduced, specifically for *U_S11*, *U_L38* and *U_L41* [109,110]. Although the reason for the cell-type dependent phenotype of ICP22 mutants is unknown, it is speculated that putative cell-specific factor or factors could determine the replication phenotype of ICP22.

The *U_S1* gene shows substantial sequence heterogeneity in the N-terminal domain of the ICP22 protein in between different HSV-1 strains [111]. Within the ICP22 protein, ten conserved motifs have been identified, out of which a core 63 aa sequence is conserved in all α-herpesvirus U_S1 homologs. The conservation of the motifs within the core region could function as a scaffold with structurally variable regions at N- and C-terminal domains. Considering that the ICP22 protein is extensively post-translationally modified, it is thus likely that N- and C-terminal domains can adopt alternative conformations. These different conformations support a complex role of ICP22 in the interaction with both host and viral proteins.

Difficulties in understanding biological functions of ICP22 protein have been due to co-expression of an in-frame, C-terminal variant of ICP22, known as $U_S1.5$. The initial study proposed that the translation start site of the $U_S1.5$ corresponds to residue 147 of ICP22. However, this was subsequently corrected and shown to initiates at methionine 171 [112,113]. More recent work indicates that the $U_S1.5$ translation starts with M90, the second AUG start codon of the ICP22 protein [114]. Although, to date, no unique function of the $U_S1.5$ protein has been reported, it may have a role in some of the functions attributed to the ICP22 protein such as (I) replication in restrictive cells (II) enhancement of the expression of late viral proteins *in vitro* (III) inhibition of ICP0-mediated gene expression in transient-transfection assays [115].

ICP22 contains two independent regions with nuclear localization signals (NLS) [116]. During the productive infection, the onset of DNA replication coincides with the migration of ICP22 from small, dense nuclear bodies to the replication compartments that contain transcription complexes. This transition requires the phosphorylation of ICP22 by the viral protein kinase U_L13 [117,118,119].

ICP22 facilitates the formation of virus-induced chaperon-enriched (VICE) domains in the nucleus of the infected cell [120]. The VICE domains are usually formed adjacent to the VRCs, where they serve as nuclear protein quality control centers during infection [121]. They contain several host chaperones (Hsp70, Hsp40, Hsp90), ubiquitinated proteins and proteasomal components that regulate protein folding, complex formation and proteolysis [105]. Recruitment of heat shock cognate protein 70 (Hsc70) to the VICE domains is dependent on ICP22. Moreover, ICP22 functions as a virally encoded cochaperone (J-protein/Hsp40) and together with Hsc70 recognizes and manages aggregated and misfolded proteins [120,122].

Recent study showed that ICP22 directly interacts and recruits cellular transcription elongation complex FACT to the viral DNA for efficient transcription elongation of viral genes. Besides FACT, interaction with two other transcription elongation factors SPT5 and SPT6 with viral genomes is considered to be ICP22-dependent [123].

To date, many viruses have evolved mechanisms to utilize the phosphorylation events as a mean to regulate function of viral proteins and to establish a cellular environment for efficient viral replication. Herpesviruses are especially of interest because, unlike most other viruses, they encode virus-specific protein kinase(s) [124]. ICP22 is extensively phosphorylated by the viral U_L13 protein kinase, and, to a lesser extent, by the U_S3 protein kinase [125,126]. ICP22 is also phosphorylated by yet unidentified cellular kinases and nucleotidylylated by casein kinase II [127].

U_L13 is an HSV-1 serine/threonine protein kinase that directly phosphorylates ICP22 [128]. Through phosphorylation of the carboxyl-terminal domain of (CTD) of ICP22, U_L13 enhances the synthesis of a set of γ2 proteins exemplified by the products of the *U_L38*, *U_L41*, and *U_S11* genes [110,126]. The ICP22-U_L13 complex mediates the activation of the cell division control protein 2 (cdc2) and degradation of its partners, cyclins A and B. Active cdc2 then binds to its new partner, the viral DNA synthesis processivity factor U_L42, forming a complex that recruits and phosphorylates

topoisomerase IIα for efficient expression of the γ2 genes, as stated above [129,130]. U_L13 and ICP22 are both involved in Pol II phosphorylation. This interaction alters the phosphorylation of the Pol II CTD, resulting in the depletion of the hyperphosphorylated (Pol IIo) and hypophosphorylated (Pol IIa) states and induction of a novel, "intermediate" form designated Pol IIi [131]. U_S3, a second HSV-1 serine/threonine protein kinase, is required for the phosphorylation of the Pol II CTD *in vitro* and interaction of ICP22 with CDK9 is highly dependent on its activity [132].

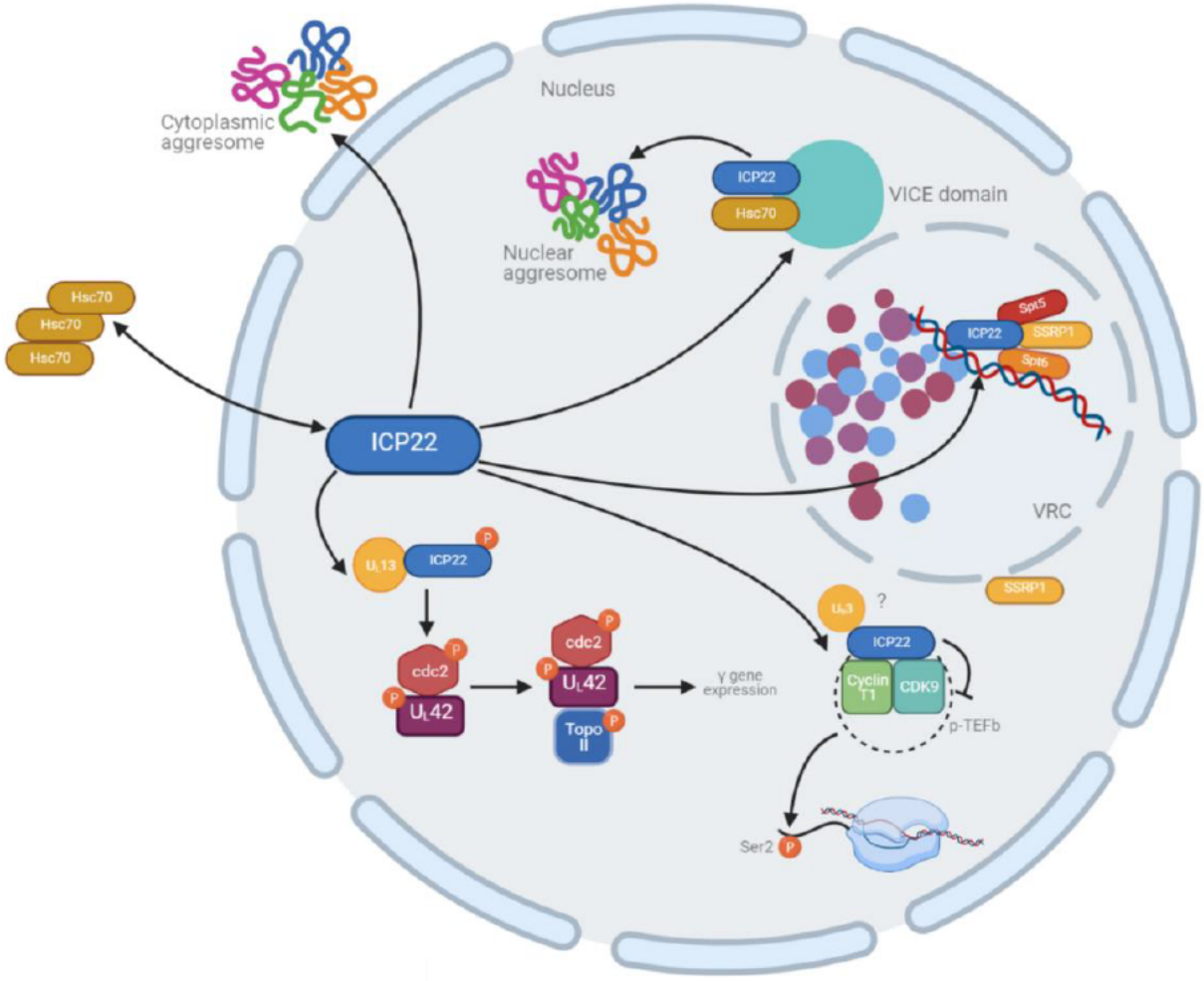

Figure 4. Known functions of the HSV-1 protein ICP22.

Schematic representation of known ICP22 functions in the host cell nucleus.

Generated with BioRender.com (2020). Retrieved from https://app.biorender.com/biorender-illustrations.

1.1.6. Immediate-early protein ICP27

Similar to ICP22, ICP27 is an essential, multifunctional HSV-1 immediate-early protein that affects both viral and cellular gene expression. It is post-translationally modified by phosphorylation and arginine methylation. This governs its functional interaction during lytic infection by causing local structural alterations, leading to either increased or decreased affinity for a binding partner [133].

Arginine residues within an RGG box are the major site of ICP27 methylation and have been shown to be involved in regulating protein-protein interactions and ICP27 export to the cytoplasm. Mutant viruses with lysine to arginine exchanges show impaired growth and delay in viral replication when compared to the WT HSV-1 [134]. ICP27 phosphorylation site mutants show impaired viral replication and viral gene expression. ICP27 colocalization with the Pol II CTD and the formation of Hsc70 nuclear foci is lost upon infection with the mutant viruses, which is normally occurring during WT infection [135]. ICP27 is necessary for the expression of early and late HSV-1 proteins in a promoter-independent manner, primarily through enhancing the expression and export of intron-less viral mRNAs by recruiting cellular mRNA export proteins and TAP/NXF1 [136,137,138].

Even though some studies provided convincing evidence that ICP27 inhibits splicing in a gene-specific manner by interacting with splicing factors such as Spliceosome Associated Protein 145 (SAP145) and the SRPK1 kinase, thus contributing to the host shut-off, most recent genome-wide transcriptomic analysis revealed that neither HSV-1 infection nor ICP27 ectopically overexpressed lead to global inhibition of splicing [139,140]. Still, ICP27 can modulate alternative splicing of a subset of cellular genes by interfering with cellular splicing factors [141].

At early times post infection, ICP27 is predominantly nuclear, however, by about 4 hpi, ICP27 shuttles between the nucleus and cytoplasm where it stimulates nuclear export and translation of bound viral mRNAs by interacting with the RNA export machinery and translation initiation factors [142,143,144].

Most recently, our lab revealed a new role for ICP27 in mediating HSV-1-induced host shut-off. When ectopically expressed, ICP27 is sufficient to induce disruption of transcription termination (DoTT) downstream of the normal transcript end site (TES) by inhibiting mRNA 3' end processing machinery (explained in more detail in section 1.5.).

Among many roles of ICP27 known to be attributed to either N- or C- terminal domain, or both, there are several other functions, so far not correlated to any structural part of the protein such as (I) inhibition of IFN type 1 signaling by downregulating phosphorylation and nuclear accumulation of STAT-1 (II) blocking the cell cycle in the G1- phase and (III) activation of stress activated protein kinases (SAPKs) c-Jun N-terminal kinase (JNK) and p38 [133].

1.2. Chromatin structure and regulation of transcription

Chromatin is a dynamic structure that helps to package the entire eukaryotic genome into the confines of the nucleus. It regulates the accessibility of DNA to transcriptional machinery, thus being closely linked to gene activity [145,146]. The basic unit of chromatin – the nucleosome , – consists of a protein core, composed of 147 bp of DNA wrapped 1.65 turns around the octamer complex of the core histone proteins [147]. The nucleosome octamer comprises two copies of each of the canonical histones – H3, H4, H2A, H2B – which, during the nucleosome assembly, interact in an ordered manner. Linker histone H1 serves to lock DNA wrapped around the histone core at the dyad axis and to contribute to the higher-order structure of chromatin [148,149].

Inside the histone core, two H3-H4 heterodimers form a four-helix-bundle structure to give rise to a symmetric tetramer. Two H2A-H2B dimers then associate with $(H3–H4)_2$ tetramer through multiple interactions to form an octamer which, along with the DNA, forms nucleosome. This structure ensures a hierarchical arrangement of histones in the nucleosome, where $(H3–H4)_2$ tetramer forms a stable core and the two H2A-H2B dimers get exchanged more easily without affecting the $(H3–H4)_2$ tetramer [145,150,151,152].

Reversible histone post-translational modifications (PTMs), reported to occur on the N-terminal and C-terminal tails of core histones, serve as ´docking stations´ for nuclear proteins (NPs) and can directly affect chromatin structure by altering histone-DNA interactions. Like core histones, linker H1 histone variants are also subjected to various PTMs, found in both the globular domain and tails of H1. Although H1 PTMs are much less understood than those of core histones, they are thought to have an important role in regulating chromatin architecture and function [153].

Histones contain various amino acids (aa) that can be post-translationally modified via

acetylation, methylation, phosphorylation, glycosylation, sumoylation, ubiquitylation and through other processes (Figure 5) [145,146]. As PTMs can affect gene expression without changing the DNA sequence, they have been often termed as 'epigenetic´ changes. By altering the chemical interactions within nucleosomes or with neighboring nucleosomes, PTMs can affect nucleosome stability resulting in either open or closed chromatin. Most PTMs added to histones are reversible, as the cell contains different enzymes that can either add or remove these covalent modifications, known as ´writers´ and ´erasers´, respectively [154]. Readers, on the other hand, consist of a diverse range of protein factors that can either recognize specific PTMs on histones or a combination of PTMs and histone variants to mediate a particular downstream transcriptional event [155,156].

Histone methylation is one of the most studied modifications which involves transfer of a methyl group (— CH_3) from the high-energy enzymatic donor S-adenosyl methionine (SAM) to ε-amino groups (— NH_3^+) of arginine (Arg or R) and lysine (Lys or K) [157]. Canonical histones H3 and H4 are the main sites of histone methylation, although the other core and linker histones display methylation as well. Histone methylation is a complex process that can have varying effects on gene activity, leading to either gene activation or gene silencing. Gene expression status depends on the specific residues that are modified, the degree and pattern of methylation, and the genomic context in which the methylation occurs. Histone lysine tails may be mono-, di-, or trimethylated by readily accessible Histone Methyltransferases (HMTs) or demethylated by Histone Demethylases (HDMs), whereas arginines can be mono-, symmetrically or asymmetrically di-methylated [158,159] .

Transcriptionally active euchromatin is mainly associated with methylation of H3 lysines 4, 36, and 79, whereas methylation of H3 lysines 9 and 27 is linked to the transcriptionally repressed chromatin regions [146,160]. H3K4me3 is found to be enriched around the transcriptional start site (TSS) of active promoters, where TFIID and Pol II are present [161,162,163], as well as in the coding sequences in human cells [164]. The loss of H3K4me3 in human cells results in decrease of transcriptional activity and reduction of TFIID at some promoters without the canonical TATA sequence, leading to the assumption that H3K4me3 may determine the core promoter by either anchoring TFIID to the activated promoter or by recruiting TFIID during promoter activation

[160,161]. In contrast, H3K36me3 is associated with transcription processes elongation and splicing. It is highly enriched throughout the gene body and is shown to be more abundant in the exonic, rather than in the intronic regions [165]. Furthermore, H3K36me3 has been shown to have a role in both preventing aberrant transcriptional initiation from cryptic gene promoters and in DDR by directly recruiting DNA repair machinery, leading to a quick chromatin response upon damage [166,167].

Typical marks of constitutive heterochromatin are H3K9me2/me3, while H4K27me2/me3 are usually enriched on facultative heterochromatin. Both marks recruit specific protein machineries and may underlie distinct biological features, although the consequence is chromatin compaction in both cases [168].

For the canonical histones H3, H2A and H2B, and for the linker histone H1, there are respective histone variants that have important regulatory and biological functions [169]. In humans, 11 histone H1 variants have been described, including seven differentially expressed subtypes in somatic cells (H1.0-H1.5 and H1x), three testis-specific subtypes (HILS1, H1t and H1T2) and one oocyte-specific subtype (H1oo) [170]. Histone variants differ from the canonical histones either by the alteration of primary amino acid sequence or by the addition of larger domains. Substitution of core histones with non-canonical histone variants contributes to the complexity of nucleosome structure and function by affecting PTMs, protein interactions and higher-order chromatin structure [147,171].

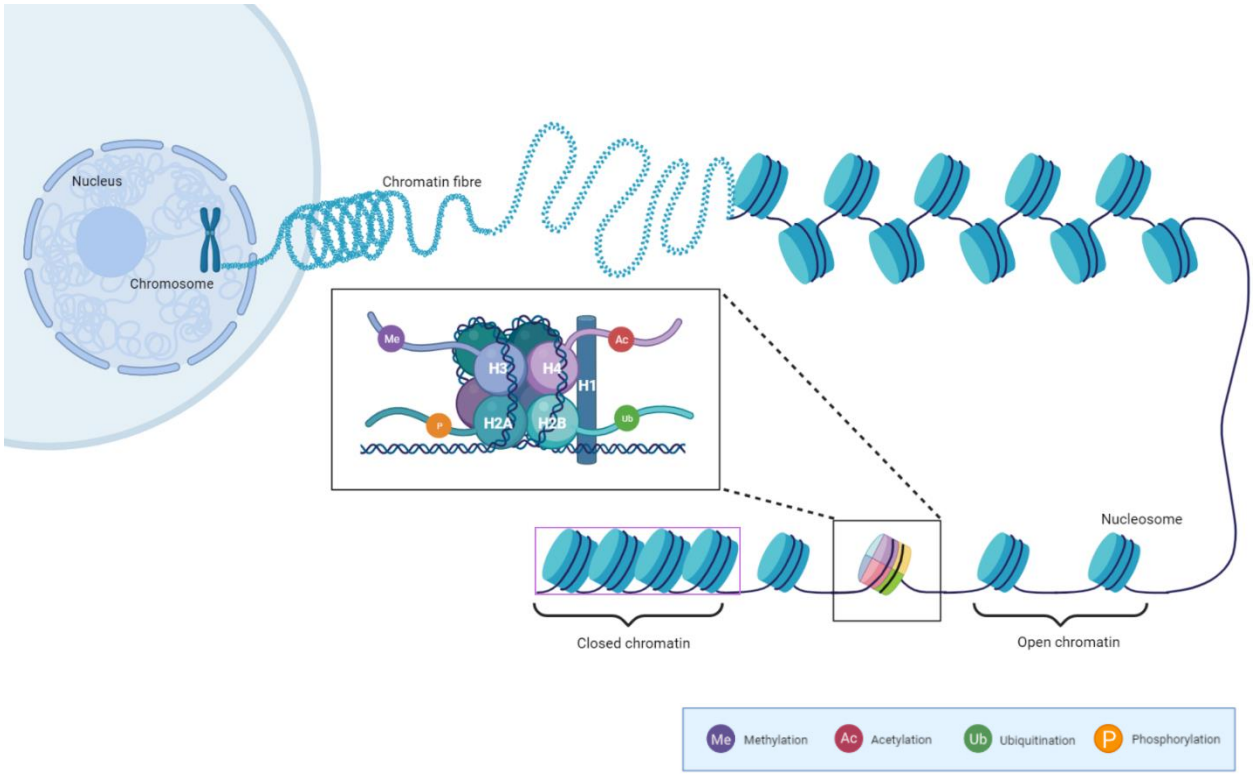

Figure 5. Chromatin structure and PTMs involved in the epigenetic regulation of gene expression.
DNA is wrapped around core histone proteins (H3, H4, H2A and H2B) thus forming the nucleosome. Nucleosomes are compacted into chromatin fibers by linker histone H1 and additional factors which med ate histone PTMs (w iters, erasers, and readers). For simplicity, only four different PTMs are depicted in the image, each on different histone tail. Depending on the epigenetic regulation, chromatin can be either in the 'open' state, thus permissive for transcription or 'closed' state, leading to silenced gene expression.
Designed with BioRender.com (2020). Retrieved from https://app.biorender.com/biorender-illustrations.

1.3. Chromatin landscape and nucleosome turnover of productive transcription elongation

Pol II carries out transcription of all protein-coding genes and a variety of non-coding RNAs [172]. The carboxy-terminal domain (CTD) of Pol II's largest subunit, Rpb1, is evolutionarily conserved and consists of heptapeptide repeats with the consensus sequence ($Y_1S_2P_3T_4S_5P_6S_7$) that is phosphorylated in the transcription cycle. This domain is an essential platform for the

recruitment of factors important in the regulation of transcriptional and co-transcriptional events, as well as gene expression in general [173]. One of the most studied phosphorylation events are the ones of serine 2 and serine 5 (Ser2P and Ser5P) that represent the transition between initiation and processive elongation, respectively. Several additional modifications have more recently been added to the CTD repertoire, with Ser7P, Thr4P, Tyr1P proposed to be associated with small nuclear RNA (snRNA) processing or histone mRNA synthesis and transcription termination [174].

Transcription elongation by Pol II is a highly regulated step of the gene expression process, where elongation accessory and/or chromatin remodeling proteins play key roles [175,176]. Upon Pol II release from the promoter-proximal pausing (PPP) region, the phase of productive elongation commences. In the elongation step, RNA chain extends until it reaches a termination signal which arrests the process and causes the release of both DNA and RNA [177]. The rate of the elongation can differ within and between neighboring genes where it has a role in co-transcriptional processes such as splicing, transcription termination and genome stability. Some factors, such as histone modification marks and certain gene features (e.g. number of exons) can efficiently modify it [178]. For productive elongation, modulation of chromatin structure through both nucleosome exchange rate and co-transcriptional modifications of DNA and histones is critical [175]. Nucleosome exchange, which is also known as nucleosome turnover, is achieved through the concerted actions of ATP-dependent nucleosome remodelers, histone modifying enzymes, and ATP-independent histone chaperones [175,179,180,181]. Nucleosome turnover is necessary to keep the chromatin fluid, which involves partial or complete removal of nucleosomes, followed by the replacement with either newly synthetized canonical histones or histone variants [145,181]. This dynamic mechanism of nucleosomes disassembly and reassembly allows Pol II to move downstream while preventing the production of cryptic intragenic transcripts [175]. This study focuses on ATP-independent histone chaperones; thus, the other components of the nucleosome turnover will not be specifically discussed.

1.3.1. ATP-independent histone chaperones

Histone chaperons are a group of acidic proteins with roles in: (I) histone trafficking between the nucleus and cytoplasm (II) correct assembly of DNA and histones into nucleosomes, and (III) disassembly of intact nucleosomes into its subcomponents during processes such as DNA replication, repair, or transcription [182,183].

These negatively charged proteins are classified as either H2A-H2B or H3-H4 chaperones, depending on their preferential interaction with different canonical histones [184]. Several histone chaperones with established roles in nucleosome assembly/disassembly during transcription have been identified. Among them, the best characterized are the well-conserved Facilitates Chromatin Transaction (FACT) and SPT6 [185].

Human FACT (hFACT) is a heterodimer composed of two subunits, Spt16 (Suppressor of Ty 16) and SSRP1 (Structure Specific Recognition Protein 1), that promotes transcription elongation by reorganizing nucleosomes through destabilization of dimer-tetramer contact points encountered by transcribing Pol II [186,187]. However, this is just one function of this highly conserved histone chaperon. Recent studies defined a broader role of FACT being involved in almost all chromatin-related processes, such as DNA replication, DDR, transcription initiation, transcription elongation and histone variant exchange [185,188,189,190].

FACT binding is dynamic, altering its contacts as the nucleosome structure undergoes changes and binding sites become available or stay inaccessible [191]. Different models of FACT's action have been proposed. The first model suggests that FACT induces dissociation of histone H2A-H2B dimer from intra-nucleosomal location thereby facilitating transcription through chromatin, while making H2A-H2B dimer either tethered to the nucleosome via FACT or displaced into the solution [187,192,193]. Subsequently, FACT-bound dimers are reinserted onto chromatin in the wake of Pol II. The second model states that FACT can function while retaining all components of the octamer, meaning, FACT can induce accessibility of nucleosome-bound DNA without histone H2A-H2B displacement, and therefore facilitate action of processive enzymes on DNA [194,195].

FACT depletion can lead to a variety of chromatin abnormalities, including; (I) destabilization of chromatin architecture and mis-localization of the yeast histone H2A.Z in transcribed regions [185,

[196]; (II) loss of nucleosomal occupancy with increased rates of bi-directional nascent transcription [197]; (III) increase of susceptibility to replication-induced DNA damage in human mammary epithelial cells [198]; (IV) reduced levels of H3K36me3 in yeast [199] and (V) aberrant transcription-coupled to H3K4me3 at immunoglobulin switch regions [200].

SPT6 is a highly conserved nuclear protein that interacts directly with both histones (with a preference for histone H3) and Rpb1, to regulate gene expression [201,202,203]. Although SPT6 is a multifunctional protein, substantial evidence suggests that its primary function is as a histone chaperone, necessary to reassemble nucleosomes in the wake of transcribing Pol II [204]. As an elongation factor, SPT6 has been shown to co-localize with elongating Pol II and to stimulate transcription elongation rate both *in vitro*, individually and in concert with DRB sensitivity-inducing factor (DSIF) [205] and *in vivo* [206].

Interestingly, the requirement for SPT6 to reassemble nucleosomes during elongation applies predominantly to genes that are transcribed at high rates [204,207]. This is consistent with studies proposing that the rate of transcription determines the fate of nucleosomes during transcription elongation. High levels of transcription suggest completely dismantled nucleosomes upstream of Pol II and reconstituted in its wake, whereas low levels of transcription suggest that hexamers devoid of an H2A-H2B dimer stay associated with the DNA while still allowing for Pol II passage through a mechanism involving the formation of small DNA loops [208,209,210]. During transcription, SPT6 is necessary for the maintenance of a chromatin architecture by hindering improper usage of cryptic promoter elements, proposing the role of SPT6 in the nucleosome reassembly to be crucial for the prevention of spurious intragenic transcription initiation [185,188,201,211]. In yeast, Tyr_1 phosphorylation of Pol II CTD has been shown to stimulate binding of SPT6 thus impairing pre-mature recruitment of termination factors [212]. Mutations in SPT6 cause genome-wide alterations of chromatin structure and impair several histone modifications, including H3K36me2/me3 catalyzed by the H3K36 methyltransferase Set2 [207,213].

1.4. Regulation of transcription termination

Termination of Pol II-mediated transcription is the final step of gene expression needed to partition the genome and preserve the accuracy of neighboring gene expression [214]. Efficient transcription termination is a prerequisite in generating and releasing functional mRNA transcripts and Pol II recycling [215].

In higher eukaryotes, once Pol II transcribes through the polyadenylation site at the 3' end of genes, elongation-to-termination transition occurs. This process consists of a few steps: (1) dissociation of DSIF (DRB Sensitivity Inducing Factor) complex comprised of elongation factors Spt4/5 [216], (2) recruitment of the multi-protein complex CPSF (Cleavage and Polyadenylation Specificity Factor) and the cleavage stimulation factor (CstF) to PAS, both necessary for pre-mRNA cleavage and polyadenylation [217,218], and (3) binding of the termination factors to disengage Pol II from its DNA template [219].

The exact mechanism of PAS-dependent termination is still not fully understood with the debate centered on two predominant, but not mutually exclusive models: the allosteric and the torpedo model. However, recent data provide strong evidence for a third model of termination that unifies both original models [220].

The allosteric model proposes that transcription of a PAS results in conformational change in the Pol II that weakens the elongation complex (EC) and favors termination, by the release of either elongation or anti-termination factors. Anti-termination factors (SCAF4 and SCAF8) have a role in suppressing termination until the desired PAS has been transcribed, and if depleted, premature cleavage and polyadenylation ensue at the PAS sequence within the gene body (Figure 6a) [221].

The torpedo model of termination includes endonucleolytic cleavage of the nascent mRNA transcript followed by 5'→3' exonuclease degradation of the Pol II-associated RNA transcript of PAS cleavage and dissociation of Pol II from the DNA template [218]. Exoribonuclease RNA-trafficking protein (XRN2/Rat1 (yeast)) is a 5'→3' exonuclease acts as the "torpedo" that facilitates transcription termination in higher eukaryotes. However, if the XRN2 active site is mutated or its passage blocked along the RNA, termination downstream of most poly(A) sites is delayed [222,220]. Consistently, when the speed of Pol II is changed by mutations, faster Pol II

extends the zone of termination further downstream while slower Pol II shifts the termination upstream [223] (Figure 6b). Even though both models depend on the recognition of the PAS, a major difference is that only the torpedo model depends on successful endonucleolytic cleavage of the nascent RNA transcript to create the entry site for the XRN2.

A unified allosteric/torpedo model is a single mechanism incorporating features of both models. The allosteric switch decelerates Pol II beyond the PAS as a result of dephosphorylation of the elongation factor SPT5 by protein phosphatase 1 (PP1) enzyme, Dis2. Once slowed, Pol II gets stranded on the template and is easily terminated by XRN2, which degrades the Pol II-associated product of PAS cleavage (Figure 6c) [220,224,225].

ALLOSTERIC MODEL

a

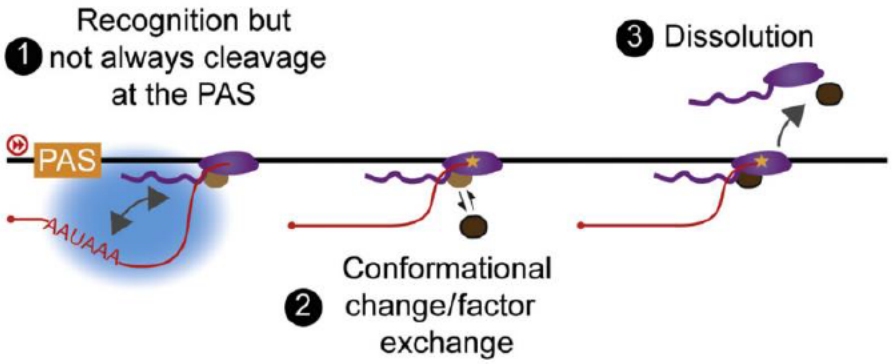

TORPEDO MODEL

b

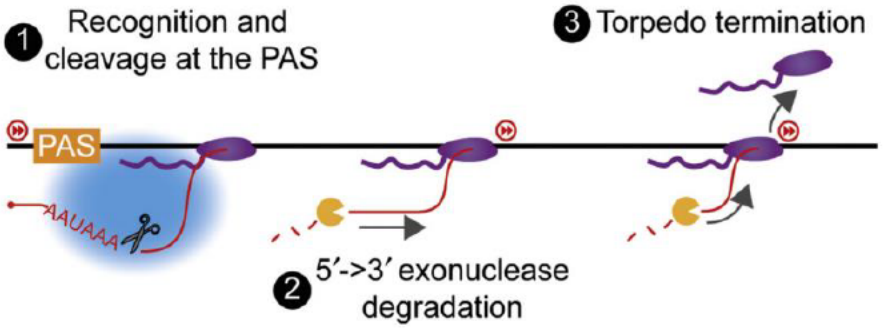

UNIFIED ALLOSTERIC/TORPEDO MODEL

c

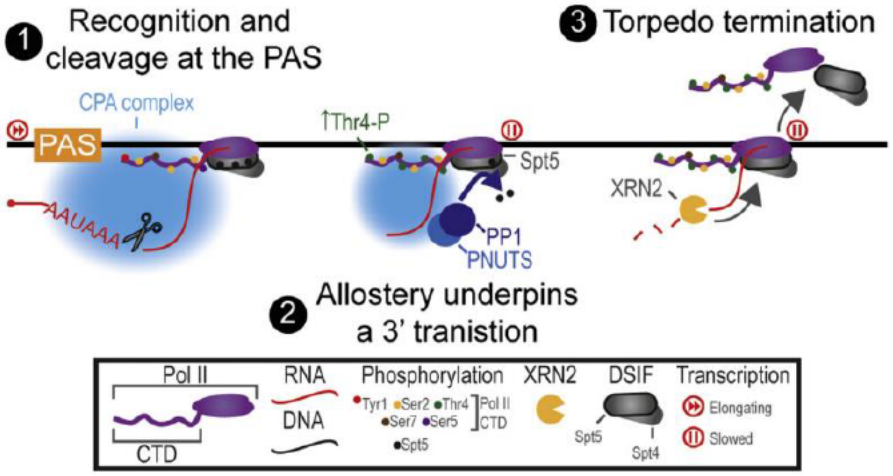

Figure 6. Proposed models of transcription termination.

(a) In the allosteric/anti-terminator model, transcription termination is caused by a conformational change caused by the destabilization of the Pol II EC after transcribing the PAS. Release of anti-termination factors or recruitment of termination factors triggers dissociation from the DNA template. **(b)** In the torpedo model, endonucleolytic cleavage at the PAS creates an entry site for the 5´→3´ exonuclease XRN2, which degrades the nascent transcript downstream of the cleavage site. **(c)** In unified allosteric/torpedo model, PAS cleavage promotes Pol II slowing (caused by dephosphorylation of SPT5 (PNUTS/PP1)) and constitutes an allosteric switch. Increased Thr4P on Pol II CTD has been associated with PAS-cleavage. The allosteric switch strands Pol II on the template and terminates it by XRN2, which degrades the Pol II-associated product of PAS cleavage.

Abbreviations: CTD (C-terminal domain); DSIF (DRB sensitivity-inducing factor); PAS (polyadenylation signal); PNUTS (PP1 nuclear targeting factor); PP1 (protein phosphatase 1); Pol II (RNA polymerase II); XRN2 (nuclear enzyme that degrades RNA in a 5'→3' direction).

Taken and adapted from Wang X et al. Eaton JD, West S. "Termination of Transcription by RNA Polymerase II: BOOM!" Trends Genet. 2020 Sep;36(9):664 675 [172]

1.5. Read-through transcription as a contributor to pervasive transcription

Transcription termination ensures the integrity of the transcriptome by determining the cellular fate of the generated transcripts. If uncontrolled, it can negatively affect transcription itself or the maintenance of genome stability by generating high levels of nonfunctional RNA transcripts toxic for the cell [226]. However, pervasive transcription is regulated remarkably well by the cell, making sure to establish the first line of defense already at the nucleosome level to prevent inappropriate Pol II initiation, followed by tight control of the transcription process and the employment of RNA decay activities to dampen the accumulation of unwanted RNA transcripts [227].

Recent studies in eukaryotes have reported that constitutive and regulated read-through transcription downstream of PASs provides a significant contribution to the pervasive transcription. This read-through transcription disrupts normal transcription termination, leading

to a production of harmful intergenic transcripts that perturb the expression of downstream genes [140,226,228–235].

By comparing the genome-wide read-through patterns after different cellular stress conditions (heat shock, oxidative stress and osmotic stress) numerous DoGs (downstream-of-gene (DoG)-containing transcript) were found common to all three stress conditions, although a certain number showed clear stress-specific differences between them [230].

Recently, it has been reported by the same group that hyperosmotic stress leads to dissociation of Integrator complex subunits (Int11 and Int3) from Pol II leading to a genome-wide loss of Integrator on DNA. Moreover, depletion of one of the catalytic subunits of the Integrator complex, Int11, was sufficient to induce read-through transcription downstream of hundreds of genes. A partial overlap of read-through genes was noted upon depletion of functional Int11 to DoGs after hyperosmotic stress [236].

Another example of widespread transcriptional read-through was observed in human cancer [229]. Transcriptome analysis revealed that patients with a higher number of read-through genes correlate significantly with poorer outcome. Moreover, they identified that mutations of SETD2 (SET Domain Containing 2) histone methyltransferase are a contributing factor for increased read-through transcription. However, when ectopically expressed, it seemed sufficient to rescue the transcription termination defects.

Furthermore, proteomic characterization reported a novel function of mammalian Pol II CTD in transcription termination at 3' ends of genes. Namely, Tyr1 residues of the CTD repeats were found to be required for termination, thereby strongly limiting the extent of read-through transcription. Further characterization revealed that the YFFF mutant, in which Tyr1 residues are replaced by Phe in the last ¾ of the CTD repeats, resulted in the loss of Pol II interaction with Mediator (Med) and Integrator (Int) complexes, suggesting that they might be involved in the pause/termination processes [174].

Another study showed that the loss of PAS endonuclease CPSF73 caused more read-through transcription, as a failure of Pol II to pause downstream of PAS, than upon loss of XRN2 [222,237]. This suggests that XRN2 can contribute in tuning termination, but not in the removal of Pol II from the DNA template.

Viruses have also been shown to antagonize normal transcription termination during infection. Upon influenza virus infection (IAV) the induction of read-through transcripts is orchestrated in part by viral non-structural protein 1 (NS1) whose ectopic expression has similar outcome. NS1 interferes with transcription termination by inhibiting CPSF subunit CPSF30, a key element in pre-mRNA 3'-end processing [233,238,239].

By employing both 4-thiouridine labeling (4sU) of RNA followed by purification of newly transcribed RNA and sequencing (4sU-seq) and ribosome profiling (Ribo-seq), we previously revealed that HSV-1 infection leads to disruption of transcription termination (DoTT) of cellular genes, thus significantly contributing to the host cell shut-off [140,234]. DoTT results in transcription for tens of thousands of nucleotides beyond the point of poly(A) sites and into the downstream regions. A detailed comparison of HSV-1-induced DoTT to DoG transcription during cellular stress (heat and salt stress) showed a strong correlation of read-through extent in both salt and heat stress to 4-5 h post HSV-1 infection. However, at the later time post HSV-1 infection (7-8 hpi) when DoTT was substantially more prominent (~3-fold), correlation was considerably lower [234].

Recently, our lab discovered that ICP27 protein is sufficient to induce DoTT when ectopically expressed in human cells (Figure 7) [235]. Mechanistically, ICP27 plays a direct bimodal role in HSV-1-mediated host shut-off. On the one hand, when bound to CPSF complex, ICP27 induces the assembly of an aberrant mRNA 3’ processing complex unable to cleave mRNA 3’ ends. On the other hand, ICP27 promotes 3’ end processing of viral/host transcripts through binding to GC-rich sequences upstream of PAS and promoting recruitment of CPSF and other mRNA 3’ processing factors [235].

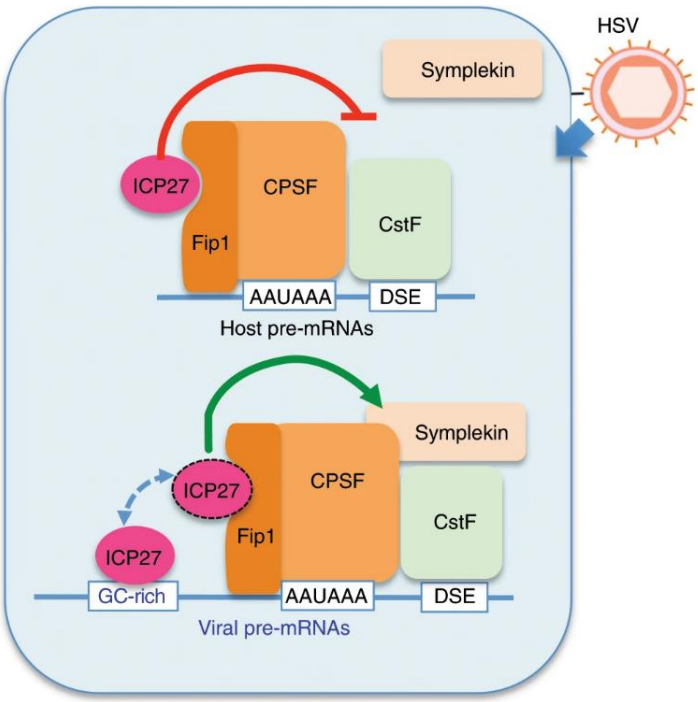

Figure 7. ICP27-mediated regulation of mRNA 3' end processing in HSV-1 infected cells.

During lytic infection, HSV-1 ICP27 interacts with the CPSF complex and induces the assembly of a dead-end 3' processing complex. Moreover, it partially displaces symplekin when bound to CPSF. Cellular or viral PASs that have GC-rich upstream sequences (UPS), bind ICP27 which promotes recruitment of CPSF and activates mRNA 3' processing. Shuttling of ICP27 between GC-rich sequences and CPSF complex is depicted with dotted line.

Taken from Wang X et al. "Herpes simplex virus blocks host transcription termination via the bimodal activities of ICP27." Nature communication, 15 Jan. 2020 [235]

1.5.1. Read-through transcription and downstream open chromatin (dOCR) induction

How transcription read-though affects host cell chromatin interactions is not completely understood. However, a recent study revealed that during IAV infection read-through transcription rapidly remodels genome 3D organization downstream of genes [233]. Read-through transcription results in chromatin decompaction and frequent switching of inactive "B" (containing gene-poor, transcriptionally inactive chromatin carrying repressive epigenetic marks) to active "A" compartment (containing gene-dense, transcriptionally active chromatin rich in ''active'' epigenetic modifications) downstream of highly transcribed genes. Upon IAV-dependent read-through, Pol II elongates hundreds of kilobases past gene termination sites, thus eliminating chromatin loops and locally de-compacting chromatin. This then causes the displacement of cohesion from the CTCF binding sites, essential for the formation and maintenance of local chromatin interaction domains [233].

Read-through transcription had a similar impact on a genome structure downstream of genes in HSV-1 infection. We previously reported that lytic HSV-1 infection leads to a DoTT-associated increase in chromatin accessibility downstream of the affected poly(A) sites already detectable at 4 hpi. Downstream open chromatin (dOCR) matched the poly(A) read-through transcription in its extent and kinetics and was shown to be caused by the DoTT as well as high levels of transcription in the downstream of the genes. Interestingly, no general increase in dOCR length was observed in cellular stress responses indicating the specific involvement of one or more viral factors in dOCR formation (Figure 8) [234].

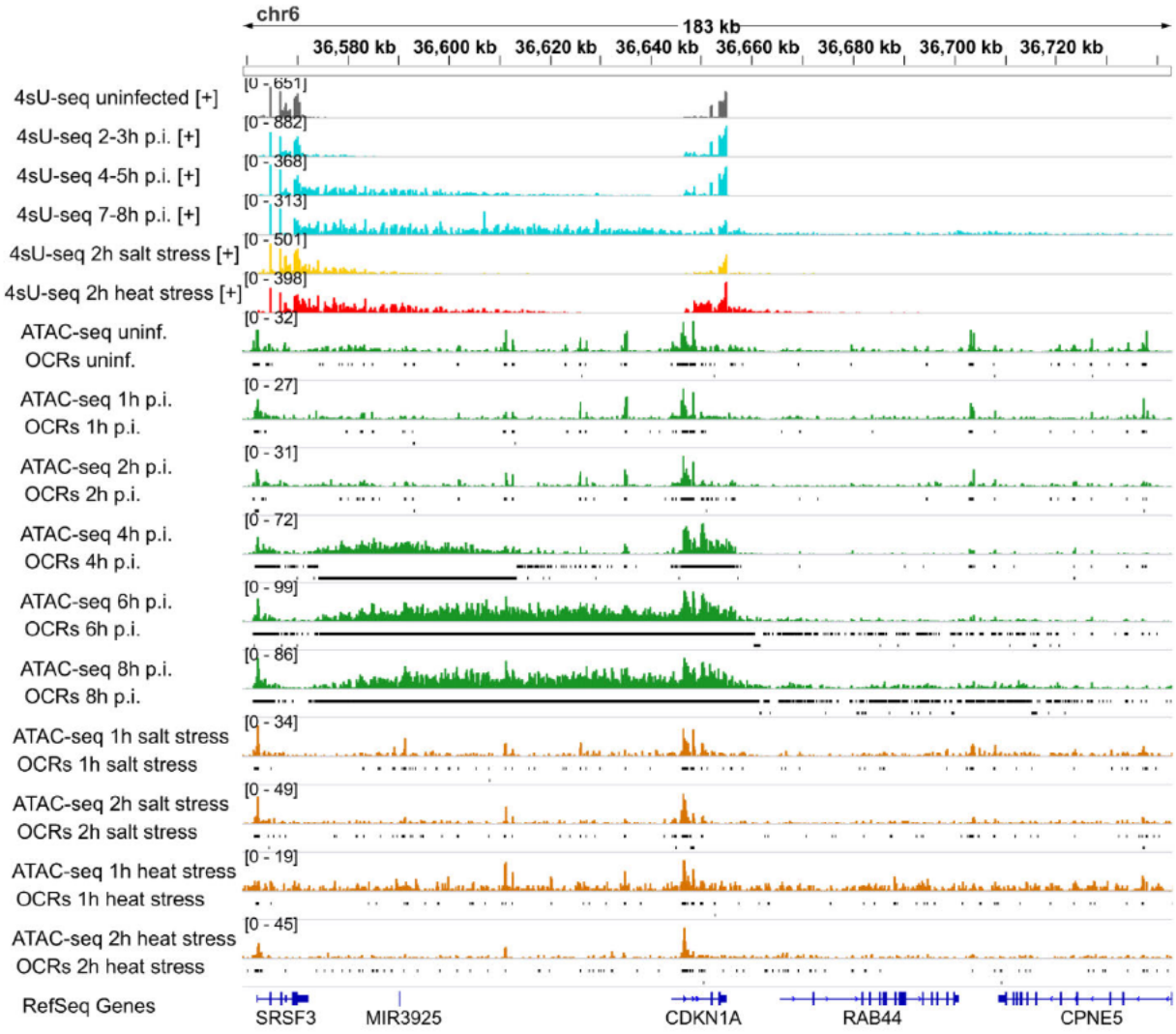

Figure 8. HSV-1 causes extensive increase in downstream open chromatin.

The upper part of the figure shows 4sU-seq read coverage for the SRSF3 gene (grey = uninfected, cyan = time-points of HSV-1 infection, yellow = 2h salt stress, red = 2h heat stress) while bottom part shows ATAC-seq data (green = HSV 1 infection, brown = heat and salt stress) and identified downstream open chromatin regions (dOCRs, black lines).

Taken from Hennig T, Michalski M, Rutkowski et al." HSV-1-induced disruption of transcription termination resembles a cellular stress response but selectively increases chromatin accessibility downstream of genes." PLoS Pathog. 2018 Mar 26;14(3) [234]

2. AIMS

The overall aim of this study was to elucidate the viral gene responsible for the formation of the dOCR during lytic HSV-1 infection and characterize the underlying molecular mechanism.

More specifically the aims were as follows:

1. Investigating the cause of differences in dOCR induction between different gene clusters

2. Establishing doxycycline-inducible cell system to investigate role of ICP22 in isolation upon disruption of transcription termination with ATAC-seq

3. Investigating roles of histone chaperons FACT and SPT6 in DoTT-associated dOCR with Omni-ATAC-seq to establish if DoTT in HSV-1 infection happens due to shifting of those factors upon direct/indirect interaction with the ICP22 protein

4. Comprehensive analysis of dOCR, identified by ATAC-seq and Omni-ATAC-seq to ChiPmentation data focusing on the deposition of canonical histone H3, histone modification marks H3K27me3 and H3K36me3 and histone linker H1

3. MATERIALS

3.1. Cell lines

All used cell lines were routinely tested for mycoplasma contamination. All cells were incubated at 37°C in a 5 % (v/v) CO_2-enriched incubator. HFFFs were utilized from passage 11 to 17 for all high-throughput experiments.

3.1.1. Human primary cells

HFFF — Human fetal foreskin fibroblasts (The European Collection of Authenticated Cell Cultures, ECACC)
Use: ChIPmentation, total RNA-seq, ATAC-seq and Omni-ATAC seq

3.1.2. Immortalized cell lines

BHK — Baby hamster kidney cell line (American Type Culture Collection, ATCC)
Use: HSV-1 production

T-HF — Human telomerase reverse transcriptase (hTERT)-Immortalized cell line (kindly provided by Dr. sc. Cyprian Rosetto [240]
Use: generation of doxycycline-inducible cell lines used for ATAC-seq and Omni-ATAC-seq

HEK-293T — Human embryonic kidney 293 cells with stable expression of the SV40 large T antigen (ATCC)
Use: lentivirus production

Vero 2.2 — African green monkey kidney Vero 2.2 cells, derivative Vero cell line expressing ICP27 under its own promoter (kindly provided by Prof. Dr. sc. Rozanne M. Sandri-Goldin)
Use: ΔICP27 virus production

U-2 OS — Human Bone Osteosarcoma Epithelial Cells (ATCC)
Use: ΔICP0 virus production

3.2. Cell culture media and supplements

Reconstituted cell culture media and solutions were stored at 4°C.

Table 1. Cell culture media and supplements

Name	Use	Supplements
DMEM (1x), High Glucose, Pyruvate (Gibco)	Cell line propagation/ infection	10 % FCS (before use, heat inactivated at 56°C for 30 min (Biochrom)) 1 % PenStrep (Sigma-Aldrich) 1 % MEM NEAA (Gibco)
DMEM (1x), High Glucose, Pyruvate (Gibco)	Virus production	2 % FCS (Biochrom) 1 % PenStrep (Sigma-Aldrich) 1 % MEM NEAA (Gibco)
DMEM (1x), High Glucose, Pyruvate (Gibco)	Virus production	1 % PenStrep (Sigma-Aldrich) 1 % MEM NEAA (Gibco)
Opti-MEM (ThermoFisher Scientific)	Cell transfection	

3.3. Viruses

All virus working stocks were kept at -80°C. HSV-1 KOS 1.1 was kindly provided by Prof. Dr. sc. Stephen Rice.

Table 2. Viruses

Virus	Strain	Producer cell line
HSV-1 WT	Strain 17	BHK
HSV-1 WT BAC	Strain 17 derived	BHK
HSV-1 WT	Strain F	BHK
HSV-1 WT	Strain KOS 1.1	BHK
HSV-1 WT BAC	Strain KOS 1.1 derived	BHK
HSV-1 ΔICP0 [241]	Strain 17	U-2 OS
HSV-1 ΔICP22 [242]	Strain F	BHK
HSV-1 ΔICP22 BAC	Strain 17 derived	V22
HSV-1 ΔICP22	Strain KOS 1.1	V22
HSV-1 ΔICP27 [243]	Strain KOS	Vero 2.2
HSV-1 Δvhs [244]	Strain 17	BHK

3.4. Plasmids

For long-term storage of plasmids, all bacterial glycerol stocks were stored at – 80°C, while plasmid DNA was kept at 4°C.

Table 3. Plasmids

Name	Description
f6GW	3rd generation lentiviral vector expressing enhanced Green Fluorescent Protein (eGFP)
LDJ5 (HA-US1)	Doxycycline-inducible lentiviral vector with US1 expression, HA-tag and blasticidin-resistance gene (derived from pW-YC1)
pLT3GGmirEPPIR#201	Doxycycline-inducible lentiviral vector with cloning site for amiRNA expression and puromycin-resistance gene [245]
psPAX2	2nd generation lentiviral packaging vector
pW-TH3	Doxycycline-inducible all-in-one lentivirus system with Multiple Cloning Site (MCS) and additional STOP codons after MCS
pW-TH57	Doxycycline-inducible all-in-one lentivirus system with UL54 expression, 3xFLAG-V5-NT1 and puromycin-resistance gene (derived from pW-TH9)
pW-TH9	Doxycycline-inducible all-in-one lentivirus system with 3xFLAG-V5-NT1 and puromycin-resistance gene
pW-YC1	Doxycycline-inducible lentiviral vector with blasticidin-resistance gene (derived from pW-TH3)
Vsv-g	Vsv-g envelope expressing plasmid, Vsv-glyco

3.5. Bacteria

All competent bacteria were kept at - 80°C.

Table 4. Bacteria

Name	Type	Manufacturer
Stellar, chemically competent cells	*E. coli*, HST08 strain	Clontech Labs
NEB 5-alpha, chemically competent cells	*E. coli*, K12 strain (DH5α derivative)	New England Biolabs

3.6. Buffers and solutions

All buffers and solutions were prepared using nuclease free H_2O, unless otherwise indicated.

All ChIPmentation, ATAC and Omni-ATAC buffers were stored at 4°C or used immediately after preparation.

Other solutions and buffers were stored at RT, unless otherwise specified.

All chemicals were purchased from Sigma-Aldrich, ThermoFisher Scientific, Carl Roth and VWR unless otherwise specified.

Table 5. Buffers and solutions

Buffer	Components
ChIPmentation	
Sonication buffer	10 mM Tris, pH 8.0 0.25 % (v/v) SDS 2 mM EDTA 1x cOmplete, Mini Protease Inhibitor Cocktail 1x PMSF
Equilibration buffer	10 mM Tris, pH 8.0 233 mM NaCl 1 mM EDTA, pH 8.0 0.166 % (w/v) Sodium deoxycholate (Na-DOC) 1.66 % (v/v) Triton x-100 1x cOmplete, Mini Protease Inhibitor Cocktail 1x PMSF
RIPA-LS buffer	10 mM Tris, pH 8.0 140 mM NaCl 1 mM EDTA, pH 8.0 0.1 % (v/v) SDS 0.1 % (w/v) Na-DOC 1 % (v/v) Triton x-100 1x cOmplete, Mini Protease Inhibitor Cocktail
RIPA-LS buffer (without the inhibitors)	10 mM Tris, pH 8.0 140 mM NaCl 1 mM EDTA, pH 8.0 0.1 % (v/v) SDS 0.1 % (w/v) Na-DOC 1 % (v/v) Triton x-100

RIPA-HS buffer	10 mM Tris, pH 8.0 500 mM NaCl 1 mM EDTA, pH 8.0 0.1 % (v/v) SDS 0.1 % (w/v) Na-DOC 1 % (v/v) Triton x-100 1x cOmplete, Mini Protease Inhibitor Cocktail
RIPA-LiCl buffer	10 mM Tris, pH 8.0 250 mM LiCl 1 mM EDTA, pH 8.0 0.5 % (w/v) Na-DOC 0.5 % (v/v) NP-40 1 x cOmplete, Mini Protease Inhibitor Cocktail
De-crosslinking buffer	160 mM NaCl 40 µg/mL RnaseA } Day 1 1x Tris-EDTA 200 µg/mL Proteinase K } Day 2 4 mM EDTA

ATAC-seq

Lysis buffer	10 mM Tris-HCl, pH 7.5 10 mM NaCl 3 mM $MgCl_2$ 0.1 % (v/v) Igepal
Transposition buffer	2x Tagmentation buffer (Ilumina) 2,5 µl Transposase (Ilumina), unknown concentration

Omni-ATAC-seq

ATAC-RSB buffer 1	10 mM Tris-HCl, pH 7.4 10 mM NaCl 3 mM $MgCl_2$
ATAC-RSB buffer 2	10 mM Tris-HCl, pH 7.4 10 mM NaCl 3 mM $MgCl_2$ 0,1 % (v/v) NP-40 0,1 % (v/v) Tween-20 0,01 % (v/v) Digitonin
ATAC-RSB buffer 3	10 mM Tris-HCl, pH 7.4 10 mM NaCl

	3 mM $MgCl_2$ 0,1 % (v/v) Tween-20
Transposition buffer	2x Tagmentation buffer (Ilumina) 100 nM Transposase (made in-house) 1x PBS 0,01 % (v/v) Digitonin 0,1 % (v/v) Tween-20

Western Blot

4x Laemmli sample buffer (-20°C)	250 mM Tris-HCl, pH 6.8 8 % (w/v) SDS 0.02 % (w/v) Bromophenol blue 40 % (v/v) glycerol 5 % (v/v) β-mercaptoethanol
10x Tris-Glycine SDS Running Buffer	30.3 g Tris-base 144 g Glycine 10 g SDS in nuclease-free H_2O to 1000 mL
10x Transfer Buffer	30.3 g Tris-base 144.2 g Glycine nuclease-free H_2O to 1000 mL
1x Transfer Buffer	100 mL 10x Transfer buffer 200 mL Methanol 700 mL nuclease-free H_20
Blocking buffer	5 % (w/v) skim-milk in 0.2 % (v/v) Tween-20 in 1x PBS
0,1 % Ponceau S staining solution	0.1 % (w/v) Ponceau S 5 % (v/v) Acetic acid
Washing buffer	0.2 % (v/v) Tween-20 in 1 x PBS

Immunoflourescence

4 % PFA (v/v) Fixing solution	16 % (w/v) Paraformaldehyde (PFA), Methanol-free in 1x PBS
0.5 % Triton (v/v) Permeabilization solution	20 % (v/v) Triton-X 100 in PBS
Blocking buffer	10 % (v/v) fetal calf serum (FCS) 250 mM glycine

	1x PBS
Primary/Secondary blocking buffer	10 % (v/v) FCS 1x PBS
Other	
0,1 % Crystal violet solution	1 g crystal violet dissolved in 50 mL ethanol 950 mL nuclease-free H_20
PMSF	200 mM in Isopropanol
5 % (w/v) CMC	50 g Carboxymethylcellulose 1000 mL nuclease-free H_20
1x PBS	w/o without calcium chloride and magnesium chloride (made in-house)
15 % (w/v) Polysucrose solution	15 g Polysucrose 400 100 mL sterile PBS
100 mg/mL Phosphonoacetic acid (PAA)	1 g PAA in 10 mL nuclease-free H_20
1 mg/mL doxycycline (Dox)	10 µl 100 mg/mL Dox in 1 mL nuclease-free H_20
100 mg/mL ampicillin (AMP)	1 g AMP in 10 mL nuclease-free H_20

3.7. Beads, Enzymes, Standards and Kits

3.7.1. Beads

Table 6. Beads

Product name	**Company**
Dynabeads Protein G for IP	ThermoFisher Scientific, 10008D
Dynabeads Protein A for IP	ThermoFisher Scientific, 10003D
Agencourt AMPureXP	Beckman Coulter, A63880

3.7.2. Enzymes

Table 7. Enzymes

Product name	Company
AgeI-HF	New England Biolabs, R3552S
BamHI-HF	New England Biolabs, R3136S
BglII	New England Biolabs, R0144S
DNase I	Zymo Research, E1010
EcoRI-HF	New England Biolabs, R3101L
MluI	New England Biolabs, R0198S
NEBNext Ultra II Q5 Master Mix	New England Biolab, M0544S
NheI-HF	New England Biolabs, R3131S
Phusion Hot Start II High Fidelity DNA-Polymerase	ThermoFisher Scientific, F539S
Proteinase K, recombinant, PCR Grade	Sigma-Aldrich, 3115887001
Q5 High-Fidelity DNA Polymerase	New England Biolab, M0491S
Ribonuclease A from bovine pancreas	Sigma-Aldrich, R4642
T4 DNA Ligase	New England Biolabs, M0202S
XbaI	New England Biolabs, R0145S
XhoI	New England Biolabs, R0146S
5× qRT SuperMix	Biotool, -
5x no RT ControlMix	Biotool, -
2x SYBR Green qPCR Master Mix	Bimake, B21202

3.7.3. Standards

Table 8. Standards

Product name	Company
Gene Ruler 100 bp DNA Ladder	ThermoFisher Scientific, SM0241
Quick-Load Purple 1 kb Plus DNA Ladder	New England Biolabs, N0550S
PageRuler Plus Pre-stained Protein Ladder	ThermoFisher Scientific, 26619

3.7.4. Kits

Table 9. Kits

Product name	Company
DNA Clean & Concentrator-5 Kit	Zymo Research, D4014
GenElute HP Plasmid Miniprep Kit	Sigma-Aldrich, NA0160
High Sensitivity DNA Kit	Agilent Technologies, 5067-4626
High Sensitivity DNA Reagents	Agilent Technologies, 5067-4627
MinElute PCR Purification Kit	Qiagen, 28004
Monarch DNA Gel Extraction Kit	New England Biolabs, T1020
Nextera DNA Library Preparation Kit	Ilumina, 15028211
NucleoBond Xtra Midi kit	Macherey-Nagel, 740410.50
NucleoSpin Gel and PCR Clean-up Kit	Macherey-Nagel, 12303368
Qubit dsDNA HS Assay Kit	ThermoFisher Scientific, Q32851
Quick-RNA Miniprep Kit	Zymo Research, R1054
Quick-RNA Microprep Kit	Zymo Research, R1050

3.8. Antibodies

3.8.1. Primary antibodies

ChIP: Chromatin immunoprecipitation followed by sequencing, ChIPmentation

IF: Immunofluorescence

WB: Western blot

Table 10. Primary antibodies

Target	Use	Concentration	Company
Anti-GAPDH (0411), mouse mAb	WB	1:1000	Santa Cruz Biotechnology, sc-47724
Anti-HA (clone 11), mouse mAb	WB	1:1000	BioLegend, 16B12
Anti-HA (F-7), mouse mAb	IF	1:1000	Santa Cruz Biotechnology, sc-7392
Anti-Histone H1 (1415-1), rabbit polyclonal	ChIP	1:50	ThermoFisher Scientific, PA5-30055
Anti-Histone H3, rabbit polyclonal	ChIP	1:50	Cell Signaling technology, 2650S
Anti-Histone H3K27me3, rabbit polyclonal	ChIP	2 µg/IP	Diagenode, C15410195

Anti-Histone H3K36me3, rabbit polyclonal	ChIP	1 µg/IP	Diagenode, C15410192
Anti-HSV-1 gD (DL6), mouse mAb	WB	1:1000	Santa Cruz Biotechnology, sc-21719
Anti-HSV-1 ICP8 (10A3), mouse mAb	WB	1:1000	Santa Cruz Biotechnology, sc-53329
Anti-IgG, normal rabbit	ChIP	Adjusted	Cell signaling technology, 2729
Anti-Spt16 (FACT) (8D2), mouse mAb	WB	1:500	BioLegend, 607008
Anti-SPT6, rabbit polyclonal	WB	1:500	Novusbio, NB100-2582
Anti-SSRP1 (FACT) (10D1), mouse mAb	WB	1:350	BioLegend, 609710
Anti-V5-Tag (D3H8Q), rabbit mAb	IF WB	1:1000 1:1000	Cell Signaling Technology, 13202S
Anti-α-Tubulin, rabbit polyclonal	WB	1:1000	Cell Signaling Technology, 2144
Anti-β-Actin (C4), mouse mAb	WB	1:1000	Santa Cruz Biotechnology, sc-47778
DAPI (4', 6-diamidino-2-phenylindole)	IF	1x	ThermoFisher Scientific, A21425

3.8.2. Secondary antibodies

Table 11. Secondary antibodies

Target	Use	Concentration	Company
Anti-Mouse IgG, Alexa Flour 488	IF	1:1000	ThermoFisher Scientific, A11017
Anti-Rabbit IgG, Alexa Flour 568	IF	1:1000	Abcam, ab175471
Goat anti-Rabbit IgG (whole molecule) – Peroxidase antibody	WB	1:10 000	Sigma-Aldrich, A0545
IRDye 680RD Goat-α-Rabbit IgG	WB	1:5000	LI-COR Biosciences GmbH, 926-68071
IRDye 800CW Goat Anti-Mouse IgG	WB	1:5000	LI-COR Biosciences GmbH, 926-32210
Rabbit anti-Mouse IgG (whole molecule) – Peroxidase antibody	WB	1:10 000	Sigma-Aldrich, A9044
Rabbit anti-Rat IgG (whole molecule) – Peroxidase antibody	WB	1: 10 000	Sigma-Aldrich, A5795

3.9. Oligonucleotides

Oligonucleotides used for generating HA-ICP22 and V5-ICP27 doxycycline-inducible cells are show in the Table 12.

Oligonucleotides were synthetized by and purchased from Sigma-Aldrich. All oligonucleotides were synthetized at 0.025 µmol scale, purified by DST, resuspended with nuclease-free H_2O to 100 µM and used at 500 nM final concentration. Stock solutions were stored at - 20°C.

Table 12. Oligonucleotides used for generating HA-ICP22 and V5-ICP27 Dox-inducible cells

Oligonucleotide name	Sequence
prW64	GCTGAGCTAGCGTTAACTGATCAGAATTCCCTAGGGTTTAAACTTCGAAAC GCGTGTCGACTACGTAACCGGTGCTAG
prW65	CTAGCACCGGTTACGTAGTCGACACGCGTTTCGAAGTTTAAACCCTAGGG AATTCTGATCAGTTAACGCTAGCTCAGC
prW110	GACTAACCGGTTAGTTAGCTAACCGCGGTTACCTATTTACCCGGGCAATG
prW111	CATTGCCCGGGTAAATAGGTAACCGCGGTTAGCTAACTAACCGGTTAGTC
prW196	GAGTCAAGCTTCTAGAGCCGCCACCATGGACTACAAAGACCATGACGGTG ATTATAAAGATCATGATATCGATTACAAGGATGACGATGACAAGATTGGT GGAAAGCCGATCCCAAACCC
prW197	CTGAGAAAGGACAGCGACGA
prW365	AGCTTGGATCCGCGACTGACATTGATATGC
prW366	AGATCTTTAGCTAACTAACCGGTTACGTAGTCGACACGCGTTTCGAAGTTT AAACCCTAGGGAATTCCCTAAAACAGGGAGTTGC
prW1656	TCGCCTGGAGAATTGGCTAGCGCCACCATGTACCCCTACGACGTGCCCGA CTACGCCGGTGGAGCCGACATTTCCCCAGGC
prW1657	GGTTACGTAGTCGACACGCGTTCACGGCCGGAGAAACGTGTC

Oligonucleotides used for generating SSRP1 and SPT6 doxycycline-inducible knock-down cells are shown in the Table 13.

Oligonucleotides were synthetized by and purchased from Sigma-Aldrich. All oligonucleotides, besides amiRNA_XhoI and amiRNA_EcoRI that were synthetized at 0.05 µmol scale, were synthetized at 0.025 µmol scale by high performance liquid chromatography (HPLC), resuspended with nuclease-free H_2O to 100 µM and used at 500 nM final concentration. Stock solutions were stored at - 20°C.

Table 13. Oligonucleotides used for generating SSRP1 and SPT6 Dox-inducible KD cells

Oligonucleotide name	Sequence
hSPT6_amiRNA_1	TGCTGTTGACAGTGAGCGACAGCACAATTCAGAAGATCAATAGTGAAG CCACAGATGTATTGATCTTCTGAATTGTGCTGGTGCCTACTGCCTCGGA
hSPT6_ amiRNA_2	TGCTGTTGACAGTGAGCGATAGGAGCATCTTTGAAATGTATAGTGAAG CCACAGATGTATACATTTCAAAGATGCTCCTACTGCCTACTGCCTCGGA
hSSRP1_ amiRNA_1	TGCTGTTGACAGTGAGCGAAAAGAAGAAGAAGAAAGTAAATAGTGAA GCCACAGATGTATTTACTTTCTTCTTCTTCTTTGTGCCTACTGCCTCGGA
hSSRP1_ amiRNA_2	TGCTGTTGACAGTGAGCGAGTCTGTGAAAATGATTTAATATAGTGAAGC CACAGATGTATATTAAATCATTTTCACAGACCTGCCTACTGCCTCGGA
amiRNA_XhoI	TACAATACTCGAGAAGGTATATTGCTGTTGACAGTGAGCG
amiRNA_EcoRI	TTAGATGAATTCTAGCCCCTTGAAGTCCGAGGCAGTAGGCA

PCR primers used for the amplification of the ChIPmentation, ATAC and Omni-ATAC-DNA libraries are shown in the table below.

Unique dual (UD) adapter sequences were synthetized by and purchased from IDT. UD index adapters are 8 bases long. All UD adapter sequences were synthetized at 0.025 µmol scale, purified by high performance liquid chromatography (HPLC), resuspended with nuclease free H_2O to 10 µM and used at the same concentration.

Stock solutions were stored at - 20°C.

Index 1 Read

5′ AATGATACGGCGACCACCGAGATCTACAC **[i5]** TCGTCGGCAGCGTC

Index 2 Read

5′ CAAGCAGAAGACGGCATACGAGAT **[i7]** GTCTCGTGGGCTCGG

Table 14. Oligonucleotides used for generating ChIPmentation, ATAC and Omni-ATAC-DNA libraries

Index (i5) Adapters		Index (i7) Adapters	
I5 Index Name	I5 Bases in Adapter	I7 Index name	I7 Bases in Adapter
i5_1	ATATGCGC	i7_1	ACGATCAG
i5_2	TGGTACAG	i7_2	TCGAGAGT
i5_3	AACCGTTC	i7_3	CTAGCTCA
i5_4	TAACCGGT	i7_4	ATCGTCTC
i5_5	GAACATCG	i7_5	TCGACAAG
i5_6	CCTTGTAG	i7_6	CCTTGGAA
i5_7	TCAGGCTT	i7_7	ATCATGCG
i5_8	GTTCTCGT	i7_8	TGTTCCGT
i5_9	AGAACGAG	i7_9	ATTAGCCG
i5_10	TGCTTCCA	i7_10	CGATCGAT
i5_11	CTTCGACT	i7_11	GATCTTGC
i5_12	CACCTGTT	i7_12	AGGATAGC
i5_13	ATCACACG	i7_13	GTAGCGTA
i5_14	CCGTAAGA	i7_14	AGAGTCCA
i5_15	TACGCCTT	i7_15	GCTACTCT
i5_16	CGACGTTA	i7_16	CTCTGGAT
i5_17	ATGCACGA	i7_17	AGATCGTC
i5_18	CCTGATTG	i7_18	GCTCAGTT
i5_19	GTAGGAGT	i7_19	GTCCTAAG
i5_20	ACTAGGAG	i7_20	TATGGCAC
i5_21	CACTAGCT	i7_21	TCGGATTC
i5_22	ACGACTTG	i7_22	AACAGCGA
i5_23	CGTGTGTA	i7_23	CCAACGAA
i5_24	GTTGACCT	i7_24	CAGTGCTT
i5_25	ACTCCATC	i7_25	GATCAAGG
i5_26	CAATGTGG	i7_26	TCTTCGAC
i5_27	TTGCAGAC	i7_27	ATCGTGGT
i5_28	CAGTCCAA	i7_28	CGGTAATC
i5_29	ACGTTCAG	i7_29	AGTTGTGC
i5_30	AACGTCTG	i7_30	AATGACGC
i5_31	TATCGGTC	i7_31	TACCGGAT
i5_32	CGCTCTAT	i7_32	TTGCAACG
i5_33	GATTGCTC	i7_33	CACTTCAC
i5_34	GATGTGTG	i7_34	TAGCCATG
i5_35	CGCAATCT	i7_35	ACAGGCAT
i5_36	TGGTAGCT	i7_36	AGGTGTTG
i5_37	GATAGGCT	i7_37	CAGTCACA
i5_38	AGTGGATC	i7_38	TCGATGAC
i5_39	TTGGACGT	i7_39	GAAGTGCT
i5_40	ATGACGTC	i7_40	CTTCCTTC

3.10. Consumables

Consumables, such as serological pipettes, pipette tips, cell culture dishes, cell culture flasks, falcon and reaction tubes, cell scrapers and other disposable material were purchased from Sarstedt, Labor Dr. Scheller, VWR, Eppendorf, Millipore, Greiner Bio-One and Hartenstein.

3.11. Equipment

Table 15. Equipment

Equipment	Product name/Manufacturer
Adjustable volume pipettes	Transferpette S pipette (BRAND) 0,1-1 µL, single-channel adjustable volume 1-20 µL, single-channel adjustable volume 20-200 µL, single-channel adjustable volume 100-1000 µL, single-channel adjustable volume
Bioanalyzer Instrument	2100 Bioanalyzer Instrument (Agilent Technologies)
Bioanalyzer Parts & Accessories	Chip priming station (Agilent Technologies) Chip Vortexer IKA MS 3 (Agilent Technologies)
Cell culture incubator	Heracell™ 240i CO_2 (Thermo Fisher Scientific)
Cell culture hood	BSB 4A, Safety Cabinet (GELAIRE Flow Laboratories)
Centrifuges	Centrifuge 5427 R (Eppendorf) Eppendorf Minispin Plus (Eppendorf) Rotanta 460/460R (Hettich)
E-Gel precast gel electrophoresis system	Thermo Fisher Scientific
Fluorometer	The Invitrogen Qubit 3 Fluorometer (Thermo Fisher Scientific)
Freezers	Liebherr Premium (-20°C) Forma 900 series (-80°C) (Thermo Fisher Scientific) VIP Plus Series (-150°C) (Panasonic)
Fridge (+4°C)	Liebherr Premium
Fume cupboard	Standard fume cupboard (Vinitex Laboratoriuminrichtingen)
Gel electrophoresis system	Thermo Fisher Scientific
Gel hood imager	INTAS
Hemocytometer	Neubauer improved (VWR)

Imaging system	Odyssey Fc (LI-COR)
Laboratory balance	Kern EW 1500-2M Toploader balance (Sigma Aldrich)
LED transilluminator	SERVA BlueLight table (SERVA)
Magnetic stand	DynaMag™-2 Magnet (Thermo Fisher Scientific)
Magnetic stirrer	IKAMAG REO (Janke & Kunkel)
Microscopes	Leica DMi8 (Leica Microystems)
	ZEISS Primovert (Zeiss)
Microwave	MW 7890 (Severin)
Nanodrop	NanoDrop 2000 Spectrophotometer (Thermo Fisher Scientific)
PCR thermal cycler	Biometra TAdvanced Twin Thermal Cycler (Analytik Jena AG)
pH meter	FiveEasy F20 pH/mV Meter (Mettler Toledo)
Pipette controller	Accu-jet pro (BRAND)
Power supply unit	POWER Pro (Cleaver Scientific Ltd)
Quantitative RT-PCR machine	LightCycler® 96 Instrument (Roche)
Thermo-shaker	Thermomixer R dry block heating and cooling shaker (Eppendorf)
	PCMT Thermoshaker with cooling for microtubes (Grant-bio)
Tube roller machine	RS-TR 5 (Phoenix instrument)
Tube Rotator	Tube Rotator Unit with US Power Cord (VWR)
Ultrasonifier	Branson Digital Sonifier S-450
Ultra-speed centrifuges	Sorvall Discovery 90SE (Hitachi)
	Sorvall Evolution RC (Thermo Fisher Scientific)
Ultrapure water system	Barnstead GenPure Pro (Thermo Fisher Scientific)
Vortex mixer	Vortex Genie2 (Bender & Hobein AG)
Waterbath (+10°C to +95°C)	WNB 7 (Memmert)
	WNB 45 (Memmert)
Wet/tank blotting system	Mini Trans-Blot Cell (BioRad)

3.12. Online programs and software

Table 16. Online programs/Software

Online programs /Software	Company
Image J	Wayne Rasband
ImageStudioLite	LI-COR
INTAS GelDoc	INTAS Science Imaging
Integrated Genome Browser	Nicol et al, 2009
LightCycler® 480 Software	Roche
Microsoft Office 2016	Microsoft Incorporated
Prism6	GraphPad Software Incorporated
SnapGene	GSL Biotech LLC
UCSC Genome Bioinformatics	http://genome.ucsc.edu
2100 Expert Software	Agilent Technologies
NanoDrop 2000/2000c	Thermo Fisher Scientific
http://splashrna.mskcc.org/	Pelossof, Fairchild, et al.

4. METHODS

4.1. Cell biology methods

4.1.1. Cell passaging

Cells were passaged when nearly 80 % confluent. After aspirating the cell culture medium, cells were washed twice with 1x Dulbecco's Phosphate Buffered Saline (PBS) (Sigma-Aldrich) and then lifted with trypsin/EDTA (Gibco, ThermoFisher Scientific). To enhance trypsin activity and detach cells from the cell culture dish, dishes were incubated for ≈5 min in the incubator at 37°C. Once detached, cell culture medium was added to the trypsin to stop the enzymatic activity of the trypsin. Depending on the volume, cells were collected in 15- or 50-mL conical falcon tube and pelleted at 400x g for 5 min. Following centrifugation, the supernatant was aspirated, and the cell pellet resuspended in the cell culture medium. A fraction of the cell suspension was mixed with a fresh cell culture medium and plated onto new cell culture dishes. For plating cells at a specific cell number, the cell number of a suspension was determined by using Neubauer counting chamber.

4.1.2. Cell thawing and cryopreservation

Cryopreserved cells were stored in Cryo-Tubes at - 150°C (long term storage). To thaw, cells were placed for a few minutes in a water bath at 37°C. After defrosting, the cell suspension was transferred into a 15 mL conical falcon tube containing 9 mL of warm (37°C) cell culture medium and pelleted at 400x g for 5 min. Following centrifugation, supernatant containing dimethyl sulfoxide (DMSO) (Sigma-Aldrich) was removed, and the cell pellet was resuspended in 15 mL fresh cell culture medium. A day after plating, medium was aspirated and the cells were washed once with 1x PBS to remove residues of dead cells, after which fresh cell culture medium was added. Thawed cells were passaged at least 3-4 times before performing high-throughput experiments. For cryopreservation, cells were harvested when 80 % confluent by trypsinization, pelleted by centrifugation at 400x g for 5 min and resuspended in 1 mL freezing medium containing 90 % FCS and 10 % DMSO. Cells were kept in - 20°C freezer for a few hours before

subsequently transferring them to - 80°C overnight. For long term storage cells were transferred to -150°C.

4.1.3. HSV-1 infection

In this study, several HSV-1 WT strains as well as mutant viruses were used (as described in the Table 2). Cells were infected for 15 minutes or 1 hour in conditioned media 24-48 hours after seeding, depending on the experiment, at a multiplicity of infection (MOI) of 10. Subsequently, the inoculum was removed, and fresh media was applied to the cells. The time at which inoculum was replaced with growth media was marked as the 0 h timepoint of infection.

To block viral DNA replication, phosphonoacetic acid (PAA, 350 µg/mL, Merck, 284270-10G) was added in fresh media to cultured cells after the inoculum was removed.

SSRP1 and SPT6 doxycycline-inducible knock-down (KD) T-HF cells were grown in the absence or presence of doxycycline (Dox, 1 µg/mL, Merck, #AMBH2D6FB132) for 72 h at 37°C at 5 % CO_2, (adding fresh Dox after 48 hours), before Omni-ATACseq was performed.

HA-ICP22, V5-ICP27 and HA-ICP22 + V5-ICP27 doxycycline-inducible T-HF cells were grown in the absence or presence of 5 µg/mL Dox for 48 h at 37°C at 5 % CO_2.

4.1.4. Virus production

4.1.4.1. Cell infection

A day before infection, $5x10^6$ BHK cells were seeded in 40 cell culture dishes. On the day of the infection, the viral inoculum was prepared by resuspending the required amount of virus in a serum-free medium (MOI 0.001-0.005). Conditioned medium was removed, and viral medium was added for two hours. Viral medium was aspirated and 20 mL of fresh 2 % FCS cell culture medium was added to each cell culture dish. Dishes were incubated at 37°C until full cytopathic effect (CPE) was reached (2-3 days). If longer incubation was required, 10 mL of fresh 2 % FCS medium was added to the cell culture dishes.

4.1.4.2. Virus stock preparation

When CPE was fully reached, viral cell culture medium and cells were collected in 500 mL polycarbonate centrifuge bottles and pelleted for 10 minutes at 13,500x g, 4°C. Supernatant was collected leaving only a small volume (5-6 mL) with the pellet in which the cells were resuspended. Supernatant was stored on ice until further used. Resuspended cell pellets were subjected three times to freeze (liquid N_2)-thaw (water bath, 37°C) cycles to release intracellular virions, collected and pelleted for 10 minutes at 3,000x g, 4°C. Supernatant was collected in sterile Beckman ultracentrifuge bottles and mixed with the previous one while cells were discarded. Beckman ultracentrifuge bottles were placed in a precooled Sorvall Evolution RC (Sorvall GS-3 rotor) centrifuge for 2 h, 13,500x g, 4°C. Following centrifugation, the supernatant was discarded, and 1 mL of 1x PBS was added to the viral pellets were resuspended overnight on ice. Next day, viral pellets were pooled in a conical falcon tube and transferred into a precooled tissue glass dounce homogenizer. To separate viral particles, the viral suspension was dounced 40 times on ice. The viral solution was then layered over the polysucrose gradient (as described in section 4.1.5.3.) and centrifuged in a precooled Sorvall Discovery 90SE (SW28 rotor) centrifuge at 15,000x g, 2 hours, 4°C with no deceleration. In the tare tube PBS was added. After centrifugation, the viral band appeared ½ to ¾ down the tube and by using a dark background, the supernatant was removed, and viral band collected into another ultracentrifuge tube. Viral band was diluted with sterile (endotoxin-free) 1x PBS to the maximal capacity of the tube and pelleted at 35,000x g for another 2 hours at 4°C (SW28 rotor). Supernatant was removed and 2 mL of sterile 1x PBS was added. The pellet was resuspended in PBS overnight. Next day, virus was additionally resuspended, aliquoted in 20-100 µL per tube and frozen at - 80°C.

4.1.4.3. Polysucrose 400 gradient preparation

Polysucrose 400 gradient was prepared on the day of the viral stock preparation.
Solutions of decreasing polysucrose content were prepared as stated:

i. 15 % (15 ml polysucrose)
ii. 12.5 % (12.5 ml polysucrose + 2.5 mL 1x PBS)
iii. 10 % (10 ml polysucrose + 5 mL 1x PBS)

iv. 7.5 % (7.5 ml polysucrose + 7.5 mL 1x PBS)

v. 5 % (5 ml polysucrose + 10 mL 1x PBS)

Equal volumes of each solution were layered carefully (6.5 mL for a 3.5-inch 35 mL tube) with a Pasteur pipette. Tubes (virus tube and tare) were covered with a 50 mL falcon cap (to keep it sterile) and kept at 4°C overnight.

4.1.5. Virus titration

HFFF (340 000/well) or Vero/V22 cells (500 000/well) were seeded in a 6-well plate and grown until confluent. Tenfold dilutions of virus solution were prepared in a 10 % FCS conditioned medium. The virus is usually in the range of 10^{10} PFU/mL, so the dilutions were made up to 10^{10} (diluting virus 1:100 in conditioned medium → e.g. 5 µl stock + 495 µl conditioned medium (-2 dilution), then serially diluting virus 1:10 in the conditioned medium). The rest of the conditioned medium was aspirated from the wells and 500 µL of each of the dilutions were added. The plate was incubated at 37°C for either 15 minutes or 1 hour to obtain HSV-1 titer for different times of infection. Medium was aspirated and 4 mL of 0.5 % (w/v) CMC was added to each well (e.g. added 3 mL 5 % (w/v) carboxymethyl cellulose to 27 mL conditioned medium for a total of 30 mL). Plates were incubated for 3 days or until the plaques were clearly visible. Cells were then fixed by adding 400 µL of 37 % formaldehyde for at least 15 minutes at room temperature (RT). Fixing solution was aspirated and the cells were stained with 1 % crystal violet for at least one hour. Crystal violet solution was aspirated, and the plate was washed in the excess of tap water. When plates were dried, for easier plaque counting grid was made at each of the wells with thin pen. Plaques were counted from a dilution that gave ≈30 clearly discernible plaques. One plaque represents 1 PFU/mL in the given virus dilution.

4.1.6. Immunofluorescence

1 x 10^5 HA-ICP22 and HA-ICP22+V5-ICP27 cells were plated in 12 well-dishes with or without the addition of 5 µg/mL of Dox. At 48 h post-induction, cells were fixed with 4 % PFA solution for 15 min at RT, washed three times in 1x PBS, and either stored at 4°C overnight in PBS or processed immediately as follows. Cells were permeabilized in 0.5 % Triton X-100 permeabilization solution

for 5-10 minutes and blocked in 10 % FCS blocking buffer for 1 h at RT. Anti-HA or anti-V5 antibodies were incubated in 10 % primary blocking buffer for 1 h at RT at appropriate dilution. Following three 5 minute washes in 1x PBS, secondary anti-mouse IgG, Alexa Fluor 488 or anti-rabbit IgG, Alexa Flour 568 were incubated in 10 % secondary blocking buffer for 1 h at RT with 0.5 µg/mL 4',6-diamidino-2-phenylindole (DAPI) to depict cell nuclei. After incubation, cells were washed three times with 1x PBS and images were taken on Leica DMi8 fluorescence microscope.

4.2. Protein Chemistry

4.2.1. SDS-polyacrylamide gel electrophoresis (SDS-PAGE)

Samples were harvested at the indicated time points by removal of growth media, followed by wash with 1x PBS and lysis in 1x Laemmli buffer. Samples were sonicated and heated for 5 min at 95°C before loading onto a Novex WedgeWell 4–20 % Tris-Glycine Gel (Thermo Fisher Scientific, XP04200BOX). Unlike fixed concentration gels, gradient gels are cast so that there is a gradual dilution from high to low concentration from the bottom region of the gel to the top. This allows for gradual separation of proteins with similar molecular weight.
The polyacrylamide gel electrophoresis was carried out at 80-100 V in 1x SDS running buffer until proteins were resolved as desired.

4.2.2. Western blot

Following SDS-PAGE (as described in section 4.2.1), electrophoretic transfer was used to elute proteins from gel and transfer them to 0.2 µm nitrocellulose membrane (Carl Roth, 5945.1). For this, wet transfer system was used where gel and membrane are submerged under 1x transfer buffer in tank. Before setting up the transfer apparatus, fiber pads, Whatman filter papers, membrane, and gel were soaked in 1x transfer buffer. For electrophoretic transfer, gel and membrane setup was as follows: on the cathode (-) side of the gel holder cassette fiber pad is placed followed by two Whatman filter papers, gel, membrane, two Whatman filter papers and fiber pad ending on the anode (+) side of the gel holder cassette. After the transfer at 260 mA for 90 minutes, the nitrocellulose membrane was incubated in Ponceau S staining solution for 5

minutes at RT to visualize protein bands. To remove Ponceau S color the membrane was washed five times with ddH_2O. The membrane was blocked for 1 h at RT in 1x PBS with 0.2 % Tween (PBS-T) containing 5 % (w/v) milk and probed using primary antibodies (Table 10) overnight at 4°C at a 1:1000 dilution unless differently specified. Before addition of secondary antibody, blots were washed three times for 5 min with 1x PBS-T. After incubation with secondary antibodies (Table 11) for 2 hours at RT, blots were washed three times for 5 min with 1x PBS-T and bands visualized with a LI-COR Odyssey FC Imaging System.

4.3. Molecular biology methods

4.3.1. Heat-shock transformation of bacteria

For transformation, chemically competent *E. Coli* cells were used to amplify plasmid of interest. To 50 µL of bacteria either 10-50 ng of plasmid or 10 µL ligation reaction was added and mixed by flicking the tube 4-5 times. The mixture was incubated on ice for 30 minutes after which the cells were heat-shocked by placing the tube on 42°C for 45 s, followed by another 5 min on ice. Room temperature super optimal broth (SOC) medium (ThermoFisher Scientific, 15544034) was added to the mixture up to 1 ml and the mixture was incubated on a shaker at 220 rpm for 60 min at 37°C. In the next step, 1 %, 10 % and the rest of the mixture were spread out on ampicillin agar plates (100 µg/ml) and placed in 37°C room overnight before individual clones were picked and inoculated in LB medium for Mini-Prep and Midi-Prep plasmid isolation.

4.3.2. Glycerol stock preparation

Briefly, an individual bacterial colony was picked from the ampicillin agar plate, added to 10 mL of LB medium containing 100 µg/ml ampicillin, gently vortexed and incubated at 37°C on a shaker at 220 rpm overnight. 400 µL of the culture was mixed with 600 µL of sterile 50 % glycerol, transferred to a screw-capped tube and stored at -80°C for long-term.

4.3.3. Mini-prep and Midi-prep plasmid isolation

For Mini-Prep, an individual bacterial colony was picked from the agar plate and cultured in 10 ml LB medium containing 100 μg/ml ampicillin with overnight shaking at 220 rpm, 37°C. The plasmid Mini-Prep isolation was performed using the GenElute HP Plasmid Miniprep Kit according to the manufacturer's instructions. The plasmid DNA was eluted from the column at RT in 50 μl nuclease-free H_20 and used for restriction enzyme digestion to verify its integrity. For Midi-Prep, in 200 ml LB medium containing 100 μg/ml ampicillin correct bacteria clones were scraped from glycerol stocks and added into the mixture which was incubated in a shaker at 220 rpm overnight at 37°C. The plasmid Midi-Prep isolation was performed using the NucleoBond Xtra Midi Kit according to the manufacturer's instructions. The plasmid DNA was eluted from the column in 400-600 μl nuclease-free H_20 and either used immediately or stored at -20°C.

4.3.4. DNA isolation with phenol-chloroform

Phenol-Chloroform method was used for the isolation of DNA used in ChIPmentation (as described in 4.4.1.4.). Phenol:Chloroform:Isoamyl alcohol mixture (Sigma-Aldrich, P3803) was added to de-crosslinked chromatin in ratio 1:1 and vortexed for 1 minute. Samples were pelleted for 5 minutes at 19 000 x g at RT. The upper, water phase containing DNA, was taken, and transferred into a new tube. 1 μl of GlycoBlue (ThermoFisher Scientific, LSAM9515), 1:20 of NaAc and 1 volume of Isopropanol were added to the samples and briefly vortexed. Samples were subsequently incubated for 30 minutes at -20°C and then pelleted for 30 min at 19 000 x g at 4°C. Supernatant was removed and pellets washed twice with ice cold 70 % EtOH and pelleted for 10 minutes at 19 000 x g at 4°C. DNA pellets were dried at RT and resuspended in 25 μl Tris pH=8 elution buffer.

4.3.5. Polymerase chain reaction (PCR)

For standard PCR amplifications, a touch-down protocol was performed in a Biometra T Advanced system as described below. Primers used for the generation of HA-ICP22, V5-ICP27 and amiRNA insertions into plt3geppmir are listed in tables 12 and 13.

PCR products were analyzed by gel electrophoresis at 70 V for 1 h on a 1 % TAE agarose gel with 0.01 % ethidium bromide using 1 x gel loading dye and 100-1000 bp plus ladder.

Table 17. PCR reaction components

Component	Stock concentration	Final concentration
DNA template	-	0.5-5 ng
Forward primer_X	100 µM	500 nM
Reverse primer_X	100 µM	500 nM
Q5 HotStart Polymerase	2,000 U/ml	0.2 U/µl
dNTPs	10 mM	200 µM
Q5 Buffer	5 x	1 x
GC enhancer	5 x	1 x
Nuclease-free water	-	Ad 50 µl

Table 18. PCR touch-down program

Step	Cycle	Temperature	Time
Initial template denaturation	1	98°C	3 min
Denaturation	20	98°C	15 sec
Annealing		65°C (ΔT=-0.5°C)	15 sec
Extension		72°C	1:30 min
Denaturation	25	98°C	15 sec
Annealing		55°C	15 sec
Extension		72°C	1:30 min
Final extension	1	72°C	
		4°C	hold

4.3.6. Cell manipulation and generation

4.3.6.1. Generation of SSPR1 and SPT6 Dox-inducible cell lines

To generate SSRP1 and SPT6 doxycycline-inducible cell lines five different artificial microRNA (amiRNA) sequences were used. Top five hits generated by SplashRNA online tool were compared to sequences already predicted by *Fellmann et al*. To add restriction sites for XhoI and EcoRI to amiRNA sequences, two 50 µl reaction were set as follows:

Table 19. PCR reaction (SPT6 and SSPR1 Dox-inducible cell lines)

PCR component	Volume for 50 µl reaction
Template (10ng/µl amiRNA)	1 µl
5 x Phusion HF Buffer	10 µl
DMSO (5 % of the reaction volume)	2,5 µl
10 mM dNTPs	1 µl
Primer EW_880 (10 µM)	2,5 µl
Primer EW_881 (10 µM)	2,5 µl
Phusion Hot Start II DNA Polymerase	0.5 µl
H_20	30 µl

Phusion Hot Start II PCR amplification program was set up in a PCR machine as described below:

Table 20. Phusion Hot Start II PCR amplification program

Step	Cycle	Temperature	Time
Initial template denaturation	1	98°C	2 min
Denaturation		98°C	25 sec
Annealing	20	62°C	25 sec
Extension		72°C	20 sec
Final extension	1	72°C	5 min
		4°C	hold

Agarose gel electrophoresis of PCR product was performed and band at 144 bp was cut and purified with NucleoSpin Gel and PCR Clean-up Kit as described in the manufacturer's manual. Afterwards, the PCR product was digested for 3 hours at 37°C as described below:

Table 21. Digestion reaction 1

Component	Volume for 50 µl reaction
PCR product	~1,5 µg
EcoRI (10 U)	1,5 µl
XhoI (10 U)	1,5 µl
10 x Cutsmart (1 x)	5 µl
H_20	add to 50 µl

Doxycycline-inducible pLT3GGmirEPPIR vector was cut as described below and purified from the gel using the same kit as mentioned above:

Table 22. Digestion reaction 2

Component	Volume for 50 µl reaction
Vector	~5 µg
EcoRI (10 U)	1,5 µl
XhoI (10 U)	1,5 µl
10 x Cutsmart (1 x)	5 µl
H_20	add to 50 µl

After digestion, the 130 bp PCR product was purified from the gel and inserted into the linearized pLT3GGmirEPPIR vector in the overnight ligation at 16°C as described below:

Table 23. Ligation reaction

Component	Volume for 10 µl reaction
Linearized vector DNA	100 ng
PCR product	10 ng
T4 DNA Ligase (5 U)	1 µl
10 x T4 Ligase Buffer	2 µl
H_20	add to 10 µl

As a re-ligation control, linearized vector, but not the insert, was added into the ligation reaction. For transformation, NEB 5-alpha chemically competent *E.Coli* cells were used (see 4.3.1.) and the suspension was spread onto ampicillin-LB plates kept overnight in the 37°C room.

Next day, individual bacterial colonies were picked and resuspended in LB-medium containing 100 µg/ml ampicillin. MiniPrep and MidiPrep were performed according to the manufacturer's instructions and the control restriction digestion was set with enzymes MluI and XhoI. All constructs were sent for sequencing to exclude the possibility of mutations in the cloning site. All amiRNAs that were confirmed to be correctly cloned were transfected to HEK-293T cells as described in 4.3.7. Transduction of T-HF cells was done as described in 4.3.8. and the transduced cells were kept under selection with 5 µg/ml puromycin or frozen in N_2 until the experiment.

4.3.6.2. Generation of V5-ICP27, HA-ICP22 and V5-ICP27 + HA-ICP22 Dox-inducible cell lines

Lentiviral vectors encoding N-terminal 3xFLAG and V5-tagged (tandem tag) UL54 ORF under control of the doxycycline-inducible pTRE-Tight promoter were produced by cloning the corresponding ORF from the HSV-1 genome (strain 17) via intermediate vectors into pW-TH3. The pW-TH3 vector was derived from pCW57.1 by sequential insertion of a synthetic multi-cloning site (prW64/65) and three stop codons (prW110/111) between the NheI and AgeI restriction sites. pCW57.1 was a gift from David Root (Addgene plasmid #41393; http://n2t.net/addgene:41393). pW-TH7 (3xFlag-V5-NT1) was created by amplifying the N-terminal part of NT1 from the V5-NT1 vector (Bolstad et al. 2011) by using primers prW196/197 and inserted back between the BamHI and EcoRI of the same V5-NT1 vector. The 3xFlag-V5-NT1 ORF was excised with EcoRI and XbaI and inserted between the EcoRI and NheI sites of pW-TH3 (now designated pW-TH9). The UL54 ORF was amplified from the HSV-1 genome by PCR using primers prW365/366. The PCR product was digested with BamHI and BglII and inserted into BamHI cut pW-TH9 (now designated pW-TH57).

To generate doxycycline-inducible vector with HA-tagged US1 ORF (designated as LDJ5), the vector YC1 was used as backbone. YC1 was generated to carry blasticidin resistance gene instead of puromycin by restriction digestion of pW-TH3 vector with XbaI and AgeI and insertion of hPGK.blast construct (GeneArt) via infusion cloning as per manufacturer's instructions. The US1 ORF was amplified from the HSV-1 genome by PCR using primers prW1656/1657 and extracted 1359 bp band was cloned via infusion cloning in YC1, previously linearized with MluI and NheI RE.

For transformation of pW-TH57 and LDJ5 chemically competent Stellar *E.Coli* cells were used and the suspension was spread onto ampicillin-LB plates kept overnight in the 37°C room. Next day, individual bacterial colonies were picked and resuspended in LB-medium containing 100 µg/ml ampicillin. MiniPrep and MidiPrep were performed as per manufacturer's instructions. All constructs used in this study were subjected to control restriction digestion and were sent for sequencing.

To generate V5-ICP27 and HA-ICP22 doxycycline-inducible cell lines, HEK-293T cells were transfected with pW-TH57 and LDJ5, respectively, as described in 4.3.7. Transduction of T-HF cells was done as described in 4.3.8. and successfully transduced cells were kept in selection with 5 µg/ml puromycin and 5 µg/ml blasticidin, respectively. To generate V5-ICP27 + HA-ICP22 doxycycline-inducible cell lines, HEK-293T cells were transfected with LDJ5, as described in 4.3.7. Transduction of V5-ICP27 expressing T-HF cells was done as described in 4.3.8. Transduced cells were kept under selection with both 5 µg/ml puromycin and 5 µg/ml blasticidin.

4.3.7. Lentivirus production

One day prior to transfection, 4 x 10^5 HEK-293T cells were evenly seeded on 6 well-dishes. Following the instructions of Lipofectamine 3000 Reagent Protocol, the transfection mixtures were prepared as 125 µl reactions in two separate tubes (as described below) and mixed by gentle pipetting.

Table 24. Transfection components

Buffer A	Volume	Buffer B	Volume/Concentration
Lipofectamine 3000	5 µl	P3000 reagent	5 µl
OptiMEM	120 µl	Lentiviral vector	4 ng
		Packaging vector psPAX2	3 ng
		Vsv-g vector	1 ng
		OptiMEM	Add to 125 µl

Both reaction tubes were incubated for 10 min at RT before they were added to the HEK-293T cells drop by drop. For verification of successful transfection, f6GW was used as a lentiviral control vector. F6GW transfected cells express enhanced green fluorescent protein (eGFP) under fluorescent light of approximately 495 nm wavelength.

4.3.8. Transduction of T-HF cells

Transduction usually took place one day after the transfection, unless the cells transfected with control vector f6GW did not yet express eGFP. HEK-293T cell supernatant containing lentivirus particles was harvested and filtered through a 0.45 μm filter. Virus-containing supernatant was then added to T-HF cells, which were seeded in 6-well plates (2.5 x 10^5 cells/well) a day prior to transduction. To increase the efficiency of transduction, plates were centrifuged for 30 min at 800 x g and kept in incubator at 37°C, 5 % CO_2 before splitting to 60 % confluence for selection with appropriate antibiotic 3 days later. The optimal dose of antibiotic for T-HFs was determined by a range of doses and the lowest dose that killed all the cells was used as a selection dose.

4.4. Biochemical methods

4.4.1. ChIPmentation

4.4.1.1. Cell seeding and infection

Two days prior to infection, 2.5 x 10^6 HFFF cells were seeded in 15cm^2 dishes. At the day of infection, cells roughly doubled in amount to 4.5 x 10^6 (≈ 80 % confluent). Cells were either HSV-1 WT strain F/17, ΔICP22 (R325) or mock infected as described in section 4.1.3. PAA (350 μg/mL) was added to the fresh cell culture media that was supplied to the cells after removal of virus inoculum.

4.4.1.2. Cell fixation

Medium was removed 8 hpi and cells were fixed by adding ChIP Cross-link Gold chemical according to manufacturer's instructions (Diagenode, #C01019027). Briefly, cells were washed two times with 1x RT PBS. Ten milliliters of 1x PBS containing 1 mM $MgCl_2$ were added to the cells and 40 μL of ChIP cross-link Gold chemical was gently pipetted drop by drop. To get the ChIP Cross-link Gold into the solution and to dissolve white precipitate, dishes were swirled immediately after the addition of the ChIP Cross-link Gold. Cells were incubated with the fixation

buffer for 30 min at RT after which the solution was removed and washed two times with 1x RT PBS. For additional fixation 37 % formaldehyde was diluted with 1x RT PBS to a final concentration of 1 % and added to the dishes for 15 minutes. To stop the fixation, glycine was added to the cells at the final concentration of 125 mM and incubated for 5 min at RT. Fixation solution was aspirated and cells were washed twice with 1x cold PBS. Cells were then scraped in 1 mL of cold 1x PBS containing protease inhibitor cocktail (1x) with an additional 1mM phenylmethylsulfonyl fluoride (PMSF). Cells were pelleted at 1500 rpm for 20 min at 4°C. Supernatant was aspirated and cell pellets were frozen in liquid N_2.

4.4.1.3. Cell lysis and sonication

Cell pellets were resuspended in 1-1.5 mL 0.25 % [v/v] SDS sonication buffer with 1x protease inhibitors and 1 mM additional PMSF and incubated on ice for 10 minutes. Cells were sonicated in ten to fifteen 1-minute intervals, 25 % amplitude, with Branson Digital Sonifier TM S-450 until most fragments were in the range of 200-700 bp as determined by agarose gel electrophoresis. For both sonicated and non-sonicated samples, 50 µL aliquots were taken.

4.4.1.4. Analyzing fragment size after sonication

Non-sonicated and sonicated 50 µL aliquots were subjected to de-crosslinking by adding 100 µL ChIPmentation de-crosslinking buffer and incubating for 1 h at 37°C without shaking and then o/n at 65°C with 1000 rpm to revert the crosslink. The next day, 4 mM EDTA and 200 µg/mL Proteinase K were added, and samples incubated for another 2 h at 45°C with 1000 rpm shaking. Supernatant was transferred into a new tube and another 100 µL of ChIPmentation de-crosslinking buffer was added for 1 hour at 45°C with 1000 rpm shaking. DNA was isolated by Phenol/Chloroform extraction (as described in section 4.3.4) and separated on E-Gel Agarose Gels with SYBR Safe DNA Gel Stain, 1.2 % (ThermoFisher Scientific, G521801). An example of the sonicated samples after gel separation is shown in Figure 9. Before starting with the immunoprecipitation step, most of the fragments should be between 200-700 bp.

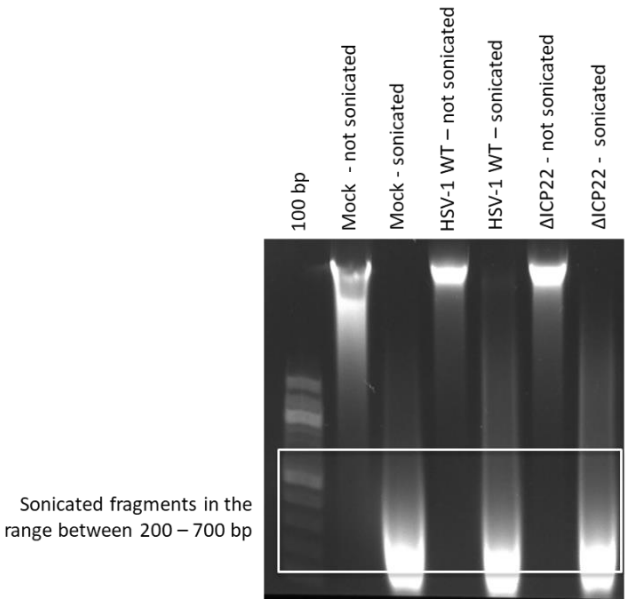

Figure 9. Sonication pattern of ChIPmentation samples.

DNA from de-crosslinked samples (Mock, HSV-1 WT and ΔICP22) was isolated with phenol/chloroform and loaded onto 1,2 % E-Gel Agarose Gels with SYBR Safe DNA Gel Stain. Unsonicated and sonicated samples represent roughly 1 % of the total sample volume. The white box indicates the ideal extent of sonication range to obtain high quality ChIPmentation data.

4.4.1.5. Immunoprecipitation and DNA-Tagmentation

Cell lysates used for the preparation of the ChIPmentation libraries were diluted 1:1.5 with equilibration buffer and spun at 14,000x g, 4°C for 10 minutes to pellet insoluble material. Supernatant was transferred to a new 1.5 mL screw-cap tube and topped up with RIPA-LS if necessary. Input and gel samples were preserved. Lysates were incubated with ChIP-antibodies (Table 10) on a rotator overnight at 4°C. Dependent on the added amount of antibody, the amount of Protein A or Protein G magnetic beads was adjusted (e.g. for 1-2 µg of antibody/IP = 15 µL of beads) and blocked overnight with 0 1 % [w/v] bovine serum albumin in RIPA buffer. On the following day, beads were added to the IP samples for 2 h on a rotator at 4°C to capture the antibody-bound fragments. The immunoprecipitated chromatin was subsequently washed twice with 150-750 µL each of cold buffers RIPA-LS, RIPA-HS, RIPA-LiCl and 10 mM Tris pH 8.0 containing

protease inhibitors. Beads were washed once more with ice-cold 10 mM Tris pH 8.0 lacking inhibitors and transferred into new tubes.

Dependent on the added amount of antibody, beads were resuspended in 25-50-75 µL of the ChIPmentation-transposition reaction mix. For 25 µL reaction, 5 µL of 5x Tagmentation buffer, 1 µL of Tagment DNA enzyme, and H_2O up to the final volume were added and incubated at 37°C for 10 minutes in a thermocycler. Beads were mixed after 5 minutes by gentle pipetting. To inactivate the Tn5 enzyme, 150-750 µL of cold RIPA-LS was added to the tagmentation reaction. Beads were washed twice with 150-750 µL of RIPA-LS and 1x Tris-EDTA and subjected to de-crosslinking by adding 100 µL ChIPmentation de-crosslinking buffer and incubating for 1 h at 37°C followed by overnight shaking at 65°C. The next day, 4 mM EDTA and 200 µg/mL Proteinase K were added, and samples incubated for another 2 h at 45°C with 1000 rpm shaking. Supernatant was transferred into a new tube and another 100 µL of ChIPmentation elution buffer was added for another hour at 45°C with 1000 rpm shaking. DNA was isolated with MinElute PCR Purification Kit according to manufacturer's instructions and eluted in 21 µL of H_2O.

4.4.1.6. Library amplification and ChIPmentation-seq

For the library quantification qPCR was set up as described below.

Table 25. ChIPmentation components – trial library

Component qPCR	Volume
100x SYBR	0,1 µL
ChIPmentation DNA	1,4 µL
IDT custom primer i5_1 (10 µm)	0,75 µL
IDT custom primer i7_1 (10 µm)	0,75 µL
NEBNext Ultra II Q5 Master Mix	5 µL
H_2O	2 µL

The following program was used:

Table 26. ChIPmentation trial library amplification program

Step	Cycle	Temperature	Time
Pre-warming	1	72°C	5 min
Initial template denaturation	1	98°C	30 sec

Denaturation		98°C	10 sec
Annealing	25	63°C	30 sec
Extension		72°C	30 sec
Final extension	1	72°C	1 min
		4°C	hold

The Cq value obtained from the library quantification, rounded up to the nearest integer plus one additional cycle, was used to amplify the rest of the ChIPmentation DNA using the same program as described above. DNA for the final library was prepared as follows:

Table 27. ChIPmentation components for final library amplification

Component qPCR	Volume
ChIPmentation DNA	13,75 µL
IDT custom primer i5_n (10 µm)	3,75 µL
IDT custom primer i7_n (10 µm)	3,75 µL
NEBNext Ultra II Q5 Master Mix	25 µL
H_20	3,75 µL

The concentration of the libraries was measured with Qubit dsDNA HS Assay Kit according to manufacturer's instructions. The quality of the purified ChIPmentation DNA was verified by Bioanalyzer before performing the sequencing at the BGI Genomics, Hong-Kong, China, or Core Unit Systemmedizin, Würzburg, Germany. All samples were sequenced at equimolar ratios. Sequencing of paired-end 35 bp reads was performed on a DNBSEQ at the same facility.

A brief workflow of ChIPmentation is shown in Figure 10.

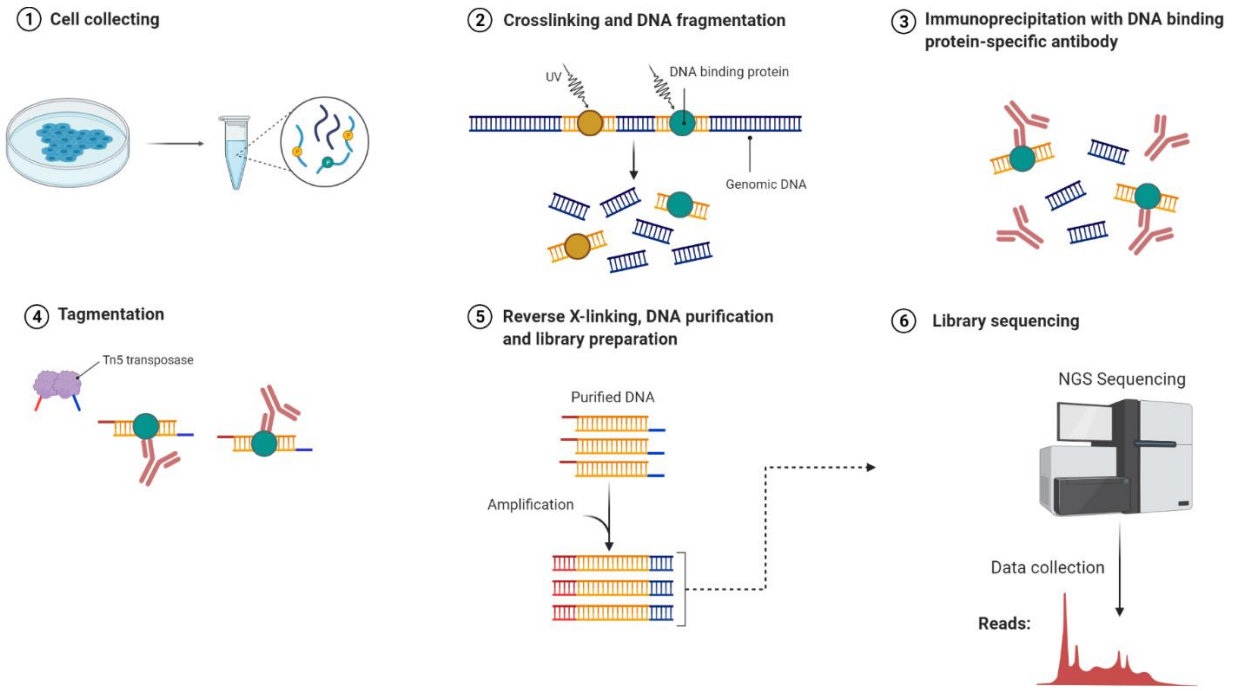

Figure 10. Schematic representation of ChIPmentation.

Cells are fixed with crosslinking reagent (e.g formaldehyde) and lysed thereafter. Chromatin is subjected to sonication followed by immunoprecipitation (IP). Standard ChIP-seq demands reverse-crosslinking followed by purification of ChIP-DNA, which is then subjected to library preparation in a multi-step procedure comprising end repair, purification, A-tailing, adapter ligation, and size exclusion. ChIPmentation however uses the sequencing adapters, 'Tn5 transposases', that are introduced in a single step by tagmentation on a bead-bound chromatin. After reverse-crosslinking, ChIP DNA is purified and subjected to library preparation.

Designed with BioRender.com (2020). Retrieved from https://app.biorender.com/biorender-illustrations.

4.4.2. Assay for Transposase-Accessible Chromatin using sequencing (ATAC-seq)

ATAC-seq was performed as described previously [246], with some modifications. Briefly, nuclei were isolated from 100 000 HFFF cells. On the day of the experiment cells were scraped, transferred to Eppendorf DNA lo-bind tubes and span at 300x g for 5 min at 4°C. The supernatant was removed, and the cells were resuspended in 1x PBS following centrifugation at 300x g for another 5 min at 4°C. PBS was carefully removed, and the cell pellets resuspended in 50 µL 1x

ice cold lysis buffer. After incubation on ice for 15 minutes cell nuclei were pelleted by spinning at 600x g for 10 min at 4°C. Lysis buffer was carefully removed, nuclei pellets were washed once more with 50 µL 1x ice cold lysis buffer and the centrifugation step was repeated.

To treat samples with transposase, lysis buffer was removed, and the nuclei pellets were resuspended in 25 µL ATAC-transposition buffer. Samples were incubated at 37°C for 30 min. Tagmented DNA was purified with the MinElute PCR purification kit according to manufacturer's instructions and eluted in 20 µL of nuclease free H_20.

ATAC-DNA for the library was prepared as a 50 µL reaction as described below.

Table 28. ATAC-seq components for library amplification

Component	Volume
DNA	20 µL
IDT custom primer i5_n (10 µm)	5 µL
IDT custom primer i7_n (10 µm)	5 µL
Nextera PCR Mix	15 µL
PPC (PCR Primer Cocktail) (10 µm)	5 µL

The following program was used:

Table 29. ATAC-seq program for library amplification

Step	Cycle	Temperature	Time
Pre-warming	1	72°C	5 min
Initial template denaturation	1	98°C	30 sec
Denaturation		98°C	10 sec
Annealing	11	63°C	30 sec
Extension		72°C	3 min
Final extension	1	72°C	2 min
		4°C	hold

PCR amplified libraries were either stored at - 80°C or processed immediately as follows. To purify the libraries and remove excess primers smaller than 100 bp, Agencourt AMPureXP beads were used according to manufacturer's instructions. Per each 1.0 µL of sample, 1.8 µL AMPure XP beads was added (in total, 90 µL of beads for 50 µL reaction). Purified DNA library was eluted from the beads in 20 µL nuclease-free H_20 and its concentration was measured with Qubit dsDNA

HS Assay Kit according to manufacturer's instructions. Fragment size distribution was determined using the Agilent 2100 Bioanalyzer and High Sensitivity DNA Kit according to manufacturer's instructions. To pool libraries equimolarly, size selection was performed between 150 bp and 1000 bp and molar concentration for each library was calculated. Library pool was loaded on E-Gel EX Gel 1.2 % Agarose gel with SYBR Gold II and visualized on E-Gel precast gel electrophoresis system. Gel was excised between 150 and 1000 bp and the DNA isolated with Monarch DNA Gel Extraction Kit was eluted in 20 µL nuclease free H_20. Ready library pool was sequenced by NextSeq 500 (Ilumina) at the Core Unit Systemmedizin, Würzburg, Germany (35bp paired-end reads).

A brief workflow of ATAC-seq is shown in Figure 11.

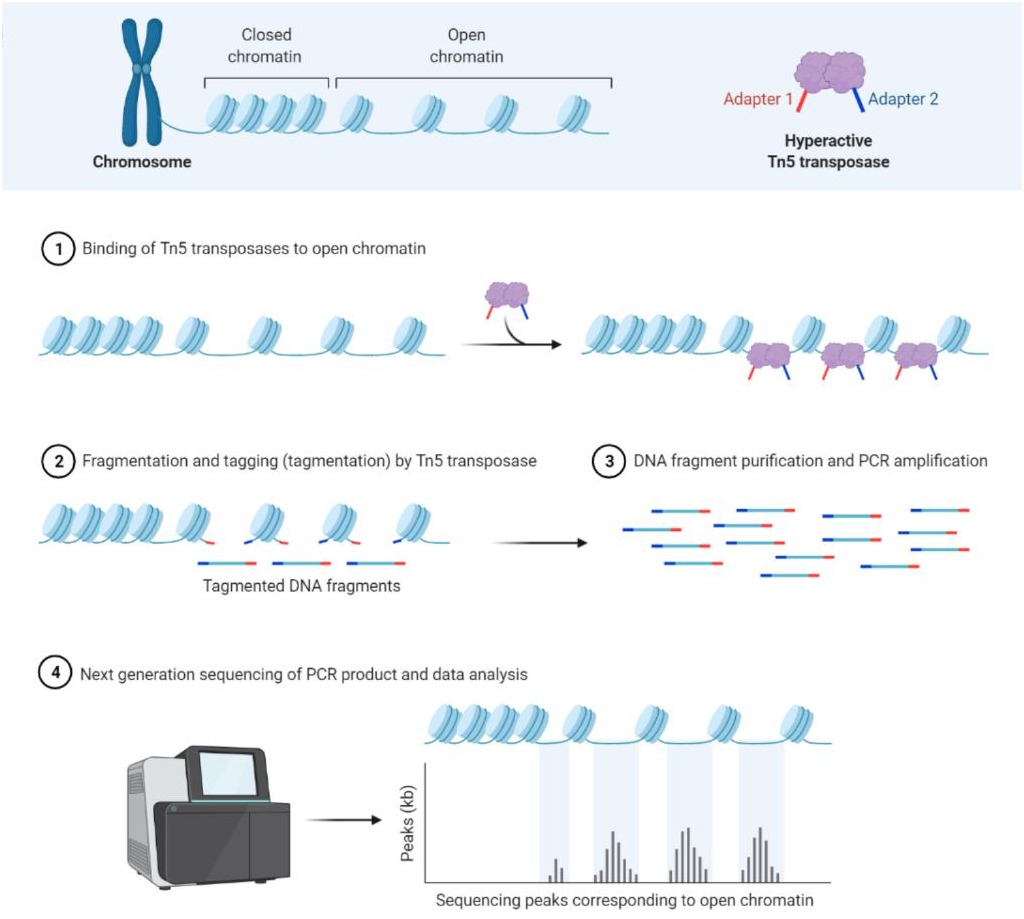

Figure 11. Schematic representation of ATAC-seq (Assay for Transposase-Accessible Chromatin using sequencing).

ATAC-seq is a high-throughput technique that facilitates studying chromatin accessibility across the genome. (1) In ATAC-Seq, genomic DNA incorporates highly active, genetically engineered Tn5 transposase. (2) Tn5 simultaneously fragments DNA, leaving a 9-bp staggered nick, and into open chromatin sites adds sequencing-compatible primers (a process known as 'tagmentation'). During this process, 9-bp duplication is created as the nick is repaired. (3)(4) Purified and amplified DNA fragments are then subjected to paired-end sequencing (facilitates higher unique alignment rates of OCRs) which identifies open chromatin regions and subsequential data analysis provides insight into the gene regulation [246,247].

Designed with BioRender.com (2020). Retrieved from https://app.biorender.com/biorender-illustrations.

4.4.3. Omni-ATAC-seq

During the course of this work, the ATAC-seq protocol for chromatin accessibility profiling was updated to an improved version, termed Omni-ATAC-seq, with increased signal-to-background ratio thus requiring reduced sequencing depth. It was performed as described previously [248].

Briefly, cells were seeded in 24-well plates 24 hours before the experiment. On the day of the experiment cells were scraped, transferred to Eppendorf DNA lo-bind tubes and span at 500x g for 5 min at 4°C. The supernatant was aspirated, and the cells were washed with 1x PBS following centrifugation at 500x g for another 5 min at 4°C. PBS was carefully removed, and the cell pellets resuspended in 50 µL 1x cold ATAC-RSB buffer 2. The samples were incubated for 3 minutes on ice and the lysis reaction was stopped with addition of 1 mL of 1x ATAC-RSB buffer 3. Cell nuclei were pelleted at 500x g for 10 min at 4°C and the supernatant was aspirated. Cell nuclei were resuspended in 50 µL Omni-ATAC transposition buffer by pipetting up and down few times and incubated at 37°C for 30 minutes in a thermo-shaker with 1000 RPM mixing. Tagmented DNA was purified with the DNA Clean & Concentrator-5 Kit according to manufacturer's instructions and eluted in 20 µL of nuclease free H_20. To determine cycles necessary to amplify the libraries a pre-amplification qPCR was set as described below.

Table 30. Omni-ATAC-seq trial library amplification program

Component	Volume
DNA	2 µL
IDT custom primer i5_n (10 µm)	1.5 µL
IDT custom primer i7_n (10 µm)	1.5 µL
2 x NEBNext Ultra II Q5 Master Mix	6.25 µL
SYBR (100 x)	0.125 µL
H_20	1 µL

The following program was used:

Table 31. Omni-ATAC-seq trial library amplification program

Step	Cycle	Temperature	Time
Pre-warming	1	72°C	5 min
Initial template denaturation	1	98°C	30 sec
Denaturation		98°C	10 sec
Annealing	20	63°C	30 sec
Extension		72°C	1 min
		4°C	hold

To set the number of PCR cycles needed to amplify each sample, linear Rn value was plotted against cycle number that corresponds to 1/3 of maximum fluorescent intensity.

The remaining DNA was amplified to the cycle number determined by qPCR as follows following the same program.

Table 32. Omni-ATAC-seq components for final library amplification

Component	Volume
DNA	12.5 µl
IDT custom primer i5_n (10 µm)	6.25 µl
IDT custom primer i7_n (10 µm)	6.25 µl
2x NEBNext Ultra II Q5 Master Mix	25 µl

PCR amplified libraries were either stored at - 80°C or processed immediately as follows. The following steps in processing Omni-ATAC libraries are as described in 4.4.2.

4.4.4. Total RNA-seq (ribosomal RNA depletion)

To confirm the presence of read-through transcription, total RNA was collected on the day of ATAC/Omni-ATAC-seq experiment and sent for Total RNA-seq. Briefly, cells were collected in 500 µL TRI reagent (Sigma-Aldrich, T9424) and total RNA was isolated with Quick-RNA Microprep Kit according to manufacturer's instructions. Biological duplicates were carried out. Following steps were performed by the Core Unit Systemmedizin, Würzburg, Germany. For the total RNA libraries, both cytoplasmic and mitochondrial rRNA species were depleted. Libraries were sequenced on NextSeq 500 (Ilumina), on the same run as ATAC/Omni-ATAC samples. Quality monitoring and output settings were handled according to standards described by 't Hoen et al.

4.5. Bioinformatical analysis

4.5.1. Read alignment

Sequencing reads for ATAC-seq, Omni-ATAC-seq, total RNA-seq, 4sU-seq and ChIPmentation were mapped against (i) the human genome (GRCh37/hg19), (ii) human rRNA sequences and (iii) the HSV-1 genome (HSV-1 strain 17, GenBank accession code: JN555585, only for HSV-1 infection data) using ContextMap v2.7.9 [249] (using BWA as short read aligner [250] and allowing a maximum indel size of 3 and at most 5 mismatches). For the two repeat regions in the HSV-1 genome, only one copy each was retained, excluding nucleotides 1–9,213 and 145,590–152,222.

4.5.2. Analysis of open chromatin regions

For ATAC-seq, Omni-ATAC-seq data, BAM files with mapped reads were converted to BED format using BEDTools [251] and OCRs were determined from these BED files using F-Seq with default parameters [252]. No filtering of OCRs was performed. dOCR length for a gene was calculated as previously described [234]. In brief, downstream OCRs were assigned to each gene in the following way. First, all OCRs overlapping with the 10 kb downstream of a gene were assigned to this gene. Second, OCRs starting at most 5 kb downstream of the so far most downstream OCR of a gene were also assigned to this gene. This was performed iteratively, until no more OCRs could be assigned. Here, individual OCRs could be assigned to multiple genes. dOCR length of a gene was

then calculated as the total genomic length downstream of this gene covered by OCRs assigned to the gene. Similarly, OCR length in gene bodies was calculated as the total genomic length of the gene bodies covered by OCRs.

4.5.3. Quantification of downstream transcriptional activity and read-through

The number of read fragments per gene or in downstream regions were determined from the mapped total RNA-seq or 4sU-seq reads in a strand-specific manner using featureCounts [253] and gene annotations from Ensembl (version 87 for GRCh37). For genes, all read pairs (= fragments) overlapping exonic regions on the corresponding strand by ≥25 bp were counted for the corresponding gene. For downstream regions, all fragments overlapping the 5 kb downstream of the gene 3'end were counted. Gene expression and downstream transcriptional activity were quantified in terms of fragments per kilobase of exons per million mapped reads (FPKM) and averaged between replicates. Only reads mapped to the human genome were counted for the total number of mapped reads for FPKM calculation.

Percentage of read-through was calculated as previously described [234]. Briefly, first the percentage of transcription downstream a gene was calculated separately for each replicate as: Percentage of downstream transcription = 100 x (FPKM in 5 kb downstream of gene)/(gene FPKM). Percentage of downstream was averaged between replicates and transcription percentage of read-through was then calculated as percentage of downstream transcription in infected – percentage of downstream transcription in uninfected or untreated cells. Negative values were set to 0.

4.5.4. Metagene analysis

Metagene analysis was performed as previously described [254] using the software developed for this publication.

* The list of figures generated by the group of Prof. Dr. Caroline Friedel can be found on page 144.

5. RESULTS

5.1. Expression of HSV-1 viral late genes is not required for dOCR induction

Disruption of transcription termination (DoTT) during lytic HSV-1 infection is accompanied by an increase in chromatin accessibility downstream of the affected host genes (dOCR) [234]. We hypothesize that this results from impaired histone repositioning in the wake of elongating Pol II downstream of genes. The underlying molecular mechanism behind this phenotype, however, remains unclear. Considering that we observed dOCR induction as early as 4 hpi, we first asked whether viral genome replication and therefore viral late gene expression was required for it. To clarify this and identify the responsible viral gene, we employed ATAC-seq (Assay for Transposase-Accessible Chromatin using sequencing) to analyze changes in genome-wide chromatin accessibility between different conditions (Figure 11).

Primary HFFF cells were either mock or HSV-1 infected with strains F and 17 with or without the presence of phosphonoacetic acid (PAA). PAA is a chemical compound that inhibits the viral DNA polymerase and thus expression of viral late (γ2) genes. Considering that we previously observed less read-through transcription for infection with strain F than with strain 17 at 8 hpi, ATAC-seq was also performed at 12 hpi. Quantification of the extent of the dOCR induction for individual host genes was performed as described in the method section 4.5.2. We restricted our analysis to 4,162 cellular genes that did not show significant read-in transcription due to read-through of an upstream gene. In contrast to mock infected cells which only showed very short dOCRs, both WT strain 17 and F induced extensive dOCRs, with WT strain 17 leading to longer dOCRs (Figure 12a). Even at 12 hpi, strain F showed less dOCR induction than strain 17 at 8 hpi.

Strikingly, PAA treatment resulted in a significant increase in dOCR length for both strains. Of note, addition of PAA strongly reduced the percentage of ATAC-seq reads that mapped to the viral genome due to the inhibition of viral DNA replication. In consequence, the percentage of cellular reads substantially increased.

To normalize for differences in the number of cellular ATAC-seq reads on dOCR lengths, down-sampling analysis was performed such that all samples had approximately the same number of reads mapping to the cellular genome (Figure 12b). This confirmed the longer dOCR occurring in both strains with PAA treatment. We conclude that viral DNA replication and viral late gene expression are not required for dOCR induction.

To investigate whether longer dOCRs arise as a consequence of differential viral gene expression upon PAA treatment, we analyzed total RNA for WT strain F (Figure 12c). PAA treatment resulted in downregulation of all classes of HSV-1 genes, with the strongest reduction observed for late genes. This is of no surprise, as by inhibiting late genes the progression of HSV-1 infection is dampened and thus, to some extent, the expression of IE and E genes also affected. With this we conclude that the dOCR phenotype doesn't arise as a result of elevated expression of certain classes of HSV-1 viral genes.

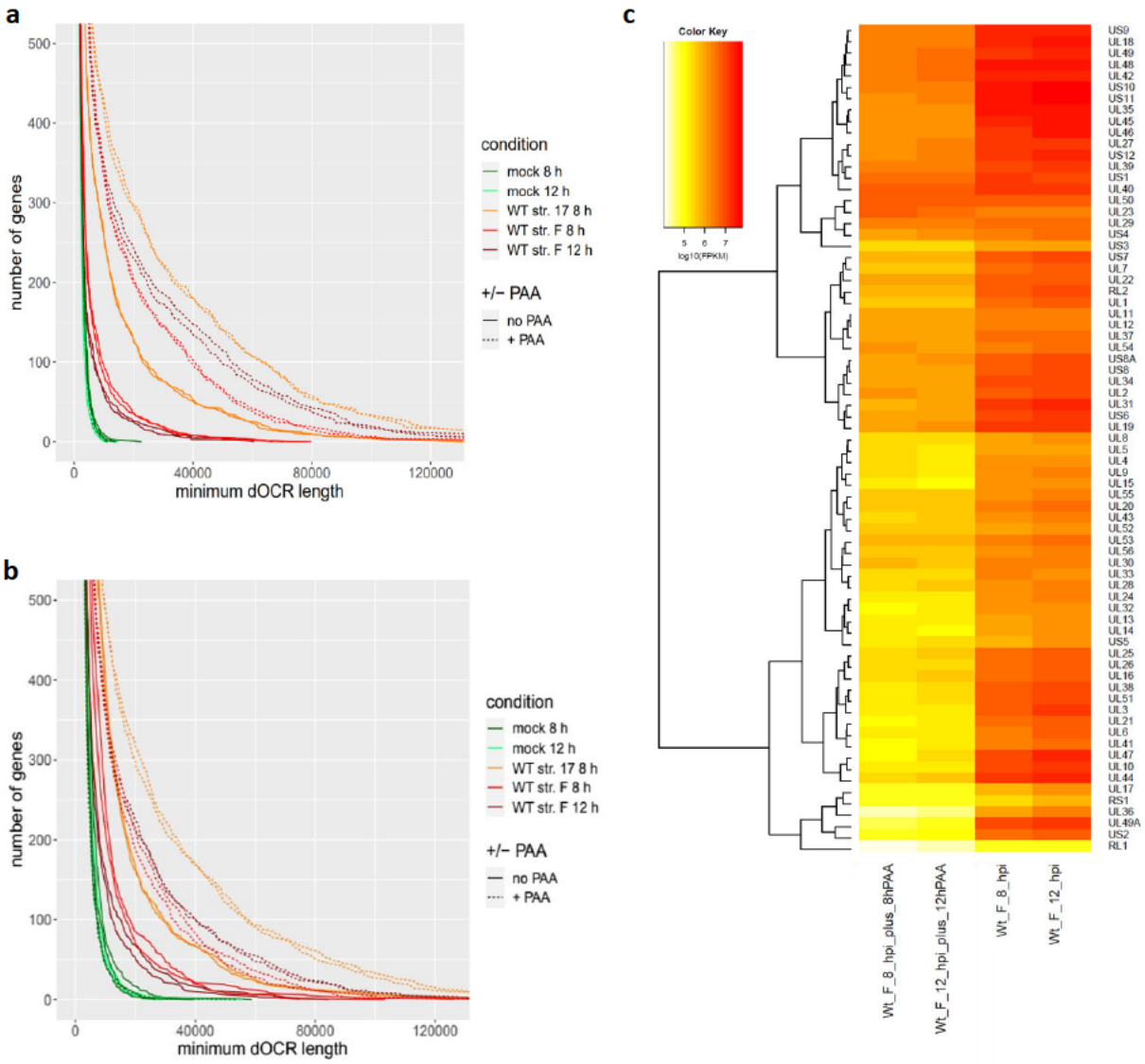

Figure 12. Induction of dOCRs in the WT HSV-1 infection.

Number of genes (y-axis) that exhibited dOCRs of at least the respective length (x-axis) in mock and WT infection (strain F and 17) at 8 and 12 hpi **(a)** without down-sampling (n=2 biological replicates) and **(b)** after down-sampling to the approximately the same number of reads mapped to the cellular genome (n=2 biological replicates). The number of genes on the y-axis is restricted to ones that have dOCR. Out of 4162 analyzed genes, many have a dOCR length of zero Dashed lines represent samples treated with PAA. **(c)** Heatmap of total RNA for WT strain F and WT strain F+PAA for two different times of infection. FPKM values were calculated by normalizing the number of fragments (=read pairs) overlapping each HSV-1 gene by the length of each gene in kb and the number of reads mapped to the human genome in million.

5.2. High level of transcriptional activity downstream of genes leads to dOCR induction

To screen for the responsible viral gene using ATAC-seq for HSV-1 null mutants of interesting candidate genes available to us, we aimed to define a subset of cellular genes with significant strong and consistent dOCR induction upon HSV-1 infection. To this end, we performed an unsupervised clustering analysis of dOCR length for mock, WT and WT+PAA condition (Figure 13). This analysis identified a total of nine gene clusters, out of which six clusters (depicted in green and blue bars) showed no dOCRs upon HSV-1 infection, regardless of the employed strain and PAA treatment. However, three gene clusters (depicted in orange and red bars) showed different degrees of significant dOCR induction. Clusters 2 (290 genes, orange bar) and 6 (701 genes, red bar) exhibited weaker dOCR induction, visible upon PAA treatment for both strains and times of infection. We observed the strongest dOCR induction for cluster 5 (305 genes, dark red bar) already in WT infection for both strains, that became even more pronounced upon PAA treatment (WT+PAA). Of note, these three clusters differed in dOCR presence prior to the onset of infection. Namely, clusters 5 and 6 showed some short dOCR induction already in mock cells that further extended upon infection, unlike in cluster 2 where we observed no dOCR induction prior to infection.

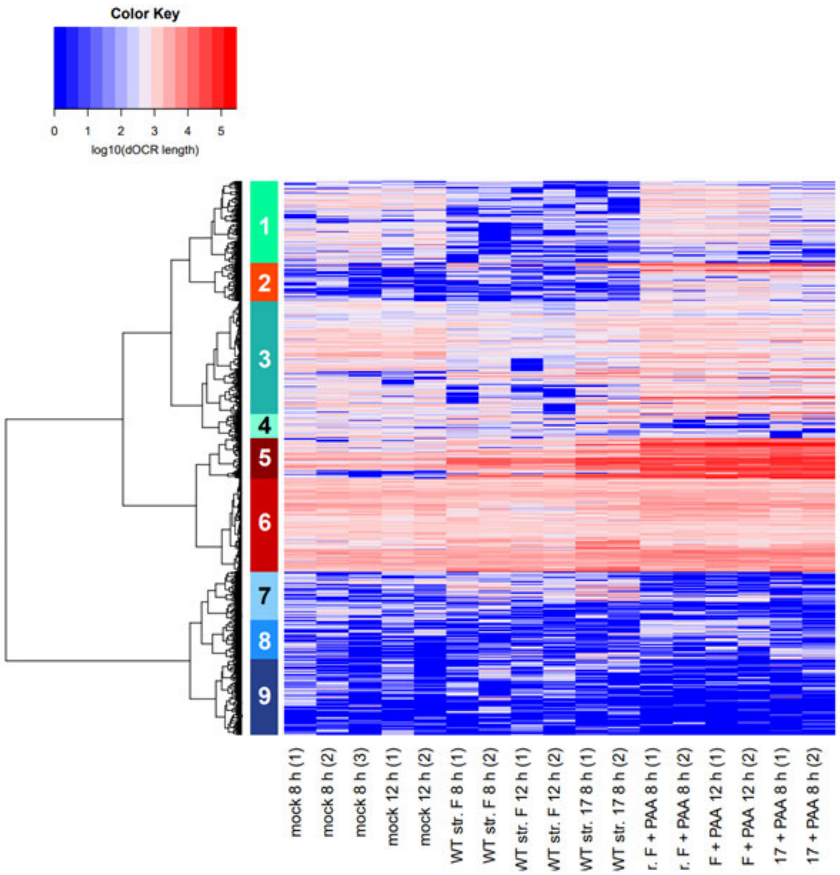

Figure 13. Hierarchical clustering analysis of cellular genes based on ATAC-seq data.

The analysis was based on log10(dOCR length) in mock, WT (strain 17 and F) and WT+PAA infection for two different times of infection. Clustering was performed according to Ward's clustering criterion and Euclidian distances. This identified nine clusters (depicted in colored bars with numbers on the left), with three of these clusters (2, 5, 6, from orange to dark red) representing different degrees of dOCR induction.

To elucidate the cause of observed differences in the dOCRs induction between the nine gene clusters, we used previously published 4sU-seq time-course data for the first 8 h of HSV-1 strain 17 infection [140]. The analysis was based on: (1) the percentage of read-through transcription (difference between HSV 1 and mock infected cells in the following ratio: FPKM within 5 kb downstream of the gene 3' end / gene FPKM x 100) and (2) the absolute extent of transcriptional read-through activity (FPKM within 5 kb downstream of the gene 3' end, indicated as 'downstream FPKM'), both previously found to correlate with dOCR induction [234]. While all clusters exhibited increasing read-through during the course of the infection, the differences

between the gene clusters were minor, with cluster 2 (orange bar, weak dOCR) characterized by the highest percentage of read-through transcription (Figure 14a). In contrast, the analysis of downstream transcriptional activity for the same data set showed that cluster 5 (dark red bar, strongest dOCR) exhibited the strongest downstream FPKM when compared to other clusters (Figure 14b). Clusters 2 and 6 (weak dOCR) were characterized by slightly increased downstream FPKM values when compared to all clusters without dOCR induction, at least late in infection. Furthermore, this observation correlated with higher gene expression values (gene FPKM in cluster 5 both prior to and throughout the infection (Figure 14c). Cluster 2 showed no significant difference when compared to clusters without dOCR induction, while cluster 6 exhibited slightly increased gene FPKMs throughout the whole time-course.

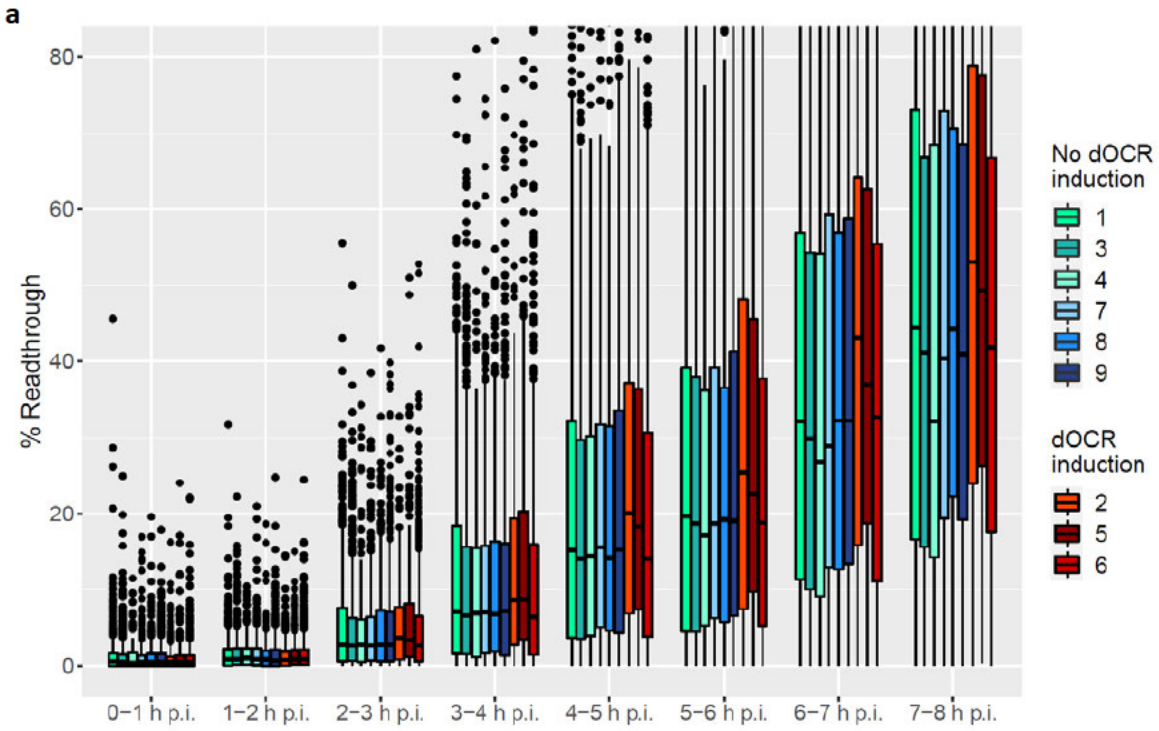

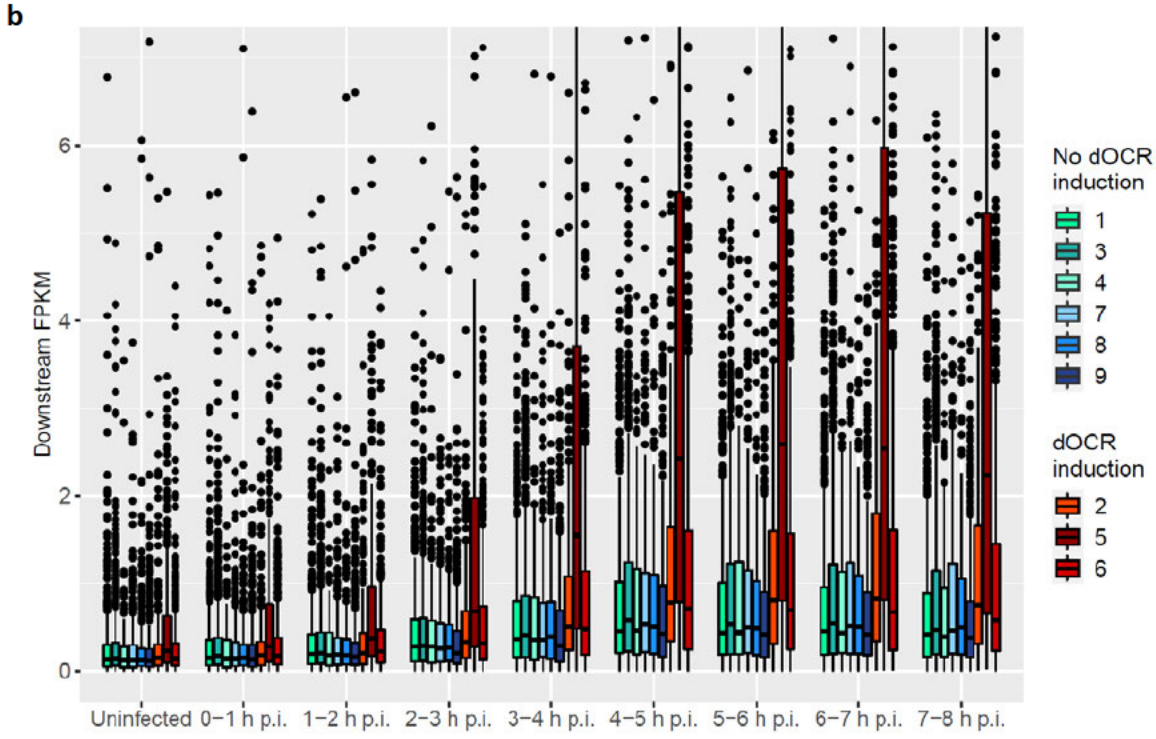
b
Downstream FPKM
0
2
4
6
Uninfected
0–1 h p.i.
1–2 h p.i.
2–3 h p.i.
3–4 h p.i.
4–5 h p.i.
5–6 h p.i.
6–7 h p.i.
7–8 h p.i.
No dOCR induction
1
3
4
7
8
9
dOCR induction
2
5
6

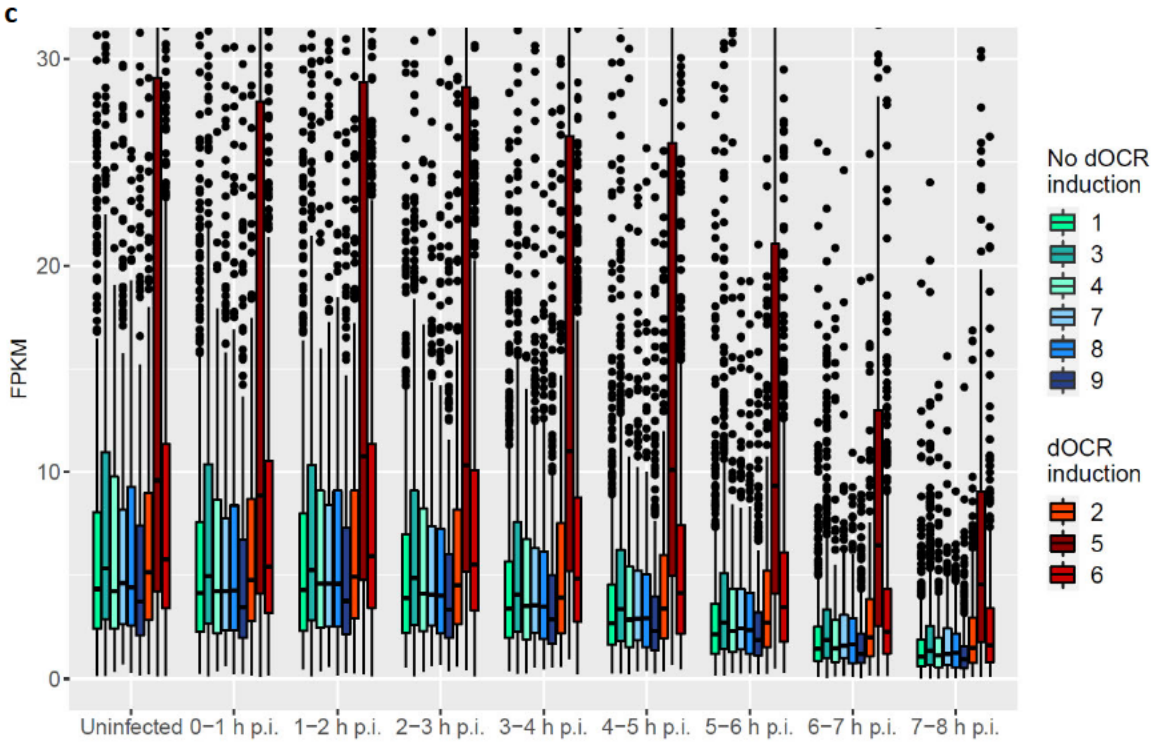
c
FPKM
0
10
20
30
Uninfected
0–1 h p.i.
1–2 h p.i.
2–3 h p.i.
3–4 h p.i.
4–5 h p.i.
5–6 h p.i.
6–7 h p.i.
7–8 h p.i.
No dOCR induction
1
3
4
7
8
9
dOCR induction
2
5
6

Figure 14. dOCR formation is dependent on the absolute extent of transcriptional activity downstream of genes, extending beyond poly(A) sites, rather than on the percentage of read-through transcription. **(a)** Boxplots showing the percentage of read-through transcription in the WT strain 17 4sU-seq time-course for nine gene clusters. Read-through transcription was calculated as described in [234]. **(b)** Boxplots showing distribution of downstream FPKM transcription in the WT strain 17 4sU-seq time-course for nine gene clusters. **(c)** Boxplots showing distribution of gene expression (gene FPKM) in the WT strain 17 4sU-seq time-course for nine gene clusters.

Of note, WT infected cells treated with PAA exhibited higher downstream FPKM and stronger dOCR induction. Thus, cellular genes comprising cluster 5 represent highly expressed genes with extensive read-through transcription. Throughout the course of the infection, clusters 2 and 6 also showed elevated downstream transcriptional activity compared to the clusters without apparent dOCR induction (Figures 14b). We conclude that the extent of dOCR induction is dependent on the absolute extent of transcriptional activity downstream of the respective genes rather than on the percentage of read-through transcription.

Induction of dOCR can thus be observed for genes with high percentage of read-through but relatively low gene expression (cluster 2) and for genes with a moderate percentage of read-through but higher gene expression (cluster 6). Both of these exhibit a similar extent of dOCR induction. Interestingly, although transcription within gene bodies was at least as high as transcription downstream, OCRs only occurred downstream of affected gene 3' ends and not within gene bodies [234]. In summary, dOCR formation selectively arises due to HSV-1-induced DoTT, when a high level of transcriptional activity extends downstream of genes beyond poly(A) sites.

5.3. ICP22 but not ICP27 is required for dOCR formation

Major HSV-1 transcriptional regulators are immediate-early (IE) genes. To identify the viral gene responsible for the dOCR phenotype, we performed ATAC-seq for a panel of HSV-1 single gene deletion mutants using infection of HFFF cells. This experiment involved null mutants of the IE genes ICP0, ICP27 and ICP22 as well as of the virion host shut-off protein (vhs), which is the major viral RNA regulator [83]. HSV-1 null mutants lacking ICP0 and ICP22 are attenuated. Therefore, ATAC-seq was performed at 12 hpi rather than 8 hpi. For WT and other null mutants, ATAC-seq was performed at 8 hpi. ICP22 triggers a loss of Pol II forms bearing Ser2 phosphorylation (Ser2P Pol II), which might be involved in dOCR induction [255]. Of note, an ICP22-independent mechanism has also been proposed to contribute to the loss of Ser2P which depends on viral late gene expression [255,256]. We thus included PAA treatment for ΔICP22 infection to address the role of Ser2P in dOCR induction. The following analysis were performed on cluster 5 containing genes to focus on the strongest dOCR induction (Figure 15a). Cells infected with ΔICP0 and Δvhs virus still induced strong dOCR comparable to WT strain 17 infection. However, infection with ΔICP27 virus led to a reduced dOCR induction. This is in accordance with the reduced read-through transcription upon infection with ICP27-null mutant [235]. These data suggest that residual DoTT and therefore weak dOCR induction are presumably stress induced. Surprisingly, dOCR induction in the ΔICP22 mutant virus was comparable to mock infected cells, suggesting that ICP22 may be responsible for dOCR induction. This phenotype was quite striking considering that ΔICP22 exhibited substantially more read-through transcription in comparison to ΔICP27 infection [235]. Furthermore, PAA treatment, which increased dOCR in WT infection, had no discernible effect on dOCR formation in ΔICP22 infection.

To validate this finding, ATAC-seq was repeated for the ΔICP22 mutant compared to its parental WT strain F at 8 and 12 hpi ± PAA treatment (Figure 15b). Again, we observed no induction of dOCR in the absence of ICP22 protein. Additionally, ΔICP22 mutants derived from KOS 1.1 and from BAC-derived WT strain 17 further confirmed previous finding (Figure 16a, b).

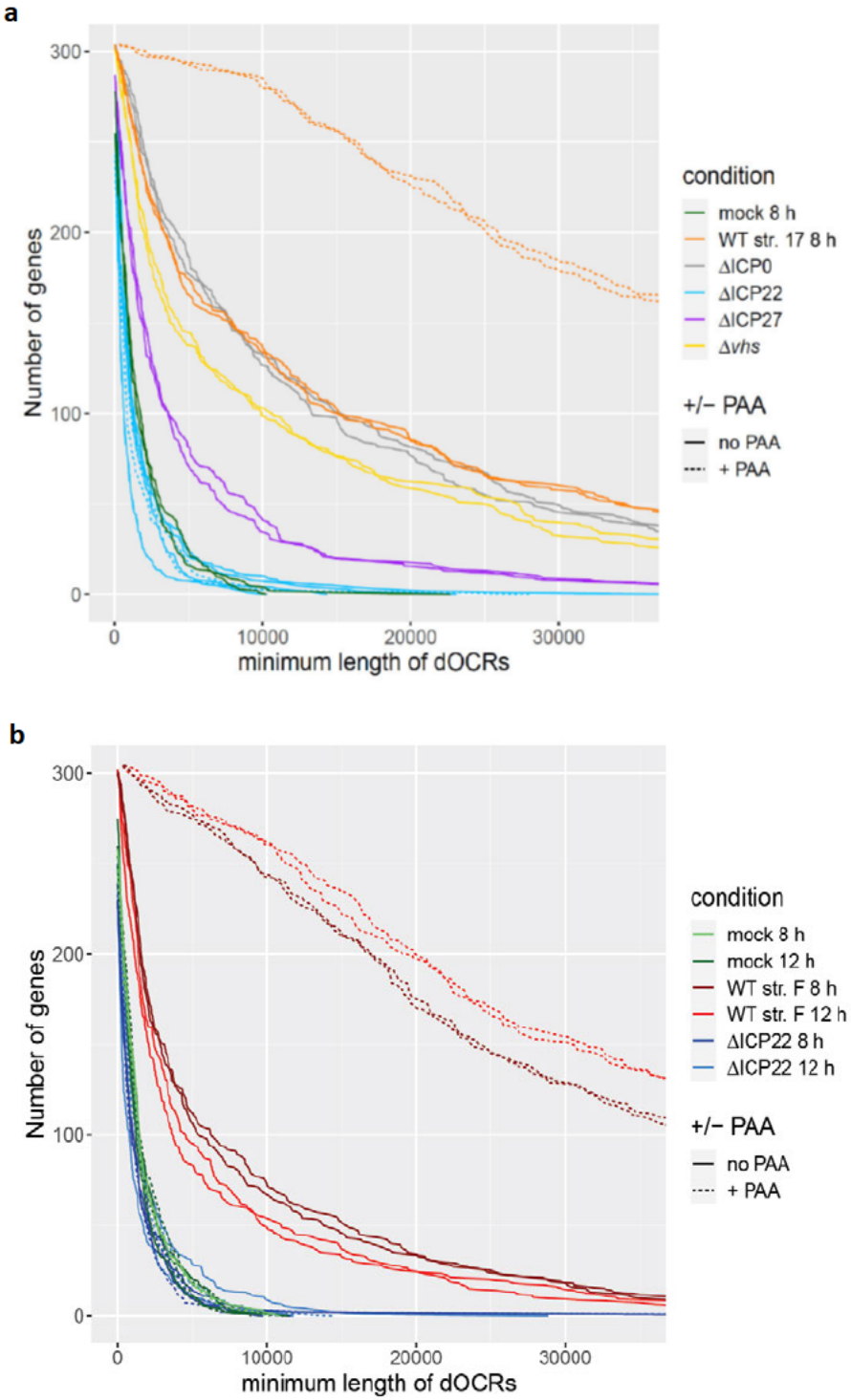

Figure 15. Induction of dOCR in a single-gene deletion mutant infection

(a) Number of genes (y-axis) in cluster 5 that exhibit dOCR of at least the respective length (x-axis) in mock, WT strain 17 (± PAA treatment), ΔICP27, Δvhs (8 hpi, respectively), ΔICP22 (± PAA treatment) and ΔICP0

(12 hpi, respectively) infection (n=2 biological replicates). **(b)** Number of genes (y-axis) in cluster 5 that exhibit dOCR of at least the respective length (x-axis) in mock, WT strain F, and ΔICP22 (± PAA treatment at 8 and 12 hpi respectively) (n=2 biological replicates). Dashed lines represent samples treated with PAA.

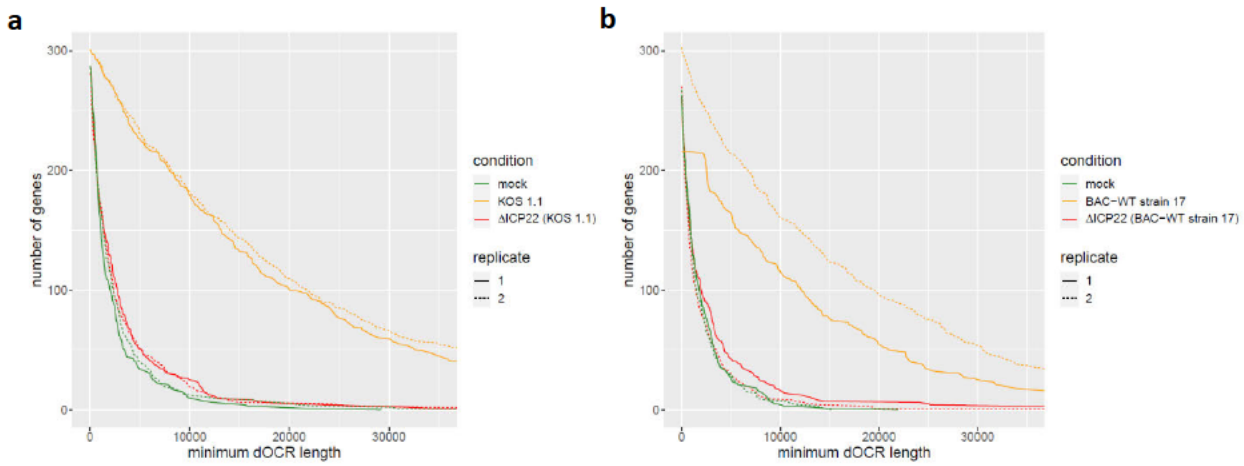

Figure 16. Induction of dOCR in ΔICP22 infection.

Number of genes (y-axis) in cluster 5 that exhibit dOCR of at least the respective length (x-axis) in **(a)** mock, WT strain KOS1.1 infection and infection with a ΔICP22 mutant derived from KOS1.1 (all with PAA treatment) and **(b)** mock, WT strain 17 (BAC-derived) infection and infection with a ΔICP22 mutant derived from BAC-WT strain 17 (no PAA treatment) (n=2 biological replicates).

In parallel to ATAC-seq we performed total RNA-seq and confirmed the presence of extensive DoTT and strong downstream transcriptional activity in both Wt strain F and ΔICP22 infection regardless of time point and PAA treatment (Figure 17). The following data for WT strain F infection confirmed a strong correlation between dOCR induction and high downstream transcriptional activity (FPKM downstream) (Figure 17a, b). After the PAA treatment this correlation was even more prominent, where the number of genes with strong downstream FPKM also increased (Figure 17c, d). Although we observed the same increase in the number of genes with strong downstream FPKM in ΔICP22 infection, no dOCRs were induced (Figure 17 e-h). We conclude that ICP22 is required for dOCR induction as no correlation between the two parameters was observed.

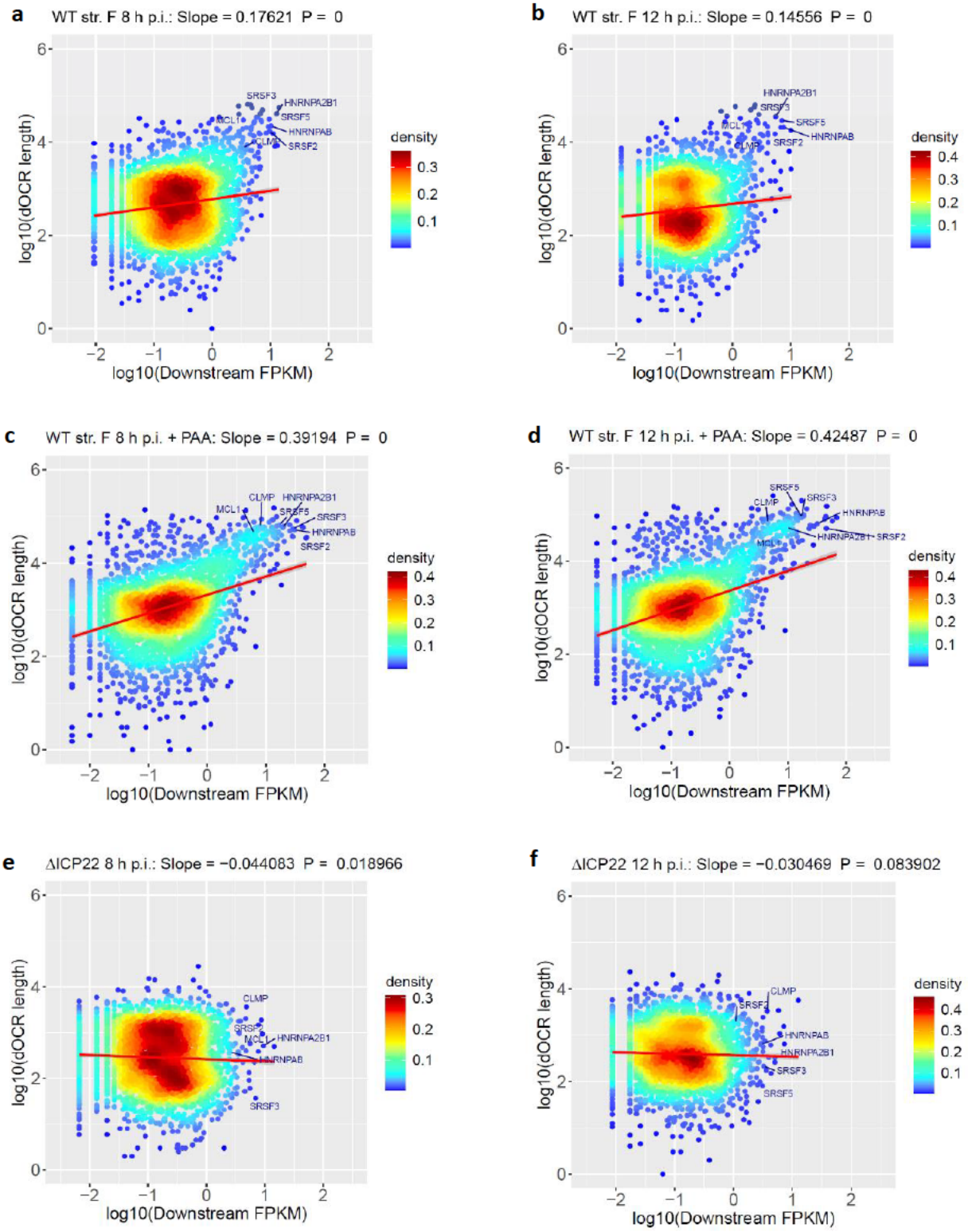
a
WT str. F 8 h p.i.: Slope = 0.17621 P = 0
b
WT str. F 12 h p.i.: Slope = 0.14556 P = 0
c
WT str. F 8 h p.i. + PAA: Slope = 0.39194 P = 0
d
WT str. F 12 h p.i. + PAA: Slope = 0.42487 P = 0
e
ΔICP22 8 h p.i.: Slope = −0.044083 P = 0.018966
f
ΔICP22 12 h p.i.: Slope = −0.030469 P = 0.083902
log10(dOCR length)
log10(Downstream FPKM)
density
SRSF3
HNRNPA2B1
SRSF5
HNRNPAB
CLMP
SRSF2
MCL1

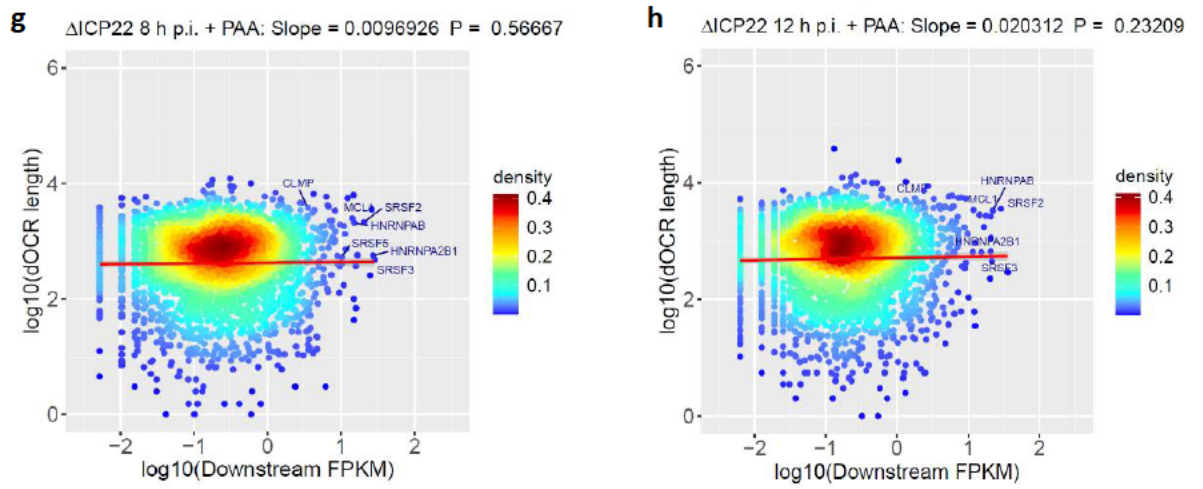

Figure 17. ICP22 is required for dOCR induction.

Scatter plots comparing downstream FPKM in total RNA against dOCR length (n=2 biological replicates). The red line indicates a linear fit of log10(dOCR length) against log10(downstream FPKM). Slope and p-value are indicated on top of each figure. Example genes with high dOCR induction in HSV-1 infection are indicated by names. Results are shown for **(a-d)** WT strain F ± PAA for 8 and 12 hpi and **(e-h)** ΔICP22 infection ± PAA for 8 and 12 hpi.

To elucidate the role of ICP27 in dOCR induction, downstream FPKM values and dOCR length were correlated for all single-gene deletion mutants from previously published 4sU-seq data [235]. When compared to the WT strain 17 infection, both ΔICP0 and Δvhs showed strong correlation in dOCR induction with transcriptional activity downstream of genes (Figure 18 a-c). This trend was also observed for ΔICP27 infection, however, to a lesser extent (Figure 18d). As previously reported, ICP27 is responsible for HSV-1 induced-DoTT both in the viral context and when ectopically expressed [235]. However, the minority of residual DoTT observed in ΔICP27 infection is probably the result of stress-induced transcriptional activity downstream of genes, sufficient to induce dOCR. As observed in the total RNA-seq data, a mutant virus lacking ICP22, irrespective of the PAA treatment, showed no dOCR induction (Figure 18 e-f). These data additionally confirm that ICP22 is required for dOCR induction.

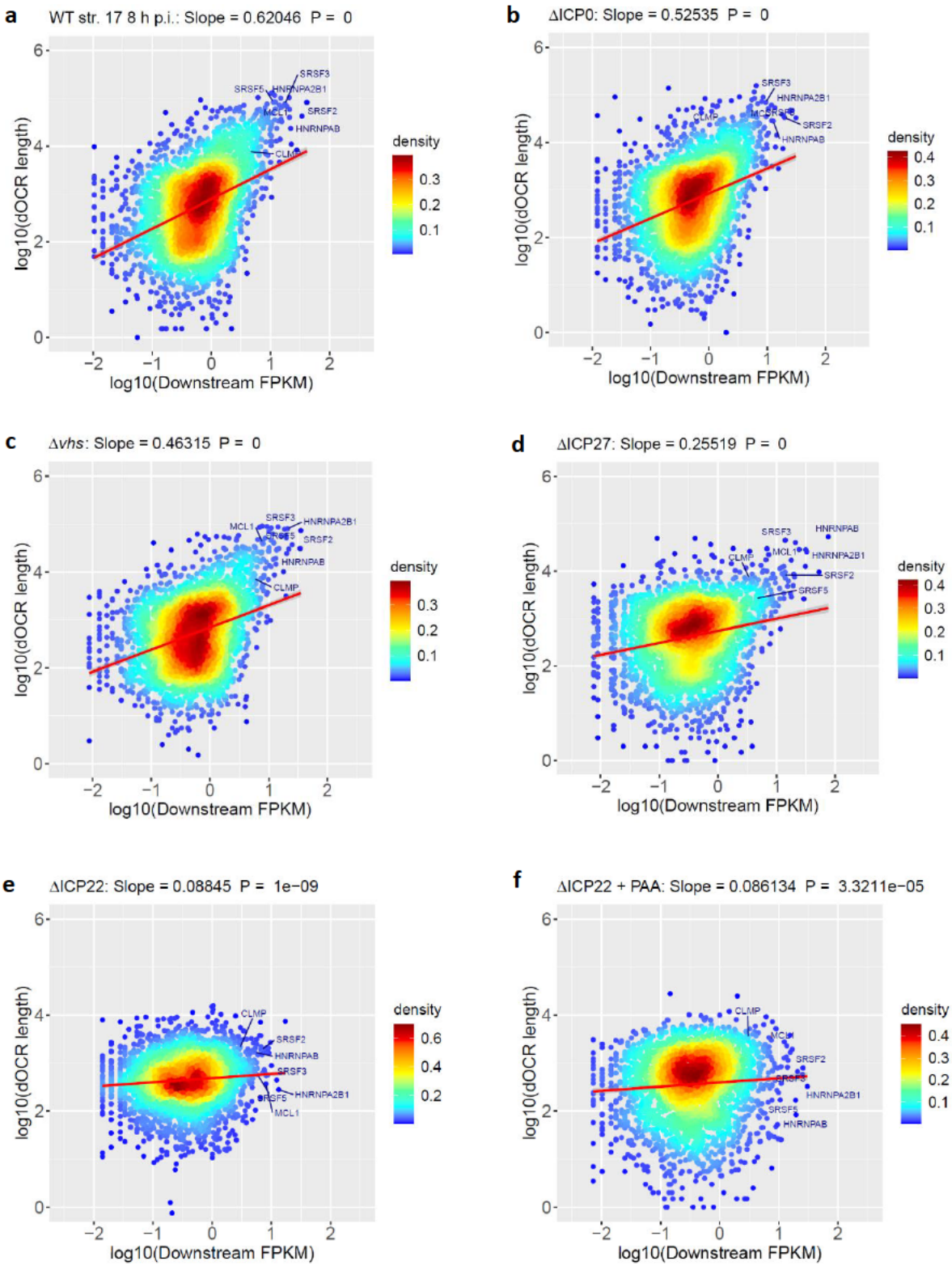
a
WT str. 17 8 h p.i.: Slope = 0.62046 P = 0
b
ΔICP0: Slope = 0.52535 P = 0
c
Δvhs: Slope = 0.46315 P = 0
d
ΔICP27: Slope = 0.25519 P = 0
e
ΔICP22: Slope = 0.08845 P = 1e−09
f
ΔICP22 + PAA: Slope = 0.086134 P = 3.3211e−05
log10(dOCR length)
log10(Downstream FPKM)
density
SRSF3
SRSF5
HNRNPA2B1
MCL1
SRSF2
HNRNPAB
CLMP

Figure 18. ICP27, vhs and ICP0 are not required for dOCR induction.

Scatter plots comparing downstream FPKM in 4sU-RNA against dOCR length (n=2 biological replicates). The red line indicates a linear fit of log10(dOCR length) against log10(downstream FPKM). Slope and p-value are indicated on top of each figure. Example genes with high dOCR induction in HSV-1 infection are indicated by names. Results are shown for **(a)** WT strain 17 for 8 hpi, **(b)** ΔICP0 infection for 12 hpi, **(c)** Δvhs infection for 8 hpi, **(d)** ΔICP27 infection for 8 hpi and **(e-f)** ΔICP22 infection ± PAA for 12 hpi.

5.4. ICP22 is sufficient to induce dOCR formation upon disruption of transcription termination

So far, transcription downstream of genes as well as ICP22 expression were shown to be necessary to induce dOCR in the context of viral infection. To test whether ectopically expressed ICP22 is sufficient to induce dOCR, Telomerase-Immortalized Human Foreskin Fibroblasts (T-HFs) were generated that conditionally express either ICP22 in isolation (T-HF ICP22 cells) or in combination with ICP27 (T-HF ICP22/ICP27 cells) upon Dox treatment (Figure 19a-d). Polyclonal T-HF cells were generated as explained in 4.3.6.2. Both proteins carried an N-terminal tag due to lack of availability of antibodies against the two target proteins. Upon 48 h treatment with Dox (5µg/mL) immunoblot and immunofluorescence analysis showed successful induction of both HA-ICP22 and HA-ICP22/V5-ICP27.

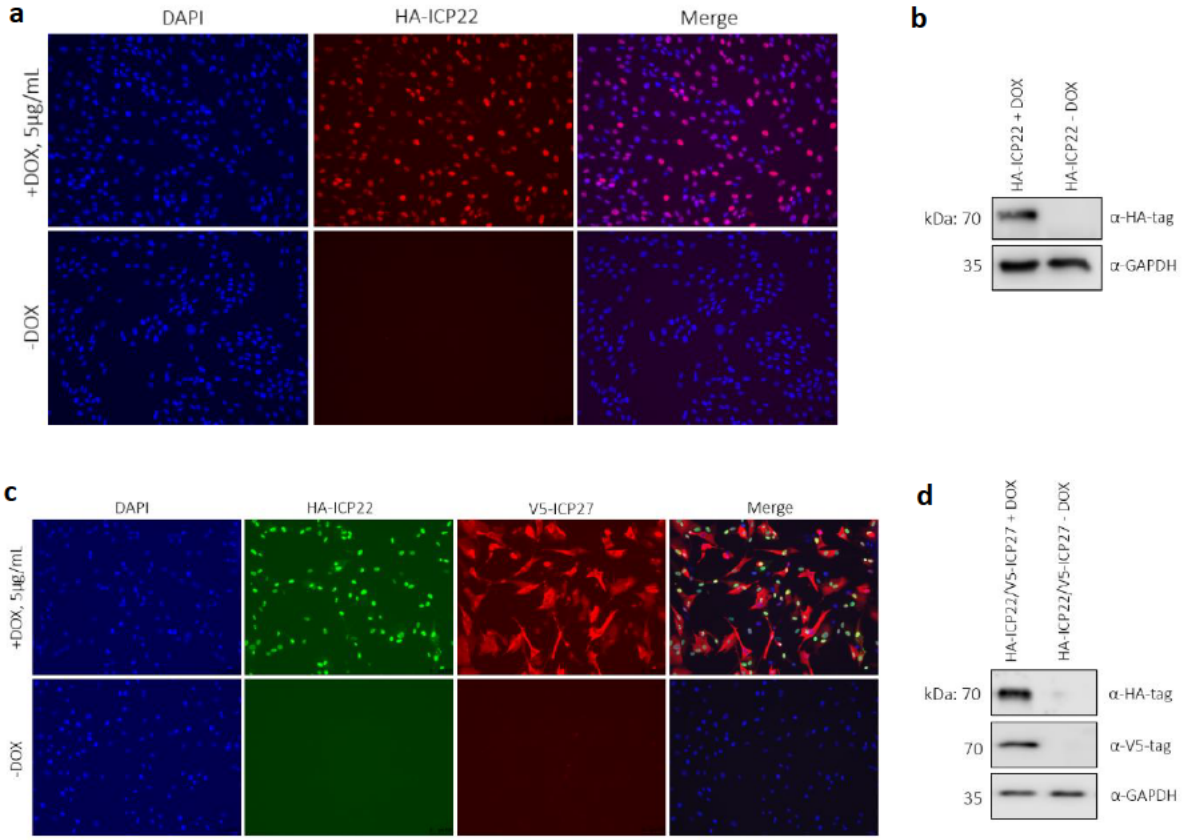

Figure 19. Ectopic expression of HA-ICP22 and HA-ICP22/V5-ICP27 in T-HF cells upon Dox exposure.
(a,b) T-HFs transduced with inducible HA-ICP22-expressing lentivirus were seeded with/without (±) the presence of 5μg/mL Dox and collected 48 h post induction Upon addition of Dox cells express HA-ICP22. Immunofluorescence and western blot images were obtained from the day of Omni-ATAC-seq experiment. **(a)** HA-ICP22 protein is shown in red and DAPI depicts cell nuclei. Mean value of cells expressing HA-ICP22 was calculated from there different fields of the same experiment and is ~88%. **(b)** Total cell lysates were collected 48 h post Dox-induction and were probed for the HA-tag. GAPDH was used as a loading control. **(c-d)** V5-ICP27 doxycycline-inducible polyclonal cells transduced with inducible HA-ICP22-expressing lentivirus were seeded with ± Dox (5μg/mL) and collected 48 h post induction. Upon addition of Dox cells express both HA-ICP22 and V5-ICP27. Immunofluorescence and western blot images were obtained from the day of Omni-ATAC-seq experiment. **(c)** HA-ICP22 protein is shown in green, V5-ICP27 is shown in red and DAPI depicts cell nuclei. Mean value of cells expressing HA-ICP22, V5-ICP27, or HA-ICP22 and V5-ICP27 was calculated from three different fields of the same experiment and is ~80%, 90%, 90% respectively. **(d)** Total cell lysates were collected 48 h post Dox-induction and were probed for the HA-tag and V5-tag. GAPDH was used as a loading control.

To test whether ICP22 is sufficient to induce DoTT-associated dOCR in a non-viral context, we generated cells with co-expression of ICP27 (T-HF ICP22/ICP27 cells) or exposed T-HF ICP22 cells to two hours of salt stress (80 mM KCl).

At this point of time in this work, we switched from ATAC-seq to Omni-ATAC-seq due to its improved signal-to-noise ratio resulting from a 13-fold reduction of reads mapping to mitochondrial DNA [248]. In parallel, we confirmed ICP27- and stress-induced read-through transcription by total RNA-seq. Of note, Dox-induced expression of ICP22 was not sufficient to trigger significant amount of dOCR formation. Due to insufficient reads mapping to the human genome in one of the two Omni-ATAC-seq replicates, we could only analyze one replicate properly (data not shown). Interestingly, co-expression of ICP27 and ICP22 resulted in extensive dOCR formation (Figure 20a, b). This was accompanied by substantial transcription downstream of genes confirming previous findings made in HeLa cells showing that ectopic expression of ICP27 is indeed sufficient to disrupt transcription termination [235] (Figure 20c). T-HF cells lacking the expression of ICP22 exposed to salt stress did not show dOCR induction, consistent with

previously published data in HFFF cells (Figure 20d) [234]. In the presence of ICP22, salt stress also triggered dOCR, although not to the same extent as when both ICP22 and ICP27 were expressed (Figure 20a, b). Moreover, fewer genes showed strong downstream transcriptional activity when compared to ICP27 induced DoTT (Figure 20e).

RNA-seq analysis confirmed that the lower extent of dOCR induction in salt stress after Dox-induced ICP22 is due to less transcriptional activity downstream of genes in salt stress compared to WT infection [234]. Consistent with some leaky expression of ICP22 and ICP27 in the absence of Dox, weak dOCR induction could also be observed in unstimulated T-HF ICP22/ICP27 cells (Figure 20a, b). Together, these data confirmed that ICP22 is both sufficient and necessary to induce dOCR upon either ICP27- or salt-stress induced DoTT.

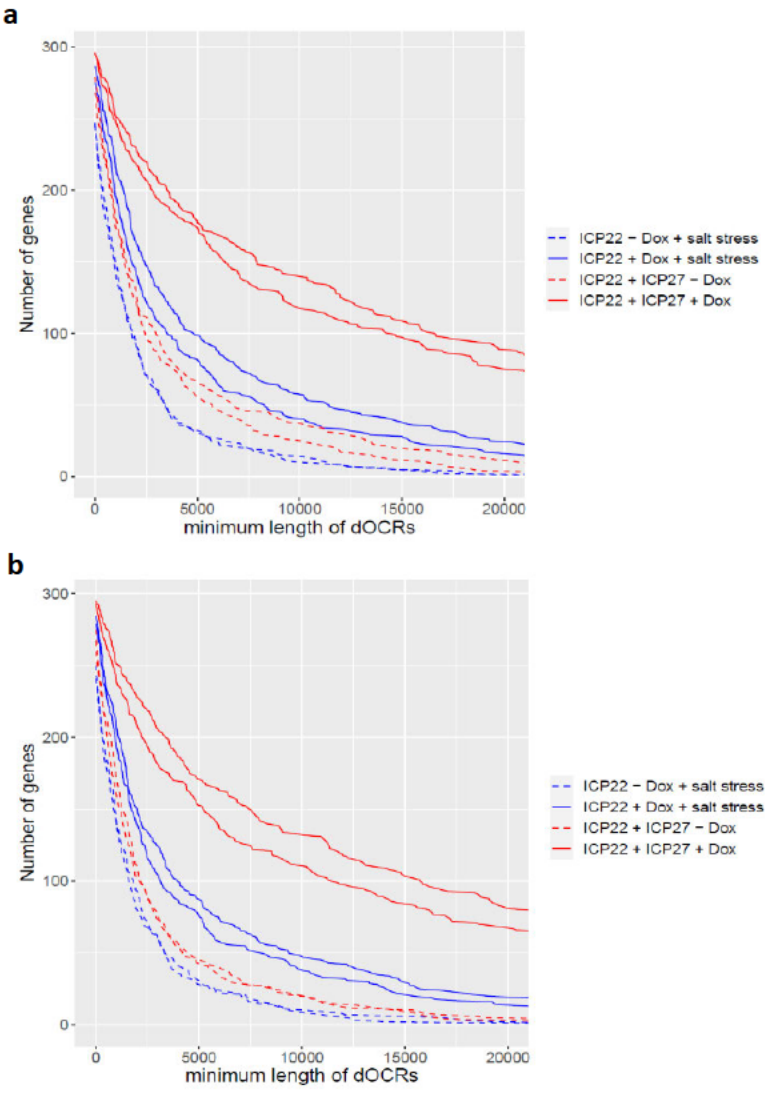

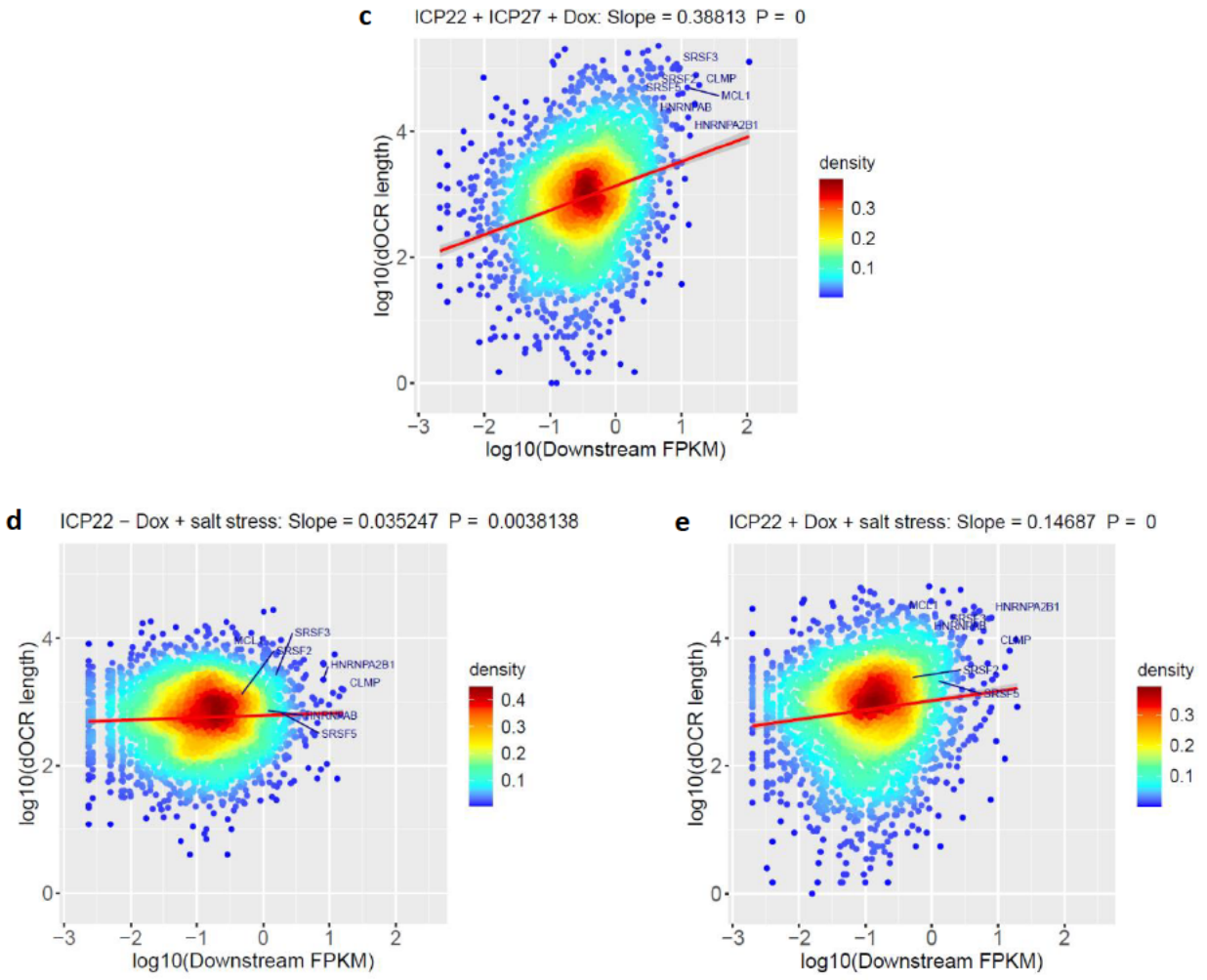

Figure 20. ICP22 is sufficient to induce dOCR upon ICP27- and salt stress-induced DoTT

(a) Number of genes (y-axis) in cluster 5 that exhibit dOCR of at least the respective length (x-axis) in T-HF ICP22/ICP27 cells ±Dox (red) and T-HF-ICP22 cells (± Dox) exposed to 2 h salt stress (blue). **(b)** Results shown after down-sampling to approximately the same number of reads on the cellular genome (n=2 biological replicates). **(c)** Scatter plot comparing downstream FPKM in total RNA (x-axis) against dOCR length (n=2 biological replicates) for cells expressing both ICP22 and ICP27 (T-HF ICP22/ICP27 cells + Dox). The red line indicates a linear fit of log10(dOCR length) against log10(downstream FPKM). Slope and p-value are indicated on top of each figure. Scatter plots comparing downstream FPKM in total RNA (x-axis) against dOCR length (n=2 biological replicates) for **(d)** ICP22-non expressing cells exposed to 2 h salt stress (T-HF ICP22 cells - Dox) or **(e)** ICP22-expressing cells exposed to 2 h salt stress (T-HF ICP22 cells + Dox). The red lines indicate a linear fit of log10(dOCR length) against log10(downstream FPKM). Slope and p-value are indicated on top of each figure.

5.5. HSV-1 infection causes alterations in histone linker H1 distribution downstream of genes

We proposed that HSV-1-induced dOCR arises due to epigenetic changes occurring in the wake of Pol II transcription downstream of cellular genes [234]. Recent studies support this hypothesis and show mobilization of histone marks during the HSV-1 infection [257–259]. Thus, to analyze HSV-1 induced changes in histone occupancy and histone modifications in the cellular genome during lytic HSV-1 infection we established a rapid and low-input chromatin immunoprecipitation (ChIP-seq) approach, termed ChIPmentation. In contrast to the adaptor ligation commonly applied in ChIP-seq, ChIPmentation utilizes adaptor insertion by 'tagmentation' via Tn5 transposase directly on a bead-bound chromatin (Figure 10).

We employed ChiPmentation to analyze genome-wide occupancy of canonical histone H3 as well as major histone modification marks associated with either heterochromatin regions (H3K27me3) or active transcription (H3K36me3) for mock and HSV-1 strain 17 infection at 8 hpi. Quality of the ChIPmentation data was confirmed by metagene analyses showing the expected chromatin occupancy profiles. For canonical H3 histone, there was a strong depletion at the transcription start site (TSS) for both mock and HSV-1, when compared to the gene bodies and downstream regions. The same pattern was observed for both genes with dOCR induction (cluster 5, strong dCOR) (Figure 21a) and genes that exhibit no dOCR (all genes except clusters 2,5 and 6) (Figure 21b). Interestingly, no notable difference in levels of histone H3 downstream of the affected genes were found (Figure 21a, b).

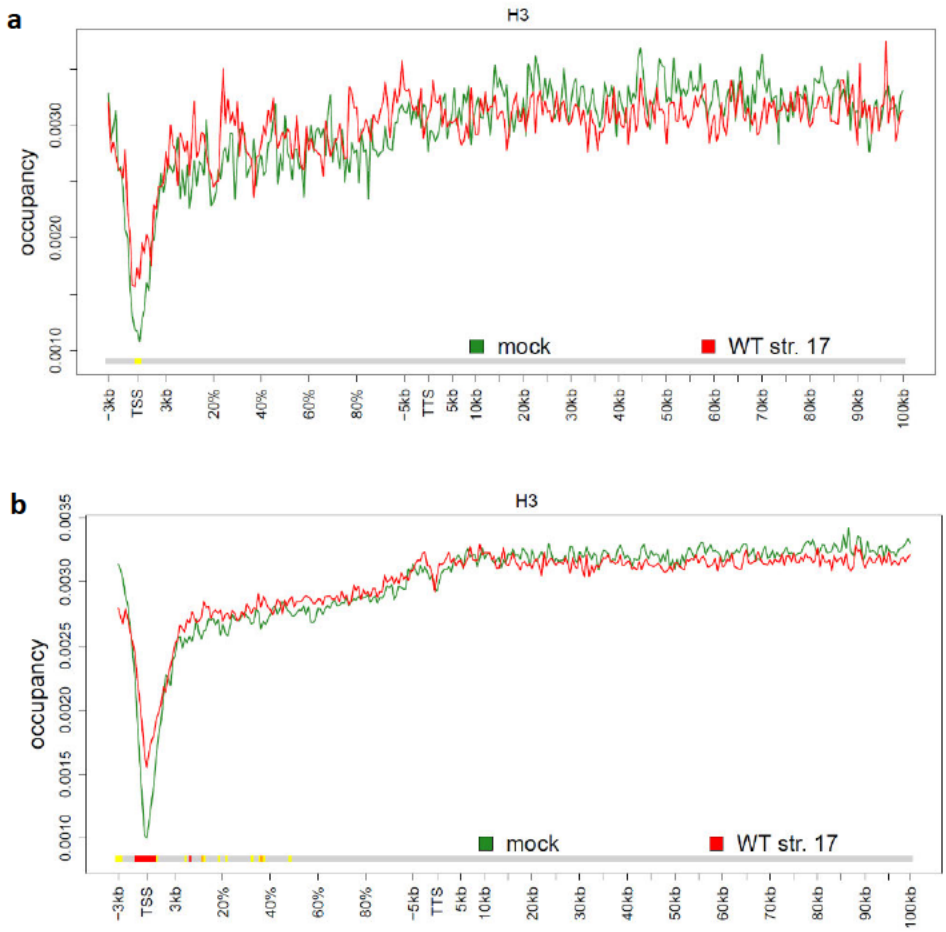

Figure 21. H3 occupancy on cellular genome does not change in dOCR during HSV-1 infection.

Metagene plots for genes **(a)** with strong dOCR induction (cluster 5) and genes **(b)** without dOCR induction, i.e. all analyzed genes apart from clusters 2,5 and 6 in mock and HSV-1 WT strain 17 infection (n=2-3 biological replicates). The color track at the bottom of each subfigure indicates the significance of paired Wilcoxon tests comparing the normalized transcript coverages for each bin between mock and WT infection. P-values are adjusted for multiple testing with the Bonferroni method within each subfigure; color code: red = adjusted p-value $\leq 10^{-5}$, orange = adjusted p-value $\leq 10^{-3}$, yellow = adjusted p-value $\leq$ 0.05.

Profiles for both active and repressive histone modification marks were in accordance with their usual distribution in untreated cells. Enrichment of heterochromatin mark H3K27me3 was observed outside of genes while it was depleted from gene bodies (Figure 22a). A mark of active

transcription, H3K36me3 was highly abundant on the gene bodies but not outside of genes (Figure 22c). Of note, a small but significant increase of H3K27me3 was found on TSS and gene bodies for genes without dOCR induction during HSV-1 infection (Figure 22b). This is presumably due to the general reduction in host transcriptional activity during infection. Similar increase at the TSS was observed for H3K36me3 in genes without dOCR (Figure 22d). In conclusion, core histone occupancy remained globally unchanged by dOCR formation.

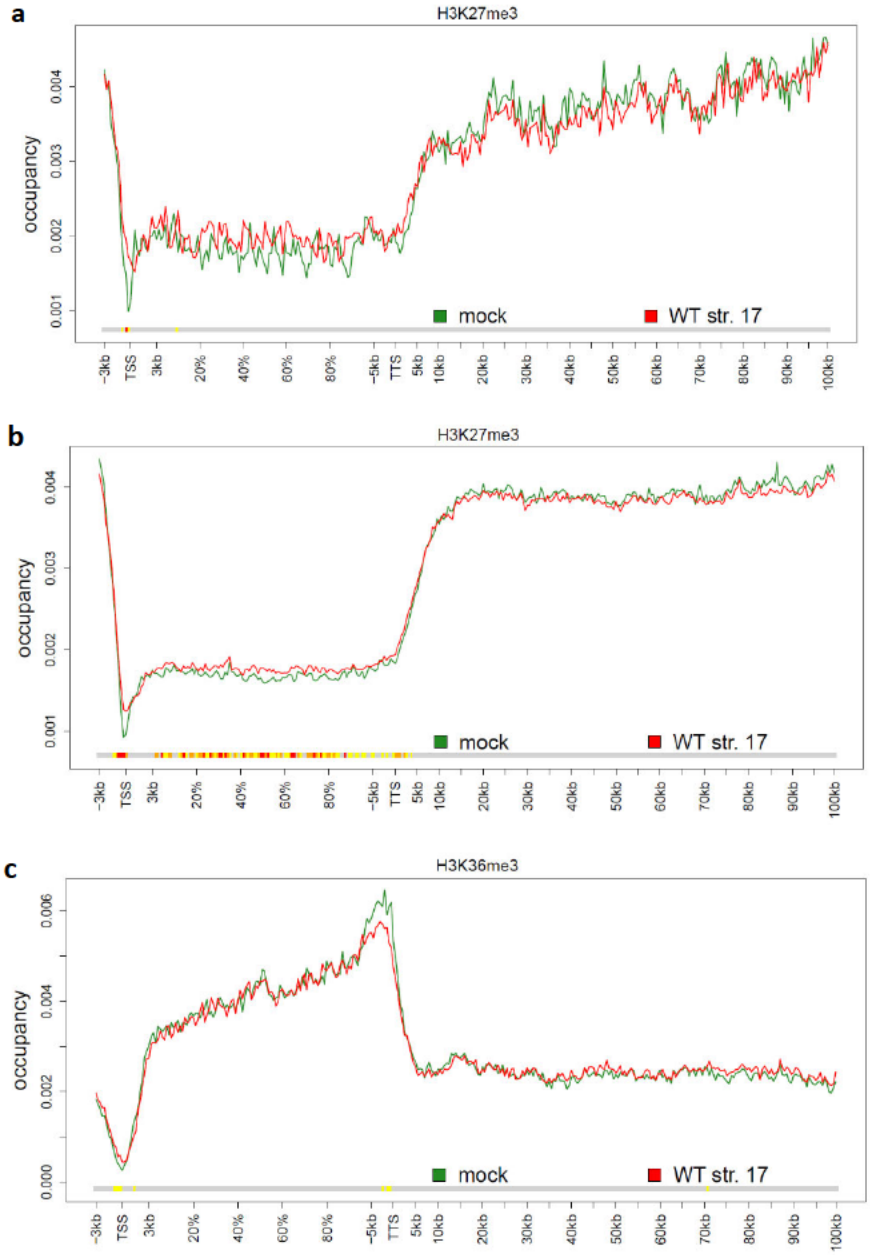

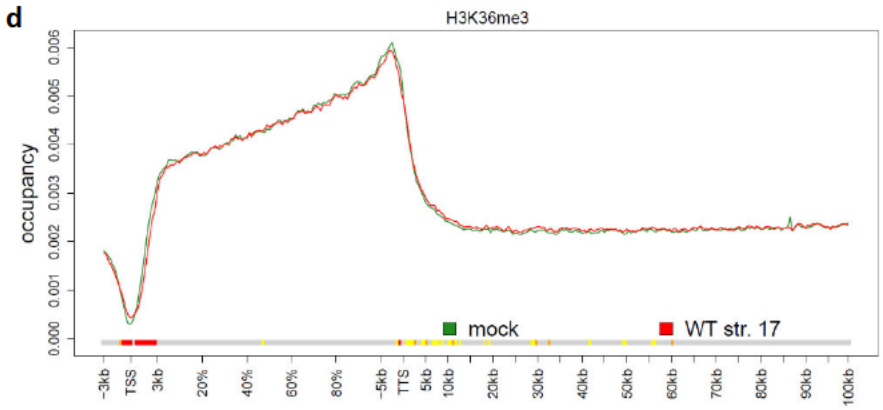

Figure 22. Occupancy of H3K27me3 and H3K36me3 on cellular genome during HSV-1 infection.
H3K27me3 metagene plots for genes **(a)** with strong dOCR induction (cluster 5) and for genes **(b)** without dOCR induction, i.e. all analyzed genes apart from cluster 2,5 and 6 in mock and HSV-1 WT strain 17 infection. H3K36me3 metagene plots for genes **(c)** with strong dOCR induction (cluster 5) and for genes **(d)** without dOCR induction, i.e. all analyzed genes apart without clusters 2,5 and 6 in mock and HSV-1 WT strain 17 infection (n=2-3 biological replicates). The color track at the bottom of each subfigure indicates the significance of paired Wilcoxon tests comparing the normalized transcript coverages for each bin between mock and WT infection. P-values are adjusted for multiple testing with the Bonferroni method within each subfigure; color code: red = adjusted p-value $\leq 10^{-5}$, orange = adjusted p-value $\leq 10^{-3}$, yellow = adjusted p-value ≤ 0.05.

Considering that we did not observe any dramatic changes in global histone occupancy within HSV-1 induced dOCR, we speculated that the dOCR induction might reflect changes in higher-order chromatin structure during the course of infection. Linker histone H1 binds neighboring nucleosomes and promotes chromatin compaction. However, displacement of histone H1 affects nucleosome density distribution and leads to a loss of higher-order chromatin structure [260].
We thus analyzed genome-wide occupancy of the H1 linker histone by ChIPmentation in mock, WT strain F and ΔICP22 infection at 8 hpi with PAA treatment. Having identified ICP22 as necessary for dOCR induction, infection with the ICP22-null mutant was included. Unlike in the previous experiment, we here used PAA treatment to increase dOCR induction and thereby enhance associated changes in H1.

Comparably to the canonical histone H3, metagene analysis showed a strong depletion of linker histone H1 at the TSS, with its levels gradually increasing throughout the gene body. This is consistent with previous reports confirming high quality of the respective ChIPmentation data [261]. Interestingly, metagene analysis of cluster 5 revealed a selective loss of H1 in WT compared to both mock and ΔICP22 infection downstream of the transcription termination site (TTS) (Figure 23a). H1 occupancy profiles for both mock and ΔICP22 infection were highly similar. The downstream increase (>50kb) in H1 observed in WT strain F infection is likely due to the normalization procedure for individual gene curves in the metagene analysis. It should be noted that occupancy profiles for each gene and replicate were first normalized to a sum of 1 before averaging across genes and replicates to avoid biases due to differences in gene expression. Thus, these profiles represent relative distributions of H1 across the gene and downstream regions. This suggests that the increase in H1 levels downstream of the TSS was shifted to further downstream regions for WT infection compared to mock or ΔICP22 infection. No such delay was observed for genes without dOCR induction between mock, WT and ΔICP22 infection (Figure 23b). Statistical analysis confirmed the differences downstream of the TTS to be significant (Wilcoxon test, $p<0.05$) at several positions when comparing WT and mock as well as WT and ΔICP22 infection (Figure 24a, b). No significant differences were observed between mock and ΔICP22 infection at a significance level of 0.05 (Figure 24c).

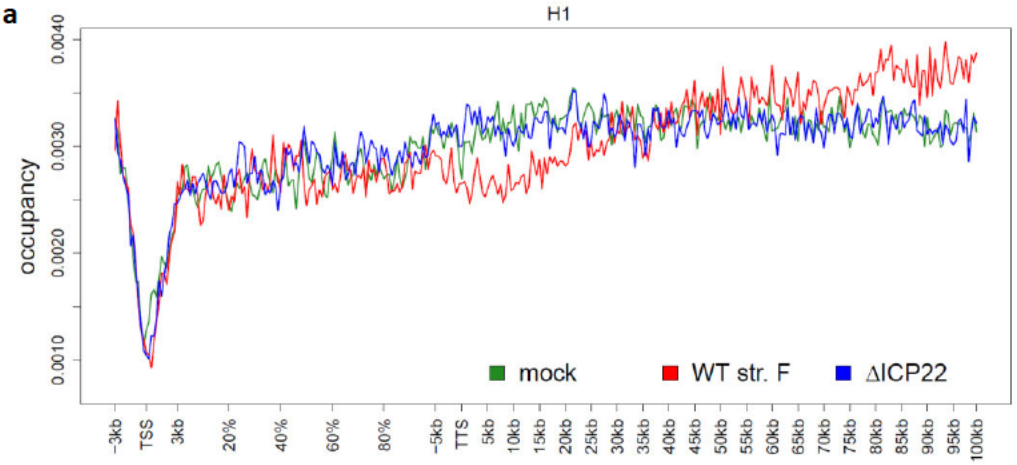

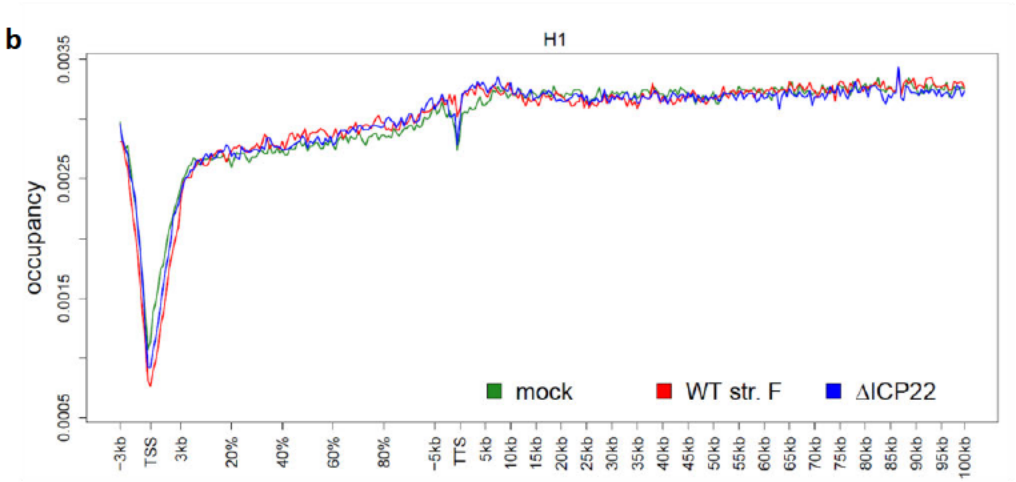

Figure 23. dOCR leads to selective loss of the histone linker H1 in cluster 5.

H1 metagene plots for genes **(a)** with strong dOCR induction (cluster 5) and for genes **(b)** without dOCR induction, i.e. all analyzed genes apart clusters 2,5 and 6 in mock and HSV-1 WT strain F and ΔICP22 infection (n=2 biological replicates).

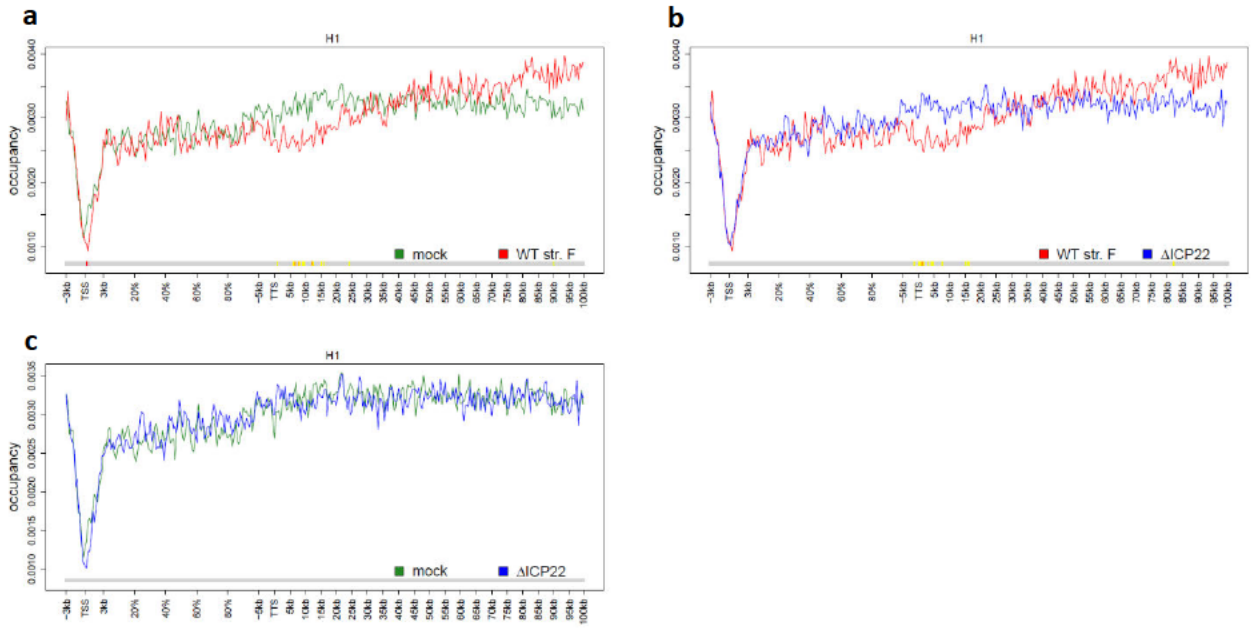

Figure 24. Selective loss of linker H1 histone is not observed in dOCR regions of mock and ΔICP22 infected cells.

Metagene plots for histone H1 on gene and downstream regions for cluster 5 for the pairwise comparison of **(a)** mock vs. WT strain F, **(b)** WT strain F vs. ΔICP22 and **(c)** mock vs. ΔICP22. The color track at the

bottom of each subfigure indicates the significance of paired Wilcoxon tests comparing the normalized transcript coverages for each bin between mock and WT infection. P-values are adjusted for multiple testing with the Bonferroni method within each subfigure; color code: red = adjusted p-value $\leq 10^{-5}$, orange = adjusted p-value $\leq 10^{-3}$, yellow = adjusted p-value ≤ 0.05.

5.6. Histone chaperons bound by ICP22 are not involved in the dOCR formation

The highly conserved histone chaperones FACT (SPT16/SSRP1) and SPT6 play critical roles in regulating the transcription process and in maintaining chromatin integrity [204]. Moreover, they bind somatic linker histone variant H1.0 [262]. Recently, both FACT and SPT6 were discovered to be recruited by the viral ICP22 protein and re-localized to the viral replication compartments (VRCs) [123]. Thus, we speculated that functional inhibition of FACT (SSRP1) or SPT6 by the ICP22 protein might explain dOCR formation. To test this hypothesis, we generated T-HF cells with doxycycline-inducible amiRNA knock-down (KD) of SSRP1 and SPT6.

To achieve efficient KD for both histone chaperons, T-HFs expressing two different amiRNAs were under 72 h-Dox-treatment (1 µg/ml) before infection (Figure 25a, b). Immunoblot confirmed strong KD of both proteins. Of note, KD of SSRP1 resulted in a concomitant loss of its interaction partner SPT16, consistent with previous reports showing that the presence of SSRP1 mRNA is critical for SPT16 protein stability [263]. On the other hand, KD of SPT6 negatively affected the expression of the proteins SSPR1 and Pol II, although cell death has not been observed [264]. It is important to note that the knockdown of neither of the two histone chaperons had any discernable effect on viral gene expression upon high MOI infection as confirmed by Western blot (Figure 26a, b).

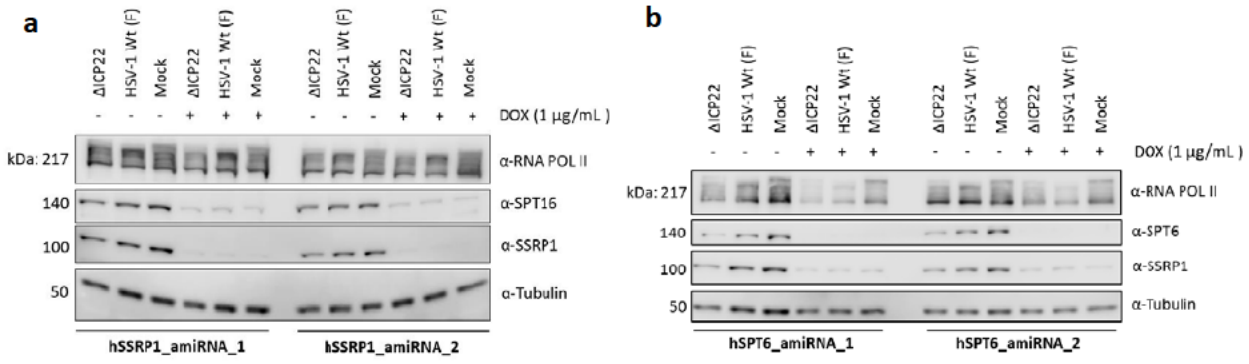

Figure 25. Knock-down of SSRP1 and SPT6 in T-HFs by an inducible, lentiviral construct encoding an artificial miRNA (amiRNAs).

(a) Knock-down of SSRP1 was induced with 1 µg/mL doxycycline (hSSRP1_amiRNA_1 and hSSRP1_amiRNA_2) and compared to the control cells. **(b)** Knock-down of SPT6 was induced with 1 µg/mL doxycycline (hSPT6_amiRNA_1 and hSPT6_amiRNA_2) and compared to control cells. Cells were infected with WT HSV-1 (F) or ΔICP22 at an MOI of 10. PAA was used at 300 µg/mL during the course of infection. Total cell lysates were collected at 72 hours post-induction with Dox and western blot was performed using antibodies, as indicated. α-Tubulin was used as a loading control.

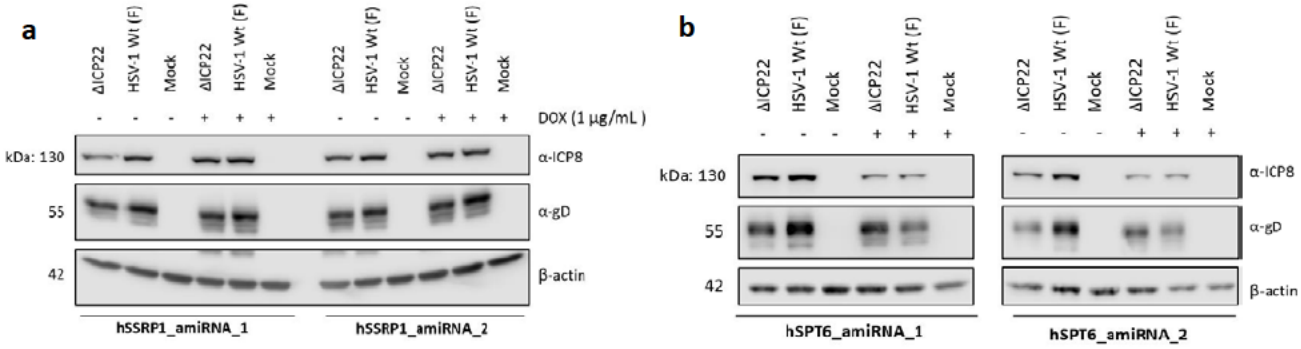

Figure 26. Expression of HSV-1 proteins in SSRP1 and SPT6 knock-down cells.

(a) T-HF cells expressing SSRP1_amiRNA and **(b)** T-HF cells expressing SPT6_amiRNA were infected with WT HSV-1 (F) or ΔICP22 at an MOI of 10 or mock infected for 8 hours. PAA was used at 300 µg/mL during the course of infection. Total cell lysates were collected at 72 hours post-induction with Dox. Western blots were probed for two HSV-1 viral proteins, ICP8 and glycoprotein D. β-actin was used as a loading control.

To assess the impact of SSRP1 and SPT6 knockdown on virus production in T-HF cells, plaque assays were performed upon HSV-1 infection. Knockdown was initiated by Dox treatment for 72 h prior to infection. To maintain the knockdown, cells were exposed to 0,5 µg/ml Dox over the next three days post inoculation. Ratio of plaques (+/-Dox), for amiRNA_SPT6_2 showed no discernible change, while amiRNA-SPT6_1 and both amiRNA_SSRP1 cells showed a slight

reduction in titer with doxycycline present in the media **(Figure 27).** We conclude that virus production in T-HF cells is not affected by KD of the two proteins.

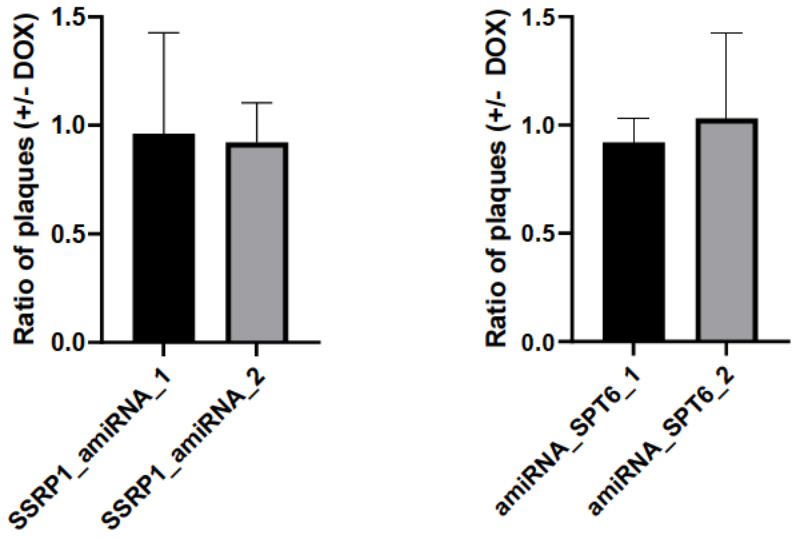

Figure 27. Virus production in T-HF cells with inducible KD of either SPT6 or SSRP1 is not affected

T-HFs expressing two different amiRNAs for SPT6 and SSRP1 were treated with 1 µg/mL Dox for 72 h. Cells were infected with WT strain F in serial dilutions for 1 hour. Fresh 0,5% CMC media was added with or without Dox (0,5 µg/mL) to maintain the knock-down. After three days, plaques were fixed, stained with crystal violet, and counted. Each bar represents mean ratio of plaques (+/- Dox) (n=2 biological replicates).

To evaluate whether SSRP1 and SPT6 had any discernable role in HSV-1-induced dOCR formation, Omni-ATAC-seq was performed on mock, HSV-1 WT strain F- and ΔICP22-infected cells (with PAA treatment in all cases). It is important to note that Omni-ATAC-seq was performed on cells from the same experiment as utilized for the Western blots in Figure 25 and 26. While infection with WT HSV-1 stain F resulted in strong dOCR formation upon depletion of either of the two histone chaperons, no dOCR induction was observed upon mock and ΔICP22 infection (Figure 28a, b). Down-sampling analysis showed the same results, detectable not only for cluster 5, but for all analyzed genes (Figure 28c-h).

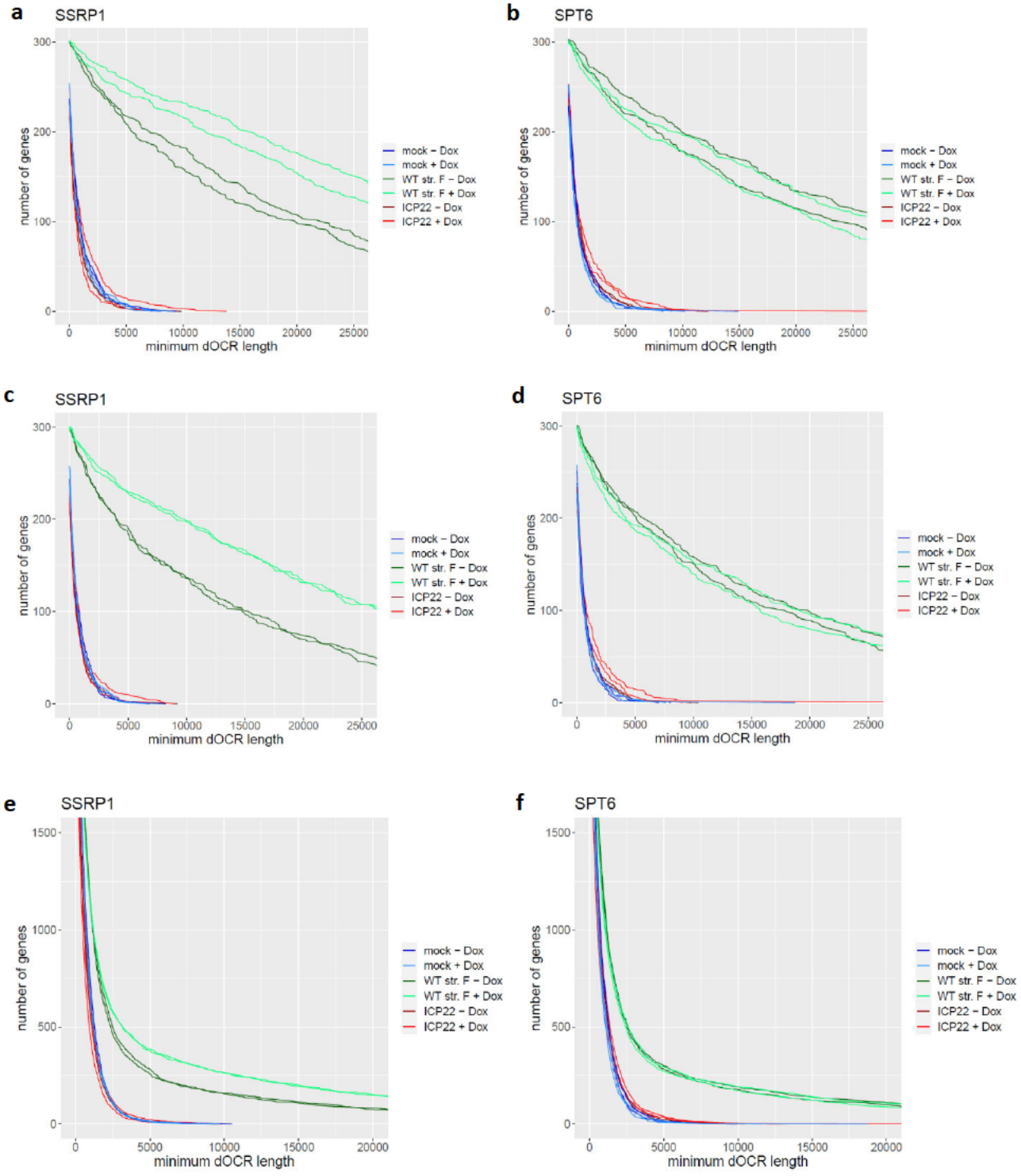
a
SSRP1
b
SPT6
c
SSRP1
d
SPT6
e
SSRP1
f
SPT6
number of genes
minimum dOCR length
mock − Dox
mock + Dox
WT str. F − Dox
WT str. F + Dox
ICP22 − Dox
ICP22 + Dox

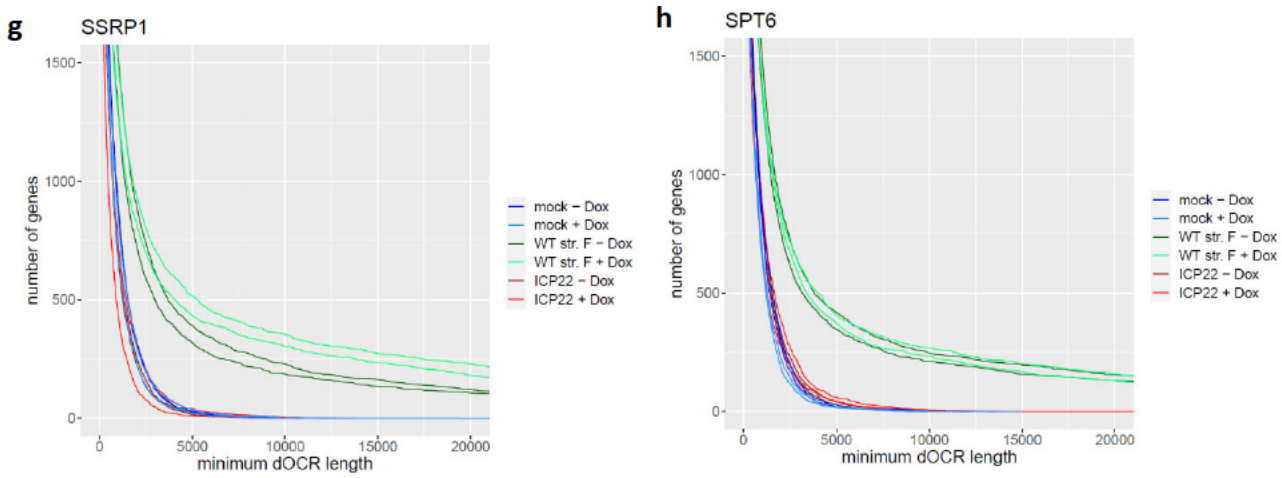

Figure 28. FACT and SPT6 are not involved in dOCR induction.

Number of genes in cluster 5 (y-axis) that exhibit dOCRs of at least the respective length (x-axis) in mock, WT strain F and ΔICP22 with or without Dox-induced knockdown of **(a)** SSRP1 and **(b)** SPT6. **(c,d)** Results shown for cluster 5 with down-sampling. Number of all genes that exhibit dOCRs of at least the respective length (x-axis) in mock, WT strain F and ΔICP22 with or without Dox-induced knockdown of **(e)** SSRP1 and **(f)** SPT6. **(g,h)** Results for all genes with dOCR with down-sampling.

Strikingly, we observed an increase in dOCR induction upon SSRP1 KD in the WT strain F infection. Manual inspection of several genes with increased dOCR revealed an increase in chromatin accessibility within the gene bodies of dOCR genes. However, cells that did not lack SSRP1 expression showed induction of open chromatin only in the downstream regions. To this end, we analyzed the effect of SPT6 or SSRP1 KD on the extent of open chromatin regions (OCRs) within gene bodies during mock, WT strain F and ΔICP22 infection. A significant number of genes (282 genes, 6.8%) showed increased (>=2-fold) chromatin accessibility upon WT infection of SSRP1-KD but not of SPT6-KD cells (Figure 29a, b) Notably, both mock and ΔICP22 infection also showed some increase in SSRP1-KD cells, but, in contrast to WT infection, this was predominantly observed for genes with relatively short areas of open chromatin in their gene bodies (Figure 29c, d). Therefore, an increase in dOCR induction in WT infection upon SSRP1-KD appears to correlate

to the general increase of chromatin accessibility in the transcribed regions, potentially tied to the role of FACT in the re-assembly of nucleosomes in the wake of Pol II.

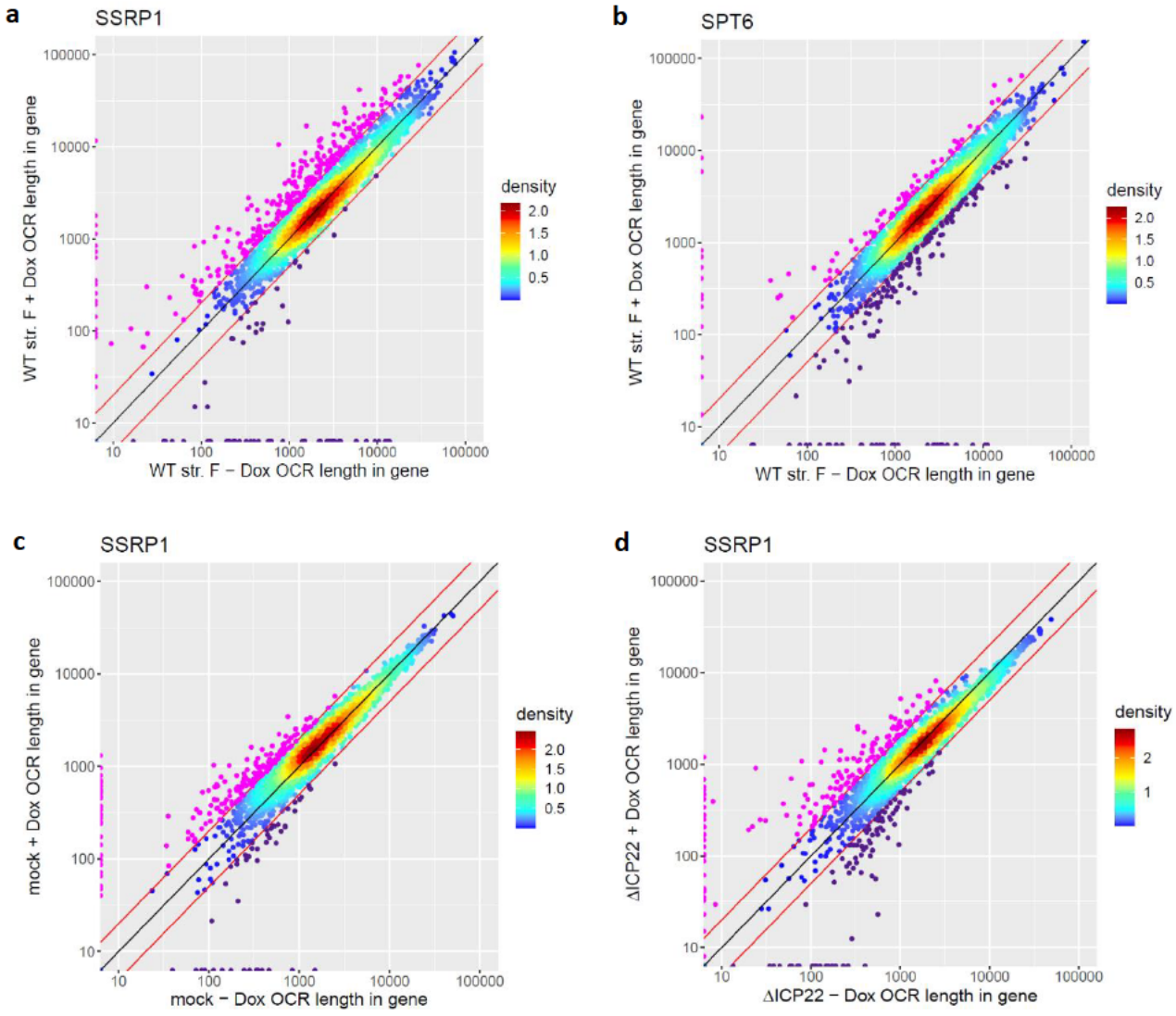

Figure 29. SSRP1 KD in the WT infection increases chromatin accessibility within the gene bodies. Comparison of the length of open chromatin regions (OCRs) in gene bodies upon WT infection of **(a)** SSRP1- KD and **(b)** SPT6-KD cells or upon **(c)** mock **(d)** ΔICP22 infection of SSRP1-KD cells for all analyzed genes. Red lines indicated a 2-fold deviation from the diagonal (black). Colors indicate density of points.

Having observed this effect, the same analysis has been performed for the T-HF ICP22 or T-HF ICP22/ICP27 cells upon Dox treatment for the corresponding ATAC-seq data (Figure 30a). Strikingly, T-HF ICP22/ICP27 cells exposed to Dox triggered a similar increase in chromatin accessibility within gene bodies (311 genes with >= 2-fold increase). However, similar to previous finding, this was predominantly observed for genes with shorter OCR regions and still resulted only in a relatively small percentage of the gene body covered by open chromatin. On the other hand, T-HF ICP22 cells exposed to 2 h salt stress with the presence of Dox had no such pronounced effect (Figure 30b).

While the underlying molecular mechanism remains unclear, these findings indicate that neither SPT6 nor FACT play a role in ICP22-induced dOCR formation.

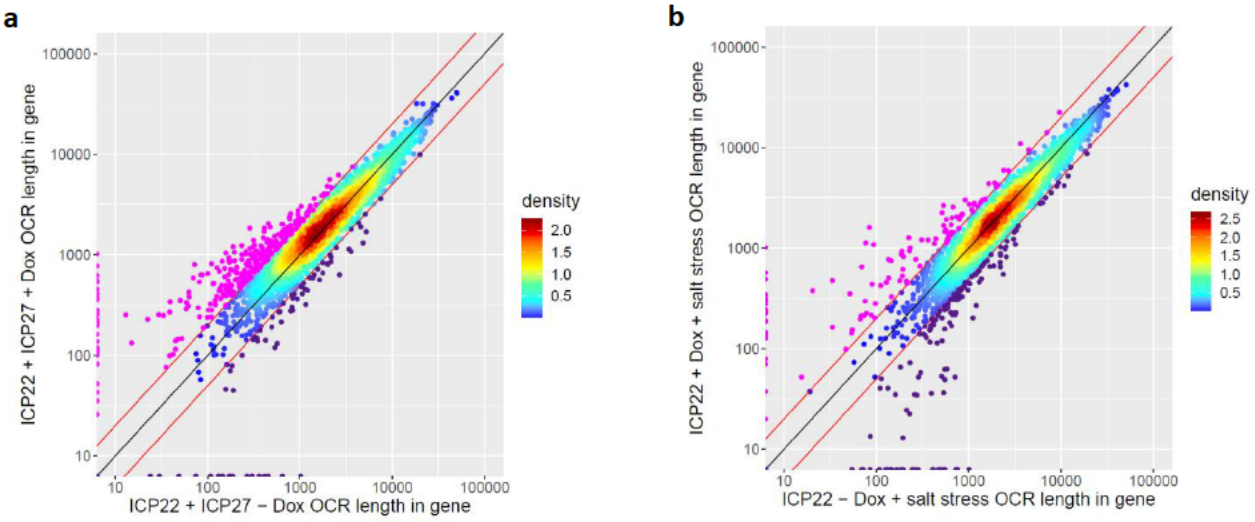

Figure 30. T-HF ICP22/ICP27 cells exposed to Dox triggered an increase in chromatin accessibility within gene bodies.

Comparison of the length of open chromatin regions (OCRs) in gene bodies for **(a)** T-HF ± expressing ICP22/ICP27 and **(b)** T-HF ± expressing ICP22/ICP27 cells upon salt stress for all analyzed genes. Red lines indicated a 2-fold deviation from the diagonal (black). Colors indicate density of points.

6. DISCUSSION

Lytic HSV-1 infection, salt and heat stress all induce a selective failure of transcription termination of thousands of genes [140,228,230,234,236]. We could recently show that HSV-1 induced DoTT is predominantly (but not exclusively) mediated by the viral ICP27 protein. By directly interacting with the cellular CPSF complex, ICP27 induces the formation of a dead-end 3' processing complex [235]. Similarly, cells exposed to heat stress show impaired recruitment of CPSF73 at the 3'end of the affected genes [265]. Interestingly, exposure to salt stress causes a decrease in binding between the Integrator complex and Pol II, rather than the loss of termination factors, although the possibility of them being involved in the mechanism is not excluded [236]. A direct comparison between HSV-1 and heat/salt stress revealed a significant overlap between gene clusters affected by read-through transcription, but also condition-specific differences [234].

Interestingly, only HSV-1 infection induces dOCRs downstream of the DoTT-affected genes [234]. This indicated the involvement of another viral gene in the induction of dOCRs. The central goal of this study was to identify the responsible viral gene, elucidate the underlying molecular mechanism and characterize the dOCR-associated changes in the cellular chromatin.

6.1. Viral DNA replication and viral late gene expression are not required for dOCR induction

To narrow down the responsible viral gene, we performed ATAC-seq on HSV-1 infected primary human fibroblasts in the presence of the viral DNA polymerase inhibitor phosphonoacetic acid (PAA) [266,267]. Interestingly, PAA treatment not only excluded a role of viral late proteins in dOCR induction but resulted in a striking increase in the extent of dOCR induction (Figure 12a). PAA treatment had no effect on mock infected cells which is in accordance with previous findings showing PAA has no inhibitory effect on cellular DNA, RNA or protein synthesis when used at concentrations known to inhibit viral replication [51,266,267,]. Down-sampling excluded that the observed increase in dOCR formation upon PAA treatment resulted from increased read numbers mapping to the cellular genome due to the reduction of reads mapping to the viral genome

(Figure 12b). Viral DNA replication is not only required for the expression of viral late genes but also results in the extensive recruitment of the host Pol II transcription machinery to the viral replication compartments [268,269]. This is at least in part responsible for the dramatic decline in host transcription during the productive infection. Therefore, PAA-triggered increase in dOCRs presumably results from significantly higher levels of transcription downstream of genes.

The observed increase in dOCRs under PAA treatment, which increases Pol II and associated factor occupancy on the cellular genome, implies that deprivation of host transcription of key cellular factors that govern chromatin conformation and accessibility is not responsible for dOCR induction.

An important feature of the induced dOCRs is that they are not observable for all cellular genes. Unsupervised clustering of the extent of dOCR induction revealed that not the percentage of failed transcription termination (percentage of transcripts experiencing read-through transcription) but rather the absolute levels of transcriptional activity downstream of gene ends was responsible for the dOCR induction (Figure 14b). Both a high basal level of transcription as well as a high percentage of read-through transcription positively correlated with the extent of dOCR induction. Accordingly, the most highly expressed genes with the highest percentage of read-though (Cluster 5) showed the highest level of dOCRs. This further supports our previous work that dOCR arise in the wake of Pol II when it transcribes into previously untranscribed regions downstream of genes [234]. For all subsequent analysis, we thus focused on the genes in cluster 5.

6.2. The viral ICP22 protein is required for dOCR induction

To identify the viral gene responsible for dOCR induction, we employed a set of mutant viruses that lacked viral genes with known important roles in host cell modulation, namely ICP0, ICP22, ICP27 and the virion host shut-off protein (vhs). As these mutants were generated on different virus strains, we included the respective parental viruses. While subtle differences were observed regarding the extent of dOCR induction by the different strains, all of them resulted in significant dOCR induction (Figure 12a, b). Importantly, we selected Cluster 5 as the set of genes that

showed strong dOCRs independent of virus strain. Subsequent ATAC-seq analysis identified the viral ICP22 protein to be essential for dOCR induction (Figure 15a, b). Importantly, PAA treatment did not rescue dOCR induction despite the positive effect of it on dOCR induction upon WT HSV-1 infection. In addition, prolonging infection from 8 to 12 h did not rescue dOCR induction demonstrating that the observed loss in dOCRs induction was not due to the attenuation of the ICP22-null mutant.

A key effect of ICP22 is the profound loss of serine 2 phosphorylation (Ser2P) of the Pol II CTD. Ser2P governs the recruitment of Pol II-associated factors to Pol II during transcription. We thus hypothesized that the loss of Ser2P may be responsible for dOCR induction. Loss of Ser2P is thought to be mediated by direct interaction and inhibition of CDK9 by the ICP22 protein [132,270,271]. While the role of ICP22 on Ser2P mediated by the other Ser2P kinases CDK12 and CDK13 have not been studied and remains unclear, infection with an ICP22-null mutant still results in reduced Ser2P levels. Importantly, however, concomitant inhibition of viral DNA replication by PAA abrogates the Ser2P loss [256]. This is why we also included PAA treated ICP22-null infections in the primary ATAC-seq experiments (Figure 15a). Of note, in contrast to the observed increase in dOCR induction by PAA treatment in WT HSV-1 infection, dOCR induction remained fully absent in infection with an ICP22-null mutant. We conclude that ICP22 is required for dOCR formation while the loss of Ser2P does not appear to be required. However, it is important to note that it remains unclear when during transcription and where on the genes Ser2P is lost from Pol II, i.e. during initiation, pausing, elongation or termination.

Although this was not within the scope of this study, a dysregulation of the other CTD residues (Tyr1 and Thr4), which are both involved in the transcription termination process, could contribute to the observed phenotype [272,273]. Therefore, a direct comparison of the Pol II CTD status downstream of genes, between HSV-1 and other cellular stressors, could potentially reveal the cause of DoTT-induced dOCR.

6.3. Expression of ICP22 is sufficient for dOCR induction upon transcription downstream of genes

To answer the question whether ICP22 was not only necessary but also sufficient for dOCR induction, we engineered cells to either express ICP22 alone or in combination with the ICP27 (Figure 19 a-d). ATAC-seq on cells expressing either ICP22 and ICP27 or ICP22 in combination with salt stress both showed clear evidence of dOCR induction (Figure 20a, b).

As previously mentioned, DoTT-associated dOCR are only induced in HSV-1 infection but not in cellular stress conditions [234]. Here, we show that the HSV-1 immediate early protein ICP22 is necessary for dOCR induction. Moreover, the context of viral infection was not required, as ectopic expression of ICP22 was also sufficient to induce dOCR in the wake of transcribing Pol II when transcription downstream of genes (DoG) was induced by salt stress (Figure 20a, b). Of note, the induction of dOCRs upon salt stress was not as pronounced as with the presence of ICP27-induced DoTT. This was explained by the much lower extent of salt stress-induced read-through transcription, which was apparent in RNA-seq data obtained from the same experiment. Less transcription downstream of genes thus explained the reduced levels of dOCR induction upon salt stress (Figure 20d, e). This work also confirmed previous findings made by our collaborator Yongsheng Shi. Similar to his observations in HeLa cells, we confirmed that ectopic expression of ICP27 is sufficient to induce DoTT in primary human fibroblasts [235]. Importantly, the induction of dOCRs upon salt stress in the ICP22 cells also demonstrated that transcription downstream of genes rather than any other of the pleiotropic effects of ICP27 on the host transcriptional machinery are required for dOCR induction.

ICP22 is known to be heavily phosphorylated by two viral kinases, U_L13 and U_S3 [128,132]. Our findings thus exclude a role of U_L13 and U_S3 in dOCR induction. However, ICP22 is also phosphorylated by an unknown cellular kinase [105]. Therefore, phosphorylation of ICP22 may still be required for dOCR induction.

6.4. The CDK9 binding domain of the ICP22 protein is likely to be involved in the dOCR phenotype

WT ICP22 consists of 420 amino acids, while the mutant ICP22 virus used in this study was a C-terminally truncated protein, only comprising the first 200 aa (Figure 31) [242]. Of note, the missing region includes the core sequence (motif 1) present in all α-herpesvirus U_S1 homologs, with the CDK9-binding sites [111]. Whether the functional part of ICP22 that is important for inducing dOCR resides in the region between 200-420 aa rather than the N-terminal part cannot be ruled out completely, since the deletion itself may well have drastically altered the protein's conformation, function, or association with other factors. However, some preliminary studies of ectopically expressed variants of U_S1 performed by our lab showed that the N-terminal region (Δ1-146) and C-terminal regions (Δ342-380) and (Δ392-420) of the protein are not involved in the dOCR formation (Figure 31). This suggests that the essential region probably resides between amino acids 147 to 341. We are currently generating a range of mutant viruses with more subtle deletions to further investigate this. Moreover, comparative analysis of different U_S1 homologs from various herpesviruses, such as HSV-2 and VZV in inducing dOCR, will be tested to decipher the region of ICP22 that is essential for the DoTT-induced dOCR phenotype.

To confirm that this finding is not strain dependent, two additional strains (KOS 1.1 and BAC derived strain 17) lacking the complete ICP22 ORF were compared to the ΔICP22 strain F in a separate ATAC-seq experiment (Figure 16a, b). This confirmed the loss of dOCR induction of the ICP22-null mutant in all three strains. Moreover, since we identified ICP22 and ICP27 to be sufficient for DoTT-induced dOCR, we assumed that the difference in their respective sequences somehow contributes to the subtle differences in the extent of DoTT-induced dOCRs, with strain 17 leading to more extensive and longer dOCRs (Figure 12a, b). Interestingly, laboratory strain 17 is known to be more virulent than other HSV-1 strains, including KOS, McKrae and F, both *in vitro and in vivo* [274,275,276,277]. Thus, it could be that the difference is simply caused by different kinetics of viral replication and viral gene expression between the two strains driven by either viral genetics or strain-specific host responses.

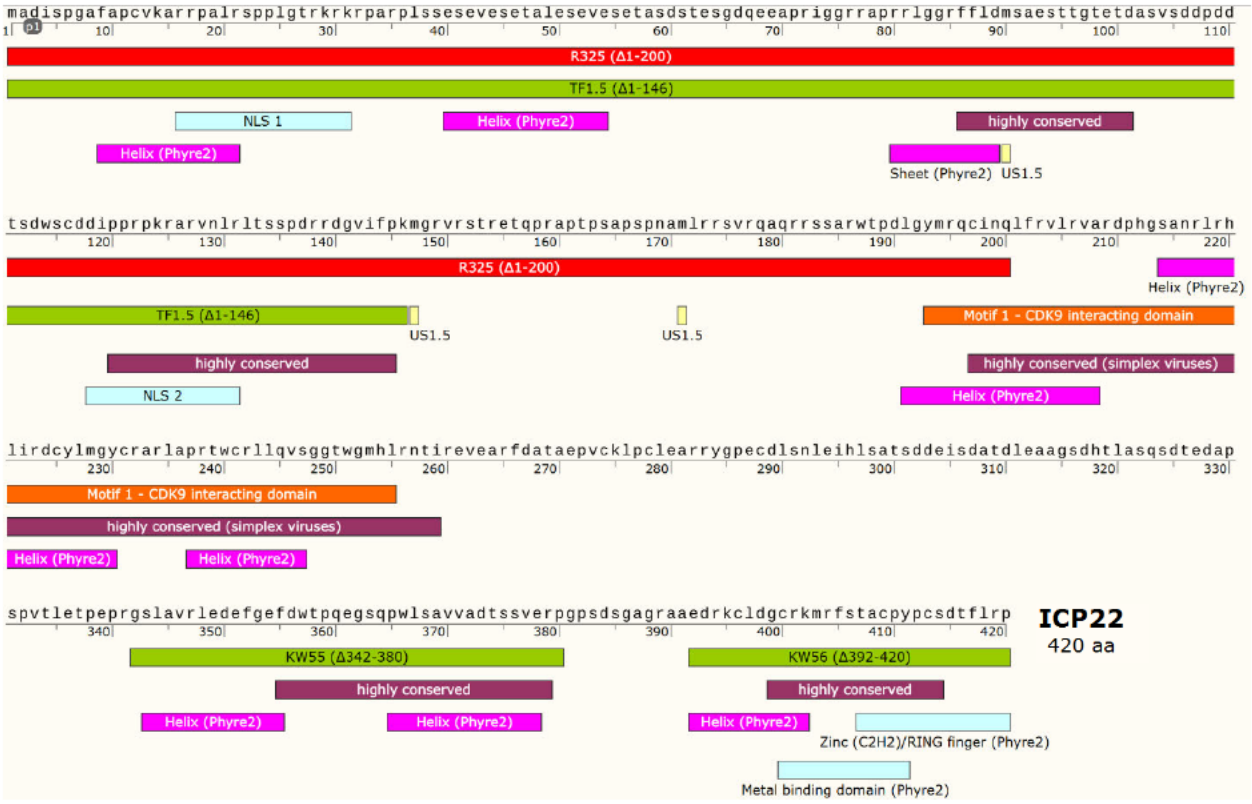

Figure 31. Schematic diagram of the 420 aa ICP22 wild-type protein.

Depicted are: ICP22 mutant virus (R325) lacking the first 200 aa (red), three ICP22 mutant viruses still able to induce dOCR (green), the location of Motif 1 – CDK9 binding domain (orange), Phyre2 predicted structural features (helix and beta sheets (pink), Zinc (C2H2)/RING finger domain and metal binding domain (light blue)) reported sites for the $U_S1.5$ protein (yellow) and highly conserved domains of the ICP22 protein in herpes simplex viruses (burgundy).

6.5. ICP22-induced dOCR causes selective loss of higher-order chromatin structure in the wake of Pol II

Transcription into the genomic regions downstream of genes should result in changes in epigenetic chromatin marks in these regions. We were surprised by the complete lack of changes in both activating and repressive chromatin marks in even the most strongly affected genes of Cluster 5. ChIPmentation data of canonical histone H3 and histone modification marks

H3K36me3 and H3K27me3 indicated unchanged histone occupancy profiles in dOCR regions during the WT HSV-1 infection (Figure 21a, Figure 22 a, c). This observation was particularly interesting considering that productive IAV infection was associated with epigenetic changes in elongation mark H3K36me3 that rose dramatically, along with increased Pol II levels in the downstream regions of highly active genes [233]. Similarly to our data, IAV infection had little effect on the heterochromatin marks H3K9me3 and H3K27me3. This indicates that these two viruses probably use different mechanisms, with IAV causing epigenetic changes in euchromatin marks.

One aspect that needs to be considered is that lytic HSV-1 infection results in a profound decrease in cellular transcription already by 8 hpi. This is reflected by the near complete absence of Pol II from gene bodies already by 4 hpi [278]. This loss of cellular transcriptional activity can be efficiently prevented by the PAA treatment [279]. Loss of global cellular transcriptional activity could thus potentially explain the lack of detectable changes in active chromatin marks downstream of genes despite extensive read-through transcription. Unfortunately, we only discovered this effect of PAA after the bulk of chromatin profiling data had already been obtained. Therefore, we are currently repeating the experiment with the PAA treatment included.

Considering that we did not observe any changes in the epigenetic modifications downstream of genes, we were wondering whether the compaction of chromatin is affected through disruption of higher-order chromatin structure. For the formation of higher order 3D structures, full nucleosomes (core histone octamer + linker histones), also known as chromatosomes, are necessary. The linker histone (H1) binds externally to the nucleosome core particles at the DNA entry/exit points and interacts with the free linker DNA (~20 bp) thereby bridging neighboring nucleosomes [280]. *In vitro* studies have shown that H1 regulates the folding of chromatin fibers into more compacted structures thus sterically occluding access of other factors to the chromatin [260]. Interestingly, ChIPmentation revealed a selective decrease in H1 occupancy downstream of genes while leaving core nucleosome occupancy unchanged (Figure 23a, b). The mechanism behind the selective loss of H1 during the WT infection is not fully understood. However, we speculate that ICP22 may affect its reassembly either (1) directly, by binding to or competing with it for nucleosome binding or (2) indirectly, by interfering with the function of H1 histone

chaperones, such as FACT and SPT6.

Importantly, conditional knockdown of SPT6 and FACT did not confirm an involvement of either of the two factors in dOCR induction. Thus, it would be of interest to look more closely into the template activating factor-I (TAF-I or protein SET), as it is identified as a specific-H1 histone chaperone [281,282]. ICP22 could potentially affect H1 localization around the TTS by interacting with TAF-I, since TAF-I is involved in eviction of histone H1. While additional experiments are required to confirm the selective loss of H1 in the exact same experimental conditions, it may explain why we did not observe any changes in other key histone modifications in genomic regions affected by DoTT and dOCR induction.

6.6. Functional relevance of dOCR induction

To date, the functional relevance of dOCR induction remains unclear. Interestingly, several studies reported that core histones (H2A, H2B, H3.1 and H4), histone variant H3.3 and linker H1 are mobilized during the HSV-1 infection. Accordingly, they can be found in the pool of free histones undergoing fast chromatin exchange [257–259]. Considering that HSV-1 inhibits synthesis of new histone proteins during productive infection by its generalized host shut-off, these free histones are most likely released from the cellular chromatin [283,284]. It is thus tempting to speculate that histone mobilization results from impaired histone repositioning downstream of DoTT-genes and is thus directly linked to dOCR induction. Free histones may be required to chromatinize both the incoming as well as the *de novo* synthesized viral genomes at the beginning of viral DNA replication. Both ICP22 and ICP27 are viral immediate-early proteins that are already expressed within the first hour of infection, while the induction of dOCRs only starts to become detectable at 2-3 h post infection and rapidly increases thereafter. It thus appears unlikely that HSV-1 impairs histone repositioning downstream of genes to increase the pool of free-histones. We prefer the hypothesis that HSV-1 (I) targets higher-order chromatin formation to govern the structural organization of viral replication centers; or that (II) dOCR induction represents a side effect of viral manipulation of the transcriptional machinery. In the latter respect, targeting of the cellular FACT complex would have been an ideal target as FACT also has an important role in

governing Pol II pause-release besides acting as a histone chaperon [285]. Considering that neither SPT6 nor FACT appear to be involved in dOCR formation the functional role of dOCR induction in HSV-1 infection remains unclear. Future work is thus required to elucidate both the underlying molecular mechanism and its functional relevance to infection.

6.7. FACT and SSRP1 do not contribute to the DoTT-induced dOCR through genome-wide nucleosome displacement

Both SPT6 and the FACT complex are involved in the modulation of gene transcription by facilitating histone displacement in front of elongating Pol II and nucleosome reassembly in the wake of Pol II passage [286]. Therefore, proper chromatin reconstitution during transcription elongation is highly dependent on these two histone chaperons.

HSV-1 is well described to efficiently recruit the cellular transcriptional machinery including both SPT6 and FACT to the VRCs to facilitate robust viral transcription and induce host shut-off [123,278,287,]. It is, however, important to note that dOCRs were even more strongly induced in the absence of viral DNA replication, indicating that dOCR induction does not result from a deprivation of SPT6 and FACT from Pol II on cellular chromatin. It does, however, not exclude any functional impairment of either factor through their interaction with ICP22. ICP22 is a key contributor to the virus-induced loss of Ser2P on the Pol II CTD, important for the recruitment of SPT6 to Pol II [288]. In contrast, FACT has been shown to be recruited to genes independently of the CTD phosphorylation [289]. It is important to note, however, that dOCR induction is selectively occurring downstream of genes in previously untranscribed genomic areas. Little is still known about the phosphorylation pattern of the Pol II CTD downstream of genes and the factors that are recruited to Pol II downstream of genes. Recently, ICP22 was shown to interact with the both FACT complex and SPT6, either directly or as a part of a complex, and thus recruits them to the growing VRCs [123]. We thus considered the two histone chaperons as prime candidates for the ICP22-induced dOCRs. However, efficient conditional knockdown of both factors did not rescue dOCR induction upon ΔICP22 infection (Figure 28a-d). Inhibition of viral DNA replication by PAA treatment also had no effect. It is important to note that knockdown of both SPT6 and FACT had

little effect on productive infection (Figure 26a-b, Figure 27). Thus, the absence of dOCR induction did not result from impaired productive HSV-1 infection. Depletion of SPT6 also resulted in a concerted loss of FACT (Figure 25b). Nevertheless, this did also not rescue dOCR induction. Finally, depletion of FACT resulted in a selective increase in chromatin accessibility within gene bodies confirming its importance in regulating nucleosome reassembly in the wake of Pol II (Figure 29a, b). This provides functional evidence that the depletion of FACT by Dox was indeed sufficiently strong to induce a phenotypic effect distinct from dOCR induction. We conclude that SPT6 and FACT are unlikely to be responsible for the ICP22-mediated dOCR induction.

This leaves us with three different models on how ICP22 triggers dOCR induction. (I) ICP22 interferes with Ser2P of the Pol II CTD, which prevents the recruitment of a histone chaperon(s) distinct from SPT6 and FACT; (II) ICP22 directly interferes with a cellular chromatin-regulating protein(s); and (III) ICP22 selectively impairs the repositioning of linker Histone 1. It is important to note, however, that any model needs to explain the selective increase in chromatin accessibility downstream of genes. Recognition of the PAS site by the transcription termination machinery is known to affect the phosphorylation of the Pol II CTD by unknown molecular mechanisms which in turn reduces the processivity of Pol II downstream of genes. We thus favor a model in which changes in Pol II CTD phosphorylation and thus the Pol II interactome downstream of genes potentially in combination with a direct interaction of ICP22 with a cellular transcription elongation factor is responsible for the observed dOCR induction. Its functional relevance to productive infection and its role in the previously reported increase in the free previously reported increase in the free histone pool requires further studies.

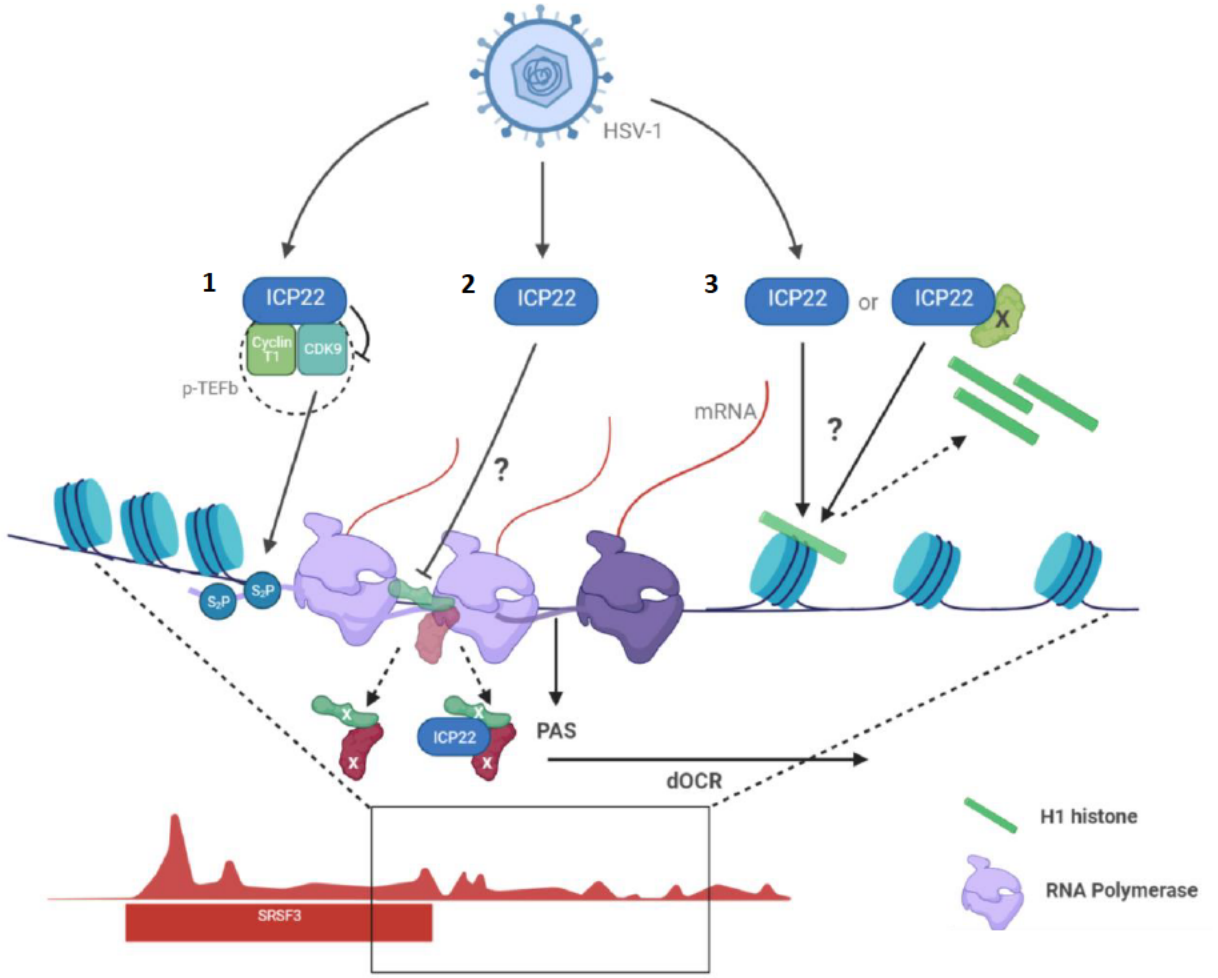

Figure 32. Three possible mechanisms involved in ICP22-induced dOCR upon read-through transcription. **(1)** ICP22 inhibits the function of CDK9 leading to loss of Ser2P through an unknown mechanism, **(2)** ICP22-mediated dOCR arises as a result of displacement of chromatin-regulating proteins through direct/indirect interaction and **(3)** ICP22, either alone or through interaction with other protein, such as TAF-I, leads to selective loss of histone linker H1 downstream of genes.

Designed in BioRender, by BioRender.com (2020). Retrieved from https://app.biorender.com/biorender-illustrations.

7. BIBLIOGRAPHY

1. Smith, T. T. & Whitley, R. J. *Infectious Diseases, Herpesviruses*. (Elsevier Ltd., 2017).
2. Payne, S. *Viruses: From Understanding to Investigation, Herpesviridae*. (Elsevier Ltd., 2017).
3. Knipe, D. M. & Howley, P. M. *Fields Virology, Herpes Simplex Virus 1*. (Lippincott Williams & Wilkins, 2013).
4. Acheson, N. H. *Fundamentals of Molecular Virology, Larger DNA Viruses of Eukaryotes*. (John Wiley & Sons, Inc., 2007).
5. Lint, A. L. & Knipe, D. M. *Encyclopedia of Microbiology, Herpesviruses*. (Elsevier Ltd., 2009).
6. Ramchandani, M. *et al.* Herpes Simplex Virus Type 1 Shedding in Tears and Nasal and Oral Mucosa of Healthy Adults. *Sex. Transm. Dis.* **43**, 756–760 (2016).
7. Dolan, A., Jamieson, F. E., Cunningham, C., Barnett, B. C. & McGeoch, D. J. The genome sequence of herpes simplex virus type 2. *J. Virol.* **72**, 2010–2021 (1998).
8. Gavins, F. N. E. & Stokes, K. Y. *Vascular Responses to Pathogens, Herpesviruses*. (Elsevier Ltd., 2015).
9. Brugha, R., Keersmaekers, K., Renton, A. & Meheus, A. Genital herpes infection: a review. *Int. J. Epidemiol.* **26**, 698–709 (1997).
10. Nicoll, M. P., Proença, J. T. & Efstathiou, S. The molecular basis of herpes simplex virus latency. *FEMS Microbiol. Rev.* **36**, 684–705 (2012).
11. Bloom, D. C., Giordani, N. V. & Kwiatkowski, D. L. Epigenetic regulation of latent HSV-1 gene expression. *Biochim. Biophys. Acta* **1799**, 246–256 (2010).
12. Harris, J. B. & Holmes, A. P. Neonatal Herpes Simplex Viral Infections and Acyclovir: An Update. *J. Pediatr. Pharmacol. Ther. JPPT Off. J. PPAG* **22**, 88–93 (2017).
13. Grünewald, K. *et al.* Three-dimensional structure of herpes simplex virus from cryo-electron tomography. *Science* **302**, 1396–1398 (2003).
14. Brown, J. C. & Newcomb, W. W. Herpesvirus capsid assembly: insights from structural analysis. *Curr. Opin. Virol.* **1**, 142–149 (2011).
15. Gibson, W. & Roizman, B. Compartmentalization of spermine and spermidine in the herpes simplex virion. *Proc. Natl. Acad. Sci. U. S. A.* **68**, 2818–2821 (1971).
16. Baines, J. D. Herpes simplex virus capsid assembly and DNA packaging: a present and future antiviral drug target. *Trends Microbiol.* **19**, 606–613 (2011).

17. Homa, null & Brown, null. Capsid assembly and DNA packaging in herpes simplex virus. *Rev. Med. Virol.* **7**, 107–122 (1997).
18. Vittone, V. *et al.* Determination of interactions between tegument proteins of herpes simplex virus type 1. *J. Virol.* **79**, 9566–9571 (2005).
19. Stannard, L. M., Fuller, A. O. & Spear, P. G. Herpes simplex virus glycoproteins associated with different morphological entities projecting from the virion envelope. *J. Gen. Virol.* **68 (Pt 3)**, 715–725 (1987).
20. Kieff, E. D., Bachenheimer, S. L. & Roizman, B. Size, composition, and structure of the deoxyribonucleic acid of herpes simplex virus subtypes 1 and 2. *J. Virol.* **8**, 125–132 (1971).
21. Denes, C. E., Everett, R. D. & Diefenbach, R. J. Tour de Herpes: Cycling Through the Life and Biology of HSV-1. *Methods Mol. Biol. Clifton NJ* **2060**, 1–30 (2020).
22. Whisnant, A. W. *et al.* Integrative functional genomics decodes herpes simplex virus 1. *Nat. Commun.* **11**, 2038 (2020).
23. Brown, J. C. High G+C Content of Herpes Simplex Virus DNA: Proposed Role in Protection Against Retrotransposon Insertion. *Open Biochem. J.* **1**, 33–42 (2007).
24. Umene, K. Recombination of the internal direct repeat element DR2 responsible for the fluidity of the a sequence of herpes simplex virus type 1. *J. Virol.* **65**, 5410–5416 (1991).
25. Hayward, G. S., Jacob, R. J., Wadsworth, S. C. & Roizman, B. Anatomy of herpes simplex virus DNA: evidence for four populations of molecules that differ in the relative orientations of their long and short components. *Proc. Natl. Acad. Sci. U. S. A.* **72**, 4243–4247 (1975).
26. Polvino-Bodnar, M., Orberg, P. K. & Schaffer, P. A. Herpes simplex virus type 1 oriL is not required for virus replication or for the establishment and reactivation of latent infection in mice. *J. Virol.* **61**, 3528–3535 (1987).
27. Denes, C. E., Miranda-Saksena, M., Cunningham, A. L. & Diefenbach, R. J. Cytoskeletons in the Closet—Subversion in Alphaherpesvirus Infections. *Viruses* **10**, (2018).
28. Wittels, M. & Spear, P. G. Penetration of cells by herpes simplex virus does not require a low pH-dependent endocytic pathway. *Virus Res.* **18**, 271–290 (1991).
29. Akhtar, J. & Shukla, D. Viral entry mechanisms: cellular and viral mediators of herpes simplex virus entry. *FEBS J.* **276**, 7228–7236 (2009).
30. Agelidis, A. M. & Shukla, D. Cell entry mechanisms of HSV: what we have learned in recent years. *Future Virol.* **10**, 1145–1154 (2015).

31. Kelly, B. J., Fraefel, C., Cunningham, A. L. & Diefenbach, R. J. Functional roles of the tegument proteins of herpes simplex virus type 1. *Virus Res.* **145**, 173–186 (2009).
32. Xu, X., Che, Y. & Li, Q. HSV-1 tegument protein and the development of its genome editing technology. *Virol. J.* **13**, 108 (2016).
33. Döhner, K., Nagel, C.-H. & Sodeik, B. Viral stop-and-go along microtubules: taking a ride with dynein and kinesins. *Trends Microbiol.* **13**, 320–327 (2005).
34. Strang, B. L. & Stow, N. D. Circularization of the herpes simplex virus type 1 genome upon lytic infection. *J. Virol.* **79**, 12487–12494 (2005).
35. Host Intrinsic and Innate Intracellular Immunity During Herpes Simplex Virus Type 1 (HSV-1) Infection - PubMed. https://pubmed.ncbi.nlm.nih.gov/31781083/.
36. Cellular proteins localized at and interacting within ND10/PML nuclear bodies/PODs suggest functions of a nuclear depot - PubMed. https://pubmed.ncbi.nlm.nih.gov/11704851/.
37. Tavalai, N. & Stamminger, T. New insights into the role of the subnuclear structure ND10 for viral infection. *Biochim. Biophys. Acta* **1783**, 2207–2221 (2008).
38. Xu, P. & Roizman, B. The SP100 component of ND10 enhances accumulation of PML and suppresses replication and the assembly of HSV replication compartments. *Proc. Natl. Acad. Sci. U. S. A.* **114**, E3823–E3829 (2017).
39. Components of promyelocytic leukemia nuclear bodies (ND10) act cooperatively to repress herpesvirus infection - PubMed. https://pubmed.ncbi.nlm.nih.gov/23221561/.
40. Xu, P., Mallon, S. & Roizman, B. PML plays both inimical and beneficial roles in HSV-1 replication. *Proc. Natl. Acad. Sci. U. S. A.* **113**, E3022-3028 (2016).
41. Burkham, J., Coen, D. M., Hwang, C. B. C. & Weller, S. K. Interactions of Herpes Simplex Virus Type 1 with ND10 and Recruitment of PML to Replication Compartments. *J. Virol.* **75**, 2353–2367 (2001).
42. Gu, H. & Roizman, B. The degradation of promyelocytic leukemia and Sp100 proteins by herpes simplex virus 1 is mediated by the ubiquitin-conjugating enzyme UbcH5a. *Proc. Natl. Acad. Sci. U. S. A.* **100**, 8963–8968 (2003).
43. Maul, G. G. & Everett, R. D. The nuclear location of PML, a cellular member of the C3HC4 zinc-binding domain protein family, is rearranged during herpes simplex virus infection by the C3HC4 viral protein ICP0. *J. Gen. Virol.* **75 (Pt 6)**, 1223–1233 (1994).
44. Jackson, S. P. & Bartek, J. The DNA-damage response in human biology and disease. *Nature* **461**, 1071–1078 (2009).

45. Weitzman, M. D., Lilley, C. E. & Chaurushiya, M. S. Genomes in conflict: maintaining genome integrity during virus infection. *Annu. Rev. Microbiol.* **64**, 61–81 (2010).
46. Put a RING on it: regulation and inhibition of RNF8 and RNF168 RING finger E3 ligases at DNA damage sites - PubMed. https://pubmed.ncbi.nlm.nih.gov/23847653/.
47. Weitzman, M. D., Lilley, C. E. & Chaurushiya, M. S. Changing the ubiquitin landscape during viral manipulation of the DNA damage response. *FEBS Lett.* **585**, 2897–2906 (2011).
48. Lilley, C. E. *et al.* A viral E3 ligase targets RNF8 and RNF168 to control histone ubiquitination and DNA damage responses. *EMBO J.* **29**, 943–955 (2010).
49. Oh, J. & Fraser, N. W. Temporal association of the herpes simplex virus genome with histone proteins during a lytic infection. *J. Virol.* **82**, 3530–3537 (2008).
50. Lu, X. & Triezenberg, S. J. Chromatin assembly on herpes simplex virus genomes during lytic infection. *Biochim. Biophys. Acta* **1799**, 217–222 (2010).
51. Lacasse, J. J. & Schang, L. M. Herpes simplex virus 1 DNA is in unstable nucleosomes throughout the lytic infection cycle, and the instability of the nucleosomes is independent of DNA replication. *J. Virol.* **86**, 11287–11300 (2012).
52. Kristie, T. M. Chromatin Modulation of Herpesvirus Lytic Gene Expression: Managing Nucleosome Density and Heterochromatic Histone Modifications. *mBio* **7**, (2016).
53. Cliffe, A. R. & Knipe, D. M. Herpes simplex virus ICP0 promotes both histone removal and acetylation on viral DNA during lytic infection. *J. Virol.* **82**, 12030–12038 (2008).
54. Liang, Y., Vogel, J. L., Narayanan, A., Peng, H. & Kristie, T. M. Inhibition of the histone demethylase LSD1 blocks alpha-herpesvirus lytic replication and reactivation from latency. *Nat. Med.* **15**, 1312–1317 (2009).
55. Narayanan, A., Ruyechan, W. T. & Kristie, T. M. The coactivator host cell factor-1 mediates Set1 and MLL1 H3K4 trimethylation at herpesvirus immediate early promoters for initiation of infection. *Proc. Natl. Acad. Sci. U. S. A.* **104**, 10835–10840 (2007).
56. Maksour, S., Ooi, L. & Dottori, M. More than a Corepressor: The Role of CoREST Proteins in Neurodevelopment. *eNeuro* **7**, (2020).
57. Gu, H., Liang, Y., Mandel, G. & Roizman, B. Components of the REST/CoREST/histone deacetylase repressor complex are disrupted, modified, and translocated in HSV-1-infected cells. *Proc. Natl. Acad. Sci. U. S. A.* **102**, 7571–7576 (2005).

58. Gu, H. & Roizman, B. Herpes simplex virus-infected cell protein 0 blocks the silencing of viral DNA by dissociating histone deacetylases from the CoREST-REST complex. *Proc. Natl. Acad. Sci. U. S. A.* **104**, 17134–17139 (2007).
59. Lomonte, P. *et al.* Functional interaction between class II histone deacetylases and ICP0 of herpes simplex virus type 1. *J. Virol.* **78**, 6744–6757 (2004).
60. Costanzo, F., Campadelli-Fiume, G., Foa-Tomasi, L. & Cassai, E. Evidence that herpes simplex virus DNA is transcribed by cellular RNA polymerase B. *J. Virol.* **21**, 996–1001 (1977).
61. Dremel, S. E. & DeLuca, N. A. Genome replication affects transcription factor binding mediating the cascade of herpes simplex virus transcription. *Proc. Natl. Acad. Sci. U. S. A.* **116**, 3734–3739 (2019).
62. Dembowski, J. A. & DeLuca, N. A. Temporal Viral Genome-Protein Interactions Define Distinct Stages of Productive Herpesviral Infection. *mBio* **9**, (2018).
63. Physical and functional interactions between herpes simplex virus immediate-early proteins ICP4 and ICP27 - PubMed. https://pubmed.ncbi.nlm.nih.gov/8995681/.
64. Batterson, W. & Roizman, B. Characterization of the herpes simplex virion-associated factor responsible for the induction of alpha genes. *J. Virol.* **46**, 371–377 (1983).
65. Campbell, M. E., Palfreyman, J. W. & Preston, C. M. Identification of herpes simplex virus DNA sequences which encode a trans-acting polypeptide responsible for stimulation of immediate early transcription. *J. Mol. Biol.* **180**, 1–19 (1984).
66. Thomas, S., Coffin, R. S., Watts, P., Gough, G. & Latchman, D. S. The TAATGARAT motif in the herpes simplex virus immediate-early gene promoters can confer both positive and negative responses to cellular octamer-binding proteins when it is located within the viral genome. *J. Virol.* **72**, 3495–3500 (1998).
67. Herrera, F. J. & Triezenberg, S. J. VP16-dependent association of chromatin-modifying coactivators and underrepresentation of histones at immediate-early gene promoters during herpes simplex virus infection. *J. Virol.* **78**, 9689–9696 (2004).
68. Fan, D. *et al.* The Role of VP16 in the Life Cycle of Alphaherpesviruses. *Front. Microbiol.* **11**, 1910 (2020).
69. Harkness, J. M., Kader, M. & DeLuca, N. A. Transcription of the herpes simplex virus 1 genome during productive and quiescent infection of neuronal and nonneuronal cells. *J. Virol.* **88**, 6847–6861 (2014).
70. DeLuca, N. A. & Schaffer, P. A. Physical and functional domains of the herpes simplex virus transcriptional regulatory protein ICP4. *J. Virol.* **62**, 732–743 (1988).

71. Smith, M. C., Boutell, C. & Davido, D. J. HSV-1 ICP0: paving the way for viral replication. *Future Virol.* **6**, 421–429 (2011).
72. Gruffat, H., Marchione, R. & Manet, E. Herpesvirus Late Gene Expression: A Viral-Specific Pre-initiation Complex Is Key. *Front. Microbiol.* **7**, 869 (2016).
73. Olesky, M., McNamee, E. E., Zhou, C., Taylor, T. J. & Knipe, D. M. Evidence for a direct interaction between HSV-1 ICP27 and ICP8 proteins. *Virology* **331**, 94–105 (2005).
74. Ryu, W.-S. *Molecular Virology of Human Pathogenic Viruses, Herpesviruses*. (Elsevier Ltd., 2016).
75. Smith, R. W. P., Graham, S. V. & Gray, N. K. Regulation of translation initiation by herpesviruses. *Biochem. Soc. Trans.* **36**, 701–707 (2008).
76. Cooper, G. M. Translation of mRNA. *Cell Mol. Approach 2nd Ed.* (2000).
77. Walsh, D. & Mohr, I. Viral subversion of the host protein synthesis machinery. *Nat. Rev. Microbiol.* **9**, 860–875 (2011).
78. Chuluunbaatar, U. *et al.* Constitutive mTORC1 activation by a herpesvirus Akt surrogate stimulates mRNA translation and viral replication. *Genes Dev.* **24**, 2627–2639 (2010).
79. Walsh, D. & Mohr, I. Assembly of an active translation initiation factor complex by a viral protein. *Genes Dev.* **20**, 461–472 (2006).
80. Hargett, D., McLean, T. & Bachenheimer, S. L. Herpes simplex virus ICP27 activation of stress kinases JNK and p38. *J. Virol.* **79**, 8348–8360 (2005).
81. Inhibition of PACT-mediated activation of PKR by the herpes simplex virus type 1 Us11 protein - PubMed. https://pubmed.ncbi.nlm.nih.gov/12368348/.
82. He, B., Gross, M. & Roizman, B. The gamma(1)34.5 protein of herpes simplex virus 1 complexes with protein phosphatase 1alpha to dephosphorylate the alpha subunit of the eukaryotic translation initiation factor 2 and preclude the shutoff of protein synthesis by double-stranded RNA-activated protein kinase. *Proc. Natl. Acad. Sci. U. S. A.* **94**, 843–848 (1997).
83. Friedel, C. C. *et al.* Dissecting Herpes Simplex Virus 1-Induced Host Shutoff at the RNA Level. *J. Virol.* **95**, (2021).
84. Kwong, A. D. & Frenkel, N. Herpes simplex virus-infected cells contain a function(s) that destabilizes both host and viral mRNAs. *Proc. Natl. Acad. Sci. U. S. A.* **84**, 1926–1930 (1987).
85. Danastas, K., Miranda-Saksena, M. & Cunningham, A. L. Herpes Simplex Virus Type 1 Interactions with the Interferon System. *Int. J. Mol. Sci.* **21**, (2020).

86. Dauber, B., Saffran, H. A. & Smiley, J. R. The herpes simplex virus host shutoff (vhs) RNase limits accumulation of double stranded RNA in infected cells: Evidence for accelerated decay of duplex RNA. *PLOS Pathog.* **15**, e1008111 (2019).
87. Taddeo, B., Sciortino, M. T., Zhang, W. & Roizman, B. Interaction of herpes simplex virus RNase with VP16 and VP22 is required for the accumulation of the protein but not for accumulation of mRNA. *Proc. Natl. Acad. Sci. U. S. A.* **104**, 12163–12168 (2007).
88. Kops, A. de B. & Knipe, D. M. Formation of DNA replication structures in herpes virus-infected cells requires a viral DNA binding protein. *Cell* **55**, 857–868 (1988).
89. Taylor, T. J., Brockman, M. A., McNamee, E. E. & Knipe, D. M. Herpes simplex virus. *Front. Biosci. J. Virtual Libr.* **7**, d752-764 (2002).
90. Wu, C. A., Nelson, N. J., McGeoch, D. J. & Challberg, M. D. Identification of herpes simplex virus type 1 genes required for origin-dependent DNA synthesis. *J. Virol.* **62**, 435–443 (1988).
91. Aslani, A., Olsson, M. & Elias, P. ATP-dependent unwinding of a minimal origin of DNA replication by the origin-binding protein and the single-strand DNA-binding protein ICP8 from herpes simplex virus type I. *J. Biol. Chem.* **277**, 41204–41212 (2002).
92. Boehmer, P. E. The herpes simplex virus type-1 single-strand DNA-binding protein, ICP8, increases the processivity of the UL9 protein DNA helicase. *J. Biol. Chem.* **273**, 2676–2683 (1998).
93. Crute, J. J. *et al.* Herpes simplex virus 1 helicase-primase: a complex of three herpes-encoded gene products. *Proc. Natl. Acad. Sci. U. S. A.* **86**, 2186–2189 (1989).
94. Trego, K. S. & Parris, D. S. Functional interaction between the herpes simplex virus type 1 polymerase processivity factor and origin-binding proteins: enhancement of UL9 helicase activity. *J. Virol.* **77**, 12646–12659 (2003).
95. Weller, S. K. & Coen, D. M. Herpes simplex viruses: mechanisms of DNA replication. *Cold Spring Harb. Perspect. Biol.* **4**, a013011 (2012).
96. Preston, V. G. & McDougall, I. M. Regions of the herpes simplex virus scaffolding protein that are important for intermolecular self-interaction. *J. Virol.* **76**, 673–687 (2002).
97. Okoye, M. E., Sexton, G. L., Huang, E., McCaffery, J. M. & Desai, P. Functional analysis of the triplex proteins (VP19C and VP23) of herpes simplex virus type 1. *J. Virol.* **80**, 929–940 (2006).
98. Gibson, W. & Roizman, B. Proteins specified by herpes simplex virus. 8. Characterization and composition of multiple capsid forms of subtypes 1 and 2. *J. Virol.* **10**, 1044–1052 (1972).
99. Loret, S., Guay, G. & Lippé, R. Comprehensive characterization of extracellular herpes simplex virus type 1 virions. *J. Virol.* **82**, 8605–8618 (2008).

100. Newcomb, W. W. *et al.* The UL6 gene product forms the portal for entry of DNA into the herpes simplex virus capsid. *J. Virol.* **75**, 10923–10932 (2001).
101. Weller, S. K. *Alphaherpesviruses: Molecular Virology, Nucleocapsid Structure, Assembly and DNA Packaging of Herpes Simplex Virus*. (Caister Academic Press, 2011).
102. Herpes simplex virus type 1 DNA-packaging protein UL17 is required for efficient binding of UL25 to capsids - PubMed. https://pubmed.ncbi.nlm.nih.gov/16474120/.
103. Albright, B. S. *et al.* The putative herpes simplex virus 1 chaperone protein UL32 modulates disulfide bond formation during infection. *J. Virol.* **89**, 443–453 (2015).
104. Reynolds, A. E. *et al.* U(L)31 and U(L)34 proteins of herpes simplex virus type 1 form a complex that accumulates at the nuclear rim and is required for envelopment of nucleocapsids. *J. Virol.* **75**, 8803–8817 (2001).
105. Rice, S. A. & Davido, D. J. HSV-1 ICP22: hijacking host nuclear functions to enhance viral infection. *Future Microbiol.* **8**, 311–321 (2013).
106. Dogrammatzis, C., Waisner, H. & Kalamvoki, M. "Non-Essential" Proteins of HSV-1 with Essential Roles In Vivo: A Comprehensive Review. *Viruses* **13**, (2020).
107. Sears, A. E., Halliburton, I. W., Meignier, B., Silver, S. & Roizman, B. Herpes simplex virus 1 mutant deleted in the alpha 22 gene: growth and gene expression in permissive and restrictive cells and establishment of latency in mice. *J. Virol.* **55**, 338–346 (1985).
108. Poffenberger, K. L., Idowu, A. D., Fraser-Smith, E. B., Raichlen, P. E. & Herman, R. C. A herpes simplex virus type 1 ICP22 deletion mutant is altered for virulence and latency in vivo. *Arch. Virol.* **139**, 111–119 (1994).
109. Poffenberger, K. L., Raichlen, P. E. & Herman, R. C. In vitro characterization of a herpes simplex virus type 1 ICP22 deletion mutant. *Virus Genes* **7**, 171–186 (1993).
110. Purves, F. C., Ogle, W. O. & Roizman, B. Processing of the herpes simplex virus regulatory protein alpha 22 mediated by the UL13 protein kinase determines the accumulation of a subset of alpha and gamma mRNAs and proteins in infected cells. *Proc. Natl. Acad. Sci. U. S. A.* **90**, 6701–6705 (1993).
111. Kolb, A. W., Schmidt, T. R., Dyer, D. W. & Brandt, C. R. Sequence variation in the herpes simplex virus U(S)1 ocular virulence determinant. *Invest. Ophthalmol. Vis. Sci.* **52**, 4630–4638 (2011).
112. Carter, K. L. & Roizman, B. The promoter and transcriptional unit of a novel herpes simplex virus 1 alpha gene are contained in, and encode a protein in frame with, the open reading frame of the alpha 22 gene. *J. Virol.* **70**, 172–178 (1996).

113. Ogle, W. O. & Roizman, B. Functional Anatomy of Herpes Simplex Virus 1 Overlapping Genes Encoding Infected-Cell Protein 22 and US1.5 Protein. *J. Virol.* **73**, 4305–4315 (1999).
114. Bowman, J. J. & Schaffer, P. A. Origin of expression of the herpes simplex virus type 1 protein U(S)1.5. *J. Virol.* **83**, 9183–9194 (2009).
115. Mostafa, H. H. & Davido, D. J. Herpes Simplex Virus 1 ICP22 but Not US1.5 Is Required for Efficient Acute Replication in Mice and VICE Domain Formation. *J. Virol.* **87**, 13510–13519 (2013).
116. Stelz, G. *et al.* Identification of two nuclear import signals in the alpha-gene product ICP22 of herpes simplex virus 1. *Virology* **295**, 360–370 (2002).
117. Jahedi, S., Markovitz, N. S., Filatov, F. & Roizman, B. Colocalization of the herpes simplex virus 1 UL4 protein with infected cell protein 22 in small, dense nuclear structures formed prior to onset of DNA synthesis. *J. Virol.* **73**, 5132–5138 (1999).
118. Leopardi, R., Ward, P. L., Ogle, W. O. & Roizman, B. Association of herpes simplex virus regulatory protein ICP22 with transcriptional complexes containing EAP, ICP4, RNA polymerase II, and viral DNA requires posttranslational modification by the U(L)13 proteinkinase. *J. Virol.* **71**, 1133–1139 (1997).
119. Dembowski, J. A. & DeLuca, N. A. Selective recruitment of nuclear factors to productively replicating herpes simplex virus genomes. *PLoS Pathog.* **11**, e1004939 (2015).
120. Bastian, T. W., Livingston, C. M., Weller, S. K. & Rice, S. A. Herpes simplex virus type 1 immediate-early protein ICP22 is required for VICE domain formation during productive viral infection. *J. Virol.* **84**, 2384–2394 (2010).
121. Livingston, C. M., Ifrim, M. F., Cowan, A. E. & Weller, S. K. Virus-Induced Chaperone-Enriched (VICE) domains function as nuclear protein quality control centers during HSV-1 infection. *PLoS Pathog.* **5**, e1000619 (2009).
122. Adlakha, M., Livingston, C. M., Bezsonova, I. & Weller, S. K. The Herpes Simplex Virus 1 Immediate Early Protein ICP22 Is a Functional Mimic of a Cellular J Protein. *J. Virol.* **94**, (2020).
123. Fox, H. L., Dembowski, J. A. & DeLuca, N. A. A Herpesviral Immediate Early Protein Promotes Transcription Elongation of Viral Transcripts. *mBio* **8**, (2017).
124. Jacob, T., Van den Broeke, C. & Favoreel, H. W. Viral Serine/Threonine Protein Kinases. *J. Virol.* **85**, 1158–1173 (2011).
125. Kato, A. *et al.* Identification of Proteins Phosphorylated Directly by the Us3 Protein Kinase Encoded by Herpes Simplex Virus 1. *J. Virol.* **79**, 9325–9331 (2005).

126. Purves, F. C. & Roizman, B. The UL13 gene of herpes simplex virus 1 encodes the functions for posttranslational processing associated with phosphorylation of the regulatory protein alpha 22. *Proc. Natl. Acad. Sci. U. S. A.* **89**, 7310–7314 (1992).
127. Mitchell, C., Blaho, J. A., McCormick, A. L. & Roizman, B. The nucleotidylylation of herpes simplex virus 1 regulatory protein alpha22 by human casein kinase II. *J. Biol. Chem.* **272**, 25394–25400 (1997).
128. Asai, R., Ohno, T., Kato, A. & Kawaguchi, Y. Identification of proteins directly phosphorylated by UL13 protein kinase from herpes simplex virus 1. *Microbes Infect.* **9**, 1434–1438 (2007).
129. Advani, S. J., Weichselbaum, R. R. & Roizman, B. Herpes simplex virus 1 activates cdc2 to recruit topoisomerase II alpha for post-DNA synthesis expression of late genes. *Proc. Natl. Acad. Sci. U. S. A.* **100**, 4825–4830 (2003).
130. Smith-Donald, B. A. & Roizman, B. The interaction of herpes simplex virus 1 regulatory protein ICP22 with the cdc25C phosphatase is enabled in vitro by viral protein kinases US3 and UL13. *J. Virol.* **82**, 4533–4543 (2008).
131. Long, M. C., Leong, V., Schaffer, P. A., Spencer, C. A. & Rice, S. A. ICP22 and the UL13 protein kinase are both required for herpes simplex virus-induced modification of the large subunit of RNA polymerase II. *J. Virol.* **73**, 5593–5604 (1999).
132. Durand, L. O., Advani, S. J., Poon, A. P. W. & Roizman, B. The Carboxyl-Terminal Domain of RNA Polymerase II Is Phosphorylated by a Complex Containing cdk9 and Infected-Cell Protein 22 of Herpes Simplex Virus 1. *J. Virol.* **79**, 6757–6762 (2005).
133. Sandri-Goldin, R. M. The many roles of the highly interactive HSV protein ICP27, a key regulator of infection. *Future Microbiol.* **6**, 1261–1277 (2011).
134. Souki, S. K., Gershon, P. D. & Sandri-Goldin, R. M. Arginine Methylation of the ICP27 RGG Box Regulates ICP27 Export and Is Required for Efficient Herpes Simplex Virus 1 Replication. *J. Virol.* **83**, 5309–5320 (2009).
135. Rojas, S., Corbin-Lickfett, K. A., Escudero-Paunetto, L. & Sandri-Goldin, R. M. ICP27 phosphorylation site mutants are defective in herpes simplex virus 1 replication and gene expression. *J. Virol.* **84**, 2200–2211 (2010).
136. Chen, I.-H. B., Li, L., Silva, L. & Sandri-Goldin, R. M. ICP27 recruits Aly/REF but not TAP/NXF1 to herpes simplex virus type 1 transcription sites although TAP/NXF1 is required for ICP27 export. *J. Virol.* **79**, 3949–3961 (2005).

137. Perkins, K. D., Gregonis, J., Borge, S. & Rice, S. A. Transactivation of a viral target gene by herpes simplex virus ICP27 is posttranscriptional and does not require the endogenous promoter or polyadenylation site. *J. Virol.* **77**, 9872–9884 (2003).
138. Sandri-Goldin, R. M. & Mendoza, G. E. A herpesvirus regulatory protein appears to act post-transcriptionally by affecting mRNA processing. *Genes Dev.* **6**, 848–863 (1992).
139. Sciabica, K. S., Dai, Q. J. & Sandri-Goldin, R. M. ICP27 interacts with SRPK1 to mediate HSV splicing inhibition by altering SR protein phosphorylation. *EMBO J.* **22**, 1608–1619 (2003).
140. Widespread disruption of host transcription termination in HSV-1 infection | Nature Communications. https://www.nature.com/articles/ncomms8126.
141. Tang, S., Patel, A. & Krause, P. R. Herpes simplex virus ICP27 regulates alternative pre-mRNA polyadenylation and splicing in a sequence-dependent manner. *Proc. Natl. Acad. Sci. U. S. A.* **113**, 12256–12261 (2016).
142. Ellison, K. S., Maranchuk, R. A., Mottet, K. L. & Smiley, J. R. Control of VP16 translation by the herpes simplex virus type 1 immediate-early protein ICP27. *J. Virol.* **79**, 4120–4131 (2005).
143. Fontaine-Rodriguez, E. C., Taylor, T. J., Olesky, M. & Knipe, D. M. Proteomics of herpes simplex virus infected cell protein 27: association with translation initiation factors. *Virology* **330**, 487–492 (2004).
144. Fontaine-Rodriguez, E. C. & Knipe, D. M. Herpes simplex virus ICP27 increases translation of a subset of viral late mRNAs. *J. Virol.* **82**, 3538–3545 (2008).
145. Venkatesh, S. & Workman, J. L. Histone exchange, chromatin structure and the regulation of transcription. *Nat. Rev. Mol. Cell Biol.* **16**, 178–189 (2015).
146. Sadakierska-Chudy, A. & Filip, M. A comprehensive view of the epigenetic landscape. Part II: Histone post-translational modification, nucleosome level, and chromatin regulation by ncRNAs. *Neurotox. Res.* **27**, 172–197 (2015).
147. Martire, S. & Banaszynski, L. A. The roles of histone variants in fine-tuning chromatin organization and function. *Nat. Rev. Mol. Cell Biol.* **21**, 522–541 (2020).
148. Izzo, A. & Schneider, R. The role of linker histone H1 modifications in the regulation of gene expression and chromatin dynamics. *Biochim. Biophys. Acta* **1859**, 486–495 (2016).
149. M. Cooper, G. & Hausman, R. *The Cell - A Molecular Approach*. (Sinauer Associates, 2009).
150. Zhou, K., Gaullier, G. & Luger, K. Nucleosome structure and dynamics are coming of age. *Nat. Struct. Mol. Biol.* **26**, 3–13 (2019).
151. McGinty, R. K. & Tan, S. Nucleosome Structure and Function. *Chem. Rev.* **115**, 2255–2273 (2015).

152. A brief review of nucleosome structure | Elsevier Enhanced Reader. https://reader.elsevier.com/reader/sd/pii/S0014579315003920?token=46FB0DA5BC204D928012CB09C7E2D90565697761016C9280D228FF0BDA8606E8AC3A71A2377250FBF712B82791838E6C doi:10.1016/j.febslet.2015.05.016.
153. Fyodorov, D. V., Zhou, B.-R., Skoultchi, A. I. & Bai, Y. Emerging roles of linker histones in regulating chromatin structure and function. *Nat. Rev. Mol. Cell Biol.* **19**, 192–206 (2018).
154. Histone Post-Translational Modifications and Nucleosome Organisation in Transcriptional Regulation: Some Open Questions | SpringerLink. https://link.springer.com/chapter/10.1007%2F5584_2017_58.
155. Gillette, T. G. & Hill, J. A. Readers, writers and erasers: Chromatin as the Whiteboard of Heart Disease. *Circ. Res.* **116**, 1245–1253 (2015).
156. Zhao, S., Yue, Y., Li, Y. & Li, H. Identification and characterization of 'readers' for novel histone modifications. *Curr. Opin. Chem. Biol.* **51**, 57–65 (2019).
157. Chemical mechanisms of histone lysine and arginine modifications. https://www.ncbi.nlm.nih.gov/pmc/articles/PMC2642981/.
158. Regulation of chromatin by histone modifications | Cell Research. https://www.nature.com/articles/cr201122.
159. Jambhekar, A., Dhall, A. & Shi, Y. Roles and regulation of histone methylation in animal development. *Nat. Rev. Mol. Cell Biol.* **20**, 625–641 (2019).
160. Vermeulen, M. *et al.* Selective anchoring of TFIID to nucleosomes by trimethylation of histone H3 lysine 4. *Cell* **131**, 58–69 (2007).
161. Okitsu, C. Y., Hsieh, J. C. F. & Hsieh, C.-L. Transcriptional activity affects the H3K4me3 level and distribution in the coding region. *Mol. Cell. Biol.* **30**, 2933–2946 (2010).
162. Distinct and predictive chromatin signatures of transcriptional promoters and enhancers in the human genome | Nature Genetics. https://www.nature.com/articles/ng1966.
163. Kim, T. H. *et al.* A high-resolution map of active promoters in the human genome. *Nature* **436**, 876–880 (2005).
164. Mapping Global Histone Methylation Patterns in the Coding Regions of Human Genes | Molecular and Cellular Biology. https://mcb.asm.org/content/25/11/4650.
165. Huang, C. & Zhu, B. Roles of H3K36-specific histone methyltransferases in transcription: antagonizing silencing and safeguarding transcription fidelity. *Biophys. Rep.* **4**, 170–177 (2018).

166. Wagner, E. J. & Carpenter, P. B. Understanding the language of Lys36 methylation at histone H3. *Nat. Rev. Mol. Cell Biol.* **13**, 115–126 (2012).
167. Sen, P. *et al.* H3K36 methylation promotes longevity by enhancing transcriptional fidelity. *Genes Dev.* **29**, 1362–1376 (2015).
168. Saksouk, N., Simboeck, E. & Déjardin, J. Constitutive heterochromatin formation and transcription in mammals. *Epigenetics Chromatin* **8**, 3 (2015).
169. Henikoff, S. & Smith, M. M. Histone variants and epigenetics. *Cold Spring Harb. Perspect. Biol.* **7**, a019364 (2015).
170. Talbert, P. B. *et al.* A unified phylogeny-based nomenclature for histone variants. *Epigenetics Chromatin* **5**, 7 (2012).
171. Post-Translational Modifications of Histones That Influence Nucleosome Dynamics | Chemical Reviews. https://pubs.acs.org/doi/abs/10.1021/cr500350x.
172. Eaton, J. D. & West, S. Termination of Transcription by RNA Polymerase II: BOOM! *Trends Genet.* **36**, 664–675 (2020).
173. The RNA Polymerase II Carboxy-Terminal Domain (CTD) Code | Chemical Reviews. https://pubs.acs.org/doi/10.1021/cr400071f.
174. Shah, N. *et al.* Tyrosine-1 of RNA Polymerase II CTD Controls Global Termination of Gene Transcription in Mammals. *Mol. Cell* **69**, 48-61.e6 (2018).
175. Chen, F. X., Smith, E. R. & Shilatifard, A. Born to run: control of transcription elongation by RNA polymerase II. *Nat. Rev. Mol. Cell Biol.* **19**, 464–478 (2018).
176. Regulation of transcription elongation in response to osmostress. https://www.ncbi.nlm.nih.gov/pmc/articles/PMC5720810/.
177. Cramer, P. Organization and regulation of gene transcription. *Nature* **573**, 45–54 (2019).
178. Jonkers, I. & Lis, J. T. Getting up to speed with transcription elongation by RNA polymerase II. *Nat. Rev. Mol. Cell Biol.* **16**, 167–177 (2015).
179. Kulaeva, O. I., Hsieh, F.-K., Chang, H.-W., Luse, D. S. & Studitsky, V. M. Mechanism of transcription through a nucleosome by RNA polymerase II. *Biochim. Biophys. Acta* **1829**, 76–83 (2013).
180. The role of chromatin modifiers in normal and malignant hematopoiesis. https://www.ncbi.nlm.nih.gov/pmc/articles/PMC3952453/.
181. C, D. & Jk, T. Histone exchange and histone modifications during transcription and aging. *Biochim. Biophys. Acta* **1819**, 332–342 (2013).

182. Fan, H.-F., Liu, Z.-N., Chow, S.-Y., Lu, Y.-H. & Li, H. Histone Chaperone-Mediated Nucleosome Assembly Process. *PLoS ONE* **10**, (2015).
183. Das, C., Tyler, J. K. & Churchill, M. E. A. The histone shuffle: histone chaperones in an energetic dance. *Trends Biochem. Sci.* **35**, 476–489 (2010).
184. Avvakumov, N., Nourani, A. & Côté, J. Histone chaperones: modulators of chromatin marks. *Mol. Cell* **41**, 502–514 (2011).
185. Jeronimo, C., Watanabe, S., Kaplan, C. D., Peterson, C. L. & Robert, F. The Histone Chaperones FACT and Spt6 Restrict H2A.Z from Intragenic Locations. *Mol. Cell* **58**, 1113–1123 (2015).
186. The chromatin-specific transcription elongation factor FACT comprises human SPT16 and SSRP1 proteins - PubMed. https://pubmed.ncbi.nlm.nih.gov/10421373/.
187. FACT facilitates transcription-dependent nucleosome alteration - PubMed. https://pubmed.ncbi.nlm.nih.gov/12934006/.
188. Kaplan, C. D., Laprade, L. & Winston, F. Transcription elongation factors repress transcription initiation from cryptic sites. *Science* **301**, 1096–1099 (2003).
189. Yang, J. *et al.* The Histone Chaperone FACT Contributes to DNA Replication-Coupled Nucleosome Assembly. *Cell Rep.* **14**, 1128–1141 (2016).
190. Formosa, T. The role of FACT in making and breaking nucleosomes. *Biochim. Biophys. Acta* **1819**, 247–255 (2012).
191. Formosa, T. & Winston, F. The role of FACT in managing chromatin: disruption, assembly, or repair? *Nucleic Acids Res.* **48**, 11929–11941 (2020).
192. Reinberg, D. & Sims, R. J. de FACTo nucleosome dynamics. *J. Biol. Chem.* **281**, 23297–23301 (2006).
193. Winkler, D. D. & Luger, K. The histone chaperone FACT: structural insights and mechanisms for nucleosome reorganization. *J. Biol. Chem.* **286**, 18369–18374 (2011).
194. Insight into the mechanism of nucleosome reorganization from histone mutants that suppress defects in the FACT histone chaperone - PubMed. https://pubmed.ncbi.nlm.nih.gov/21625001/.
195. Xin, H. *et al.* yFACT induces global accessibility of nucleosomal DNA without H2A-H2B displacement. *Mol. Cell* **35**, 365–376 (2009).
196. Feng, J. *et al.* Noncoding Transcription Is a Driving Force for Nucleosome Instability in spt16 Mutant Cells. *Mol. Cell. Biol.* **36**, 1856–1867 (2016).
197. Mylonas, C. & Tessarz, P. Transcriptional repression by FACT is linked to regulation of chromatin accessibility at the promoter of ES cells. *Life Sci. Alliance* **1**, (2018).

198. Prendergast, L., Hong, E., Safina, A., Poe, D. & Gurova, K. Histone chaperone FACT is essential to overcome replication stress in mammalian cells. *Oncogene* **39**, 5124–5137 (2020).
199. Chu, Y., Sutton, A., Sternglanz, R. & Prelich, G. The BUR1 cyclin-dependent protein kinase is required for the normal pattern of histone methylation by SET2. *Mol. Cell. Biol.* **26**, 3029–3038 (2006).
200. Stanlie, A., Aida, M., Muramatsu, M., Honjo, T. & Begum, N. A. Histone3 lysine4 trimethylation regulated by the facilitates chromatin transcription complex is critical for DNA cleavage in class switch recombination. *Proc. Natl. Acad. Sci. U. S. A.* **107**, 22190–22195 (2010).
201. Evidence that Spt6p controls chromatin structure by a direct interaction with histones - PubMed. https://pubmed.ncbi.nlm.nih.gov/8633238/.
202. Sdano, M. A. *et al.* A novel SH2 recognition mechanism recruits Spt6 to the doubly phosphorylated RNA polymerase II linker at sites of transcription. *eLife* **6**, e28723 (2017).
203. The Abundant Histone Chaperones Spt6 and FACT Collaborate to Assemble, Inspect, and Maintain Chromatin Structure in Saccharomyces cerevisiae | Genetics. https://www.genetics.org/content/201/3/1031.
204. Histone Chaperones Spt6 and FACT: Similarities and Differences in Modes of Action at Transcribed Genes. https://www.hindawi.com/journals/gri/2011/625210/.
205. Human Spt6 Stimulates Transcription Elongation by RNA Polymerase II In Vitro. https://www.ncbi.nlm.nih.gov/pmc/articles/PMC381665/.
206. Ardehali, M. B. *et al.* Spt6 enhances the elongation rate of RNA polymerase II in vivo. *EMBO J.* **28**, 1067–1077 (2009).
207. Ivanovska, I., Jacques, P.-É., Rando, O. J., Robert, F. & Winston, F. Control of chromatin structure by spt6: different consequences in coding and regulatory regions. *Mol. Cell. Biol.* **31**, 531–541 (2011).
208. Evidence for Eviction and Rapid Deposition of Histones upon Transcriptional Elongation by RNA Polymerase II. https://www.ncbi.nlm.nih.gov/pmc/articles/PMC529037/.
209. Transcription Through Chromatin by RNA polymerase II: Histone Displacement and Exchange. https://www.ncbi.nlm.nih.gov/pmc/articles/PMC1924643/.
210. Kireeva, M. L. *et al.* Nucleosome Remodeling Induced by RNA Polymerase II: Loss of the H2A/H2B Dimer during Transcription. *Mol. Cell* **9**, 541–552 (2002).

211. DeGennaro, C. M. *et al.* Spt6 regulates intragenic and antisense transcription, nucleosome positioning, and histone modifications genome-wide in fission yeast. *Mol. Cell. Biol.* **33**, 4779–4792 (2013).
212. (7) (PDF) CTD Tyrosine Phosphorylation Impairs Termination Factor Recruitment to RNA Polymerase II. https://www.researchgate.net/publication/228089265_CTD_Tyrosine_Phosphorylation_Impairs_Termination_Factor_Recruitment_to_RNA_Polymerase_II.
213. Roles for Ctk1 and Spt6 in regulating the different methylation states of histone H3 lysine 36 - PubMed. https://pubmed.ncbi.nlm.nih.gov/18541663/.
214. Kuehner, J. N., Pearson, E. L. & Moore, C. Unravelling the means to an end: RNA polymerase II transcription termination. *Nat. Rev. Mol. Cell Biol.* **12**, 283–294 (2011).
215. Proudfoot, N. J. Transcriptional termination in mammals: Stopping the RNA polymerase II juggernaut. *Science* **352**, aad9926–aad9926 (2016).
216. Genome-wide Analysis of RNA Polymerase II Termination at Protein-Coding Genes - PubMed. https://pubmed.ncbi.nlm.nih.gov/28318822/.
217. Mandel, C. R., Bai, Y. & Tong, L. Protein factors in pre-mRNA 3'-end processing. *Cell. Mol. Life Sci. CMLS* **65**, 1099–1122 (2008).
218. A functional mRNA polyadenylation signal is required for transcription termination by RNA polymerase II. http://genesdev.cshlp.org/content/2/4/440.
219. Kim, M. *et al.* The yeast Rat1 exonuclease promotes transcription termination by RNA polymerase II. *Nature* **432**, 517–522 (2004).
220. Eaton, J. D., Francis, L., Davidson, L. & West, S. A unified allosteric/torpedo mechanism for transcriptional termination on human protein-coding genes. *Genes Dev.* **34**, 132–145 (2020).
221. Gregersen, L. H. *et al.* SCAF4 and SCAF8, mRNA Anti-Terminator Proteins. *Cell* **177**, 1797-1813.e18 (2019).
222. Xrn2 accelerates termination by RNA polymerase II, which is underpinned by CPSF73 activity. http://genesdev.cshlp.org/content/32/2/127.
223. Fong, N. *et al.* Effects of Transcription Elongation Rate and Xrn2 Exonuclease Activity on RNA Polymerase II Termination Suggest Widespread Kinetic Competition. *Mol. Cell* **60**, 256–267 (2015).
224. A Cdk9–PP1 switch regulates the elongation–termination transition of RNA polymerase II | Nature. https://www.nature.com/articles/s41586-018-0214-z.

225. Kecman, T. *et al.* Elongation/Termination Factor Exchange Mediated by PP1 Phosphatase Orchestrates Transcription Termination. *Cell Rep.* **25**, 259-269.e5 (2018).
226. Candelli, T., Gros, J. & Libri, D. Pervasive transcription fine-tunes replication origin activity. *eLife* **7**, e40802 (2018).
227. Jensen, T. H., Jacquier, A. & Libri, D. Dealing with Pervasive Transcription. *Mol. Cell* **52**, 473–484 (2013).
228. Vilborg, A., Passarelli, M. C., Yario, T. A., Tycowski, K. T. & Steitz, J. A. Widespread Inducible Transcription Downstream of Human Genes. *Mol. Cell* **59**, 449–461 (2015).
229. Pervasive transcription read-through promotes aberrant expression of oncogenes and RNA chimeras in renal carcinoma | eLife. https://elifesciences.org/articles/09214.
230. Vilborg, A. *et al.* Comparative analysis reveals genomic features of stress-induced transcriptional readthrough. *Proc. Natl. Acad. Sci.* **114**, E8362–E8371 (2017).
231. Zhao, N. *et al.* Influenza virus infection causes global RNAPII termination defects. *Nat. Struct. Mol. Biol.* **25**, 885–893 (2018).
232. Control of Gene Expression in Senescence through Transcriptional Read-Through of Convergent Protein-Coding Genes - PubMed. https://pubmed.ncbi.nlm.nih.gov/29186682/.
233. Transcription Elongation Can Affect Genome 3D Structure - PubMed. https://pubmed.ncbi.nlm.nih.gov/30146161/.
234. Hennig, T. *et al.* HSV-1-induced disruption of transcription termination resembles a cellular stress response but selectively increases chromatin accessibility downstream of genes. *PLoS Pathog.* **14**, e1006954 (2018).
235. Wang, X. *et al.* Herpes simplex virus blocks host transcription termination via the bimodal activities of ICP27. *Nat. Commun.* **11**, 293 (2020).
236. Rosa-Mercado, N. A. *et al.* Hyperosmotic stress alters the RNA polymerase II interactome and induces readthrough transcription despite widespread transcriptional repression. *Mol. Cell* **81**, 502-513.e4 (2021).
237. Mammalian NET-Seq Reveals Genome-wide Nascent Transcription Coupled to RNA Processing: Cell. https://www.cell.com/fulltext/S0092-8674(15)00314-1.
238. Influenza Virus Mounts a Two-Pronged Attack on Host RNA Polymerase II Transcription - PubMed. https://pubmed.ncbi.nlm.nih.gov/29768209/.
239. Influenza virus NS1 protein interacts with the cellular 30 kDa subunit of CPSF and inhibits 3'end formation of cellular pre-mRNAs - PubMed. https://pubmed.ncbi.nlm.nih.gov/9651582/.

240. Xu, Y., Cei, S. A., Rodriguez Huete, A., Colletti, K. S. & Pari, G. S. Human cytomegalovirus DNA replication requires transcriptional activation via an IE2- and UL84-responsive bidirectional promoter element within oriLyt. *J. Virol.* **78**, 11664–11677 (2004).
241. Stow, N. D. & Stow, E. C. Isolation and characterization of a herpes simplex virus type 1 mutant containing a deletion within the gene encoding the immediate early polypeptide Vmw110. *J. Gen. Virol.* **67 (Pt 12)**, 2571–2585 (1986).
242. Post, L. E. & Roizman, B. A generalized technique for deletion of specific genes in large genomes: alpha gene 22 of herpes simplex virus 1 is not essential for growth. *Cell* **25**, 227–232 (1981).
243. Smith, I. L., Hardwicke, M. A. & Sandri-Goldin, R. M. Evidence that the herpes simplex virus immediate early protein ICP27 acts post-transcriptionally during infection to regulate gene expression. *Virology* **186**, 74–86 (1992).
244. Fenwick, M. L. & Everett, R. D. Inactivation of the shutoff gene (UL41) of herpes simplex virus types 1 and 2. *J. Gen. Virol.* **71 (Pt 12)**, 2961–2967 (1990).
245. Fellmann, C. *et al.* An optimized microRNA backbone for effective single-copy RNAi. *Cell Rep.* **5**, 1704–1713 (2013).
246. Buenrostro, J. D., Giresi, P. G., Zaba, L. C., Chang, H. Y. & Greenleaf, W. J. Transposition of native chromatin for fast and sensitive epigenomic profiling of open chromatin, DNA-binding proteins and nucleosome position. *Nat. Methods* **10**, 1213–1218 (2013).
247. Buenrostro, J. D., Wu, B., Chang, H. Y. & Greenleaf, W. J. ATAC-seq: A Method for Assaying Chromatin Accessibility Genome-Wide. *Curr. Protoc. Mol. Biol.* **109**, 21.29.1-21.29.9 (2015).
248. Corces, M. R. *et al.* An improved ATAC-seq protocol reduces background and enables interrogation of frozen tissues. *Nat. Methods* **14**, 959–962 (2017).
249. Bonfert, T., Kirner, E., Csaba, G., Zimmer, R. & Friedel, C. C. ContextMap 2: fast and accurate context-based RNA-seq mapping. *BMC Bioinformatics* **16**, 122 (2015).
250. Li, H. & Durbin, R. Fast and accurate short read alignment with Burrows-Wheeler transform. *Bioinforma. Oxf. Engl.* **25**, 1754–1760 (2009).
251. Quinlan, A. R. & Hall, I. M. BEDTools: a flexible suite of utilities for comparing genomic features. *Bioinforma. Oxf. Engl.* **26**, 841–842 (2010).
252. Boyle, A. P., Guinney, J., Crawford, G. E. & Furey, T. S. F-Seq: a feature density estimator for high-throughput sequence tags. *Bioinforma. Oxf. Engl.* **24**, 2537–2538 (2008).
253. featureCounts: an efficient general purpose program for assigning sequence reads to genomic features - PubMed. https://pubmed.ncbi.nlm.nih.gov/24227677/.

254. Chirackal Manavalan, A. P. *et al.* CDK12 controls G1/S progression by regulating RNAPII processivity at core DNA replication genes. *EMBO Rep.* **20**, e47592 (2019).
255. Fraser, K. A. & Rice, S. A. Herpes Simplex Virus Immediate-Early Protein ICP22 Triggers Loss of Serine 2-Phosphorylated RNA Polymerase II. *J. Virol.* **81**, 5091–5101 (2007).
256. ICP27 Interacts with the C-Terminal Domain of RNA Polymerase II and Facilitates Its Recruitment to Herpes Simplex Virus 1 Transcription Sites, Where It Undergoes Proteasomal Degradation during Infection | Journal of Virology. https://jvi.asm.org/content/80/7/3567.
257. Conn, K. L., Hendzel, M. J. & Schang, L. M. Linker histones are mobilized during infection with herpes simplex virus type 1. *J. Virol.* **82**, 8629–8646 (2008).
258. Conn, K. L., Hendzel, M. J. & Schang, L. M. Core histones H2B and H4 are mobilized during infection with herpes simplex virus 1. *J. Virol.* **85**, 13234–13252 (2011).
259. Conn, K. L., Hendzel, M. J. & Schang, L. M. The differential mobilization of histones H3.1 and H3.3 by herpes simplex virus 1 relates histone dynamics to the assembly of viral chromatin. *PLoS Pathog.* **9**, e1003695 (2013).
260. Harshman, S. W., Young, N. L., Parthun, M. R. & Freitas, M. A. H1 histones: current perspectives and challenges. *Nucleic Acids Res.* **41**, 9593–9609 (2013).
261. Krishnakumar, R. *et al.* Reciprocal binding of PARP-1 and histone H1 at promoters specifies transcriptional outcomes. *Science* **319**, 819–821 (2008).
262. Kalashnikova, A. A., Rogge, R. A. & Hansen, J. C. Linker histone H1 and protein-protein interactions. *Biochim. Biophys. Acta* **1859**, 455–461 (2016).
263. Safina, A. *et al.* Complex mutual regulation of facilitates chromatin transcription (FACT) subunits on both mRNA and protein levels in human cells. *Cell Cycle* **12**, 2423–2434 (2013).
264. Li, J. *et al.* SPT6 promotes epidermal differentiation and blockade of an intestinal-like phenotype through control of transcriptional elongation. *Nat. Commun.* **12**, 784 (2021).
265. Cardiello, J. F., Goodrich, J. A. & Kugel, J. F. Heat Shock Causes a Reversible Increase in RNA Polymerase II Occupancy Downstream of mRNA Genes, Consistent with a Global Loss in Transcriptional Termination. *Mol. Cell. Biol.* **38**, (2018).
266. Honess, R. W. & Watson, D. H. Herpes simplex virus resistance and sensitivity to phosphonoacetic acid. *J. Virol.* **21**, 584–600 (1977).
267. Crumpacker, C. S. Mechanism of action of foscarnet against viral polymerases. *Am. J. Med.* **92**, S3–S7 (1992).

268. RNA polymerase II is aberrantly phosphorylated and localized to viral replication compartments following herpes simplex virus infection. *Journal of Virology* https://journals.asm.org/doi/abs/10.1128/jvi.68.2.988-1001.1994.
269. Dembowski, J. A., Dremel, S. E. & DeLuca, N. A. Replication-Coupled Recruitment of Viral and Cellular Factors to Herpes Simplex Virus Type 1 Replication Forks for the Maintenance and Expression of Viral Genomes. *PLOS Pathog.* **13**, e1006166 (2017).
270. Guo, L. *et al.* Herpes simplex virus 1 ICP22 inhibits the transcription of viral gene promoters by binding to and blocking the recruitment of P-TEFb. *PloS One* **7**, e45749 (2012).
271. Zaborowska, J. *et al.* Herpes Simplex Virus 1 (HSV-1) ICP22 protein directly interacts with cyclin-dependent kinase (CDK)9 to inhibit RNA polymerase II transcription elongation. *PloS One* **9**, e107654 (2014).
272. Harlen, K. M. *et al.* Comprehensive RNA Polymerase II Interactomes Reveal Distinct and Varied Roles for Each Phospho-CTD Residue. *Cell Rep.* **15**, 2147–2158 (2016).
273. RNA polymerase II termination involves C-terminal-domain tyrosine dephosphorylation by CPF subunit Glc7 - PubMed. https://pubmed.ncbi.nlm.nih.gov/24413056/.
274. Szpara, M. L., Parsons, L. & Enquist, L. W. Sequence Variability in Clinical and Laboratory Isolates of Herpes Simplex Virus 1 Reveals New Mutations. *J. Virol.* **84**, 5303–5313 (2010).
275. Sedarati, F. & Stevens, J. G. Biological Basis for Virulence of Three Strains of Herpes Simplex Virus Type 1. *J. Gen. Virol.* **68**, 2389–2395 (1987).
276. Hill, J. M., Rayfield, M. A. & Haruta, Y. Strain specificity of spontaneous and adrenergically induced HSV-1 ocular reactivation in latently infected rabbits. *Curr. Eye Res.* **6**, 91–97 (1987).
277. Bowen, C. D. *et al.* Comparison of Herpes Simplex Virus 1 Strains Circulating in Finland Demonstrates the Uncoupling of Whole-Genome Relatedness and Phenotypic Outcomes of Viral Infection. *J. Virol.* **93**, (2019).
278. Birkenheuer, C. H., Danko, C. G. & Baines, J. D. Herpes Simplex Virus 1 Dramatically Alters Loading and Positioning of RNA Polymerase II on Host Genes Early in Infection. *J. Virol.* **92**, (2018).
279. Evidence for DNA-mediated nuclear compartmentalization distinct from phase separation | eLife. https://elifesciences.org/articles/47098.
280. Öztürk, M. A., Cojocaru, V. & Wade, R. C. Dependence of Chromatosome Structure on Linker Histone Sequence and Posttranslational Modification. *Biophys. J.* **114**, 2363–2375 (2018).
281. Kajitani, K., Kato, K. & Nagata, K. Histone H1 chaperone activity of TAF-I is regulated by its subtype-dependent intramolecular interaction. *Genes Cells Devoted Mol. Cell. Mech.* **22**, 334–347 (2017).

282. Mandemaker, I. *Unraveling the Chromatin in the DNA Damage Response*. (Erasmus University Rotterdam, 2018).
283. Schek, N. & Bachenheimer, S. L. Degradation of cellular mRNAs induced by a virion-associated factor during herpes simplex virus infection of Vero cells. *J. Virol.* **55**, 601–610 (1985).
284. Yager, D. R. & Bachenheimer, S. L. Synthesis and metabolism of cellular transcripts in HSV-1 infected cells. *Virus Genes* **1**, 135–148 (1988).
285. Tettey, T. T. *et al.* A Role for FACT in RNA Polymerase II Promoter-Proximal Pausing. *Cell Rep.* **27**, 3770-3779.e7 (2019).
286. Duina, A. A. Histone Chaperones Spt6 and FACT: Similarities and Differences in Modes of Action at Transcribed Genes. *Genet. Res. Int.* **2011**, (2011).
287. Abrisch, R. G., Eidem, T. M., Yakovchuk, P., Kugel, J. F. & Goodrich, J. A. Infection by Herpes Simplex Virus 1 Causes Near-Complete Loss of RNA Polymerase II Occupancy on the Host Cell Genome. *J. Virol.* **90**, 2503–2513 (2016).
288. Yoh, S. M., Cho, H., Pickle, L., Evans, R. M. & Jones, K. A. The Spt6 SH2 domain binds Ser2-P RNAPII to direct Iws1-dependent mRNA splicing and export. *Genes Dev.* **21**, 160–174 (2007).
289. Jeronimo, C. *et al. FACT is recruited to the +1 nucleosome of transcribed genes and spreads in a Chd1-dependent manner*. http://biorxiv.org/lookup/doi/10.1101/2020.08.20.259960 (2020) doi:10.1101/2020.08.20.259960.

8. LIST OF FIGURES

9. LIST OF TABLES

The following figures of the results section were generated by the group of our collaborator Prof. Dr. Caroline Friedel based on the data I generated, followed by intensive discussion on how to best perform these bioinformatics analyses.